UNIVERSITÀ DEGLI STUDI
DI MILANO

Ph.D. in Agriculture, Environment and Bioenergy
XXX Cycle

Improving decision support tools via integration of remotely sensed data in crop models

Ph.D. Thesis

Carlo Gilardelli
N° R11019

Supervisor	Academic Year	*Coordinator*
Prof. Roberto Confalonieri	2016-2017	Prof. Daniele Bassi

Carlo GILARDELLI

Improving decision support tools via integration of remotely sensed data in crop models

Ph. D. Thesis
Department of Agricultural and Environmental Sciences – Production, Landscape, Agroenergy

University of Milan
Via Celoria 2, 20133 Milan – Italy
carlo.gilardelli@unimi.it

Reference to the contents of Chapters 2 and 3 should be made by citing the original publications.

ABSTRACT

The need to fulfil sustainability requirements while increasing productions to feed the raising world's population represents a big challenge for the agricultural sector. To achieve this goal, improving management of resources at farm level is acknowledged as one of the most effective solutions. However, this requires intensive activities targeting cropping system monitoring and data processing. The advances in remote sensing and simulation technologies – especially when used in an integrated way – provide a valuable solution to support farmers and technicians in such a context.

This research aims at setting up and evaluating pre-operational tools based on the integration of crop models and remotely sensed information to support decision making in cropping systems management. The research was articulated in two main preliminary activities before the application of crop models and remote sensing in a case study. Extensive sensitivity analysis experiments were performed to deepen the knowledge about model behaviour and to identify the most influential parameters for yield simulation. A wide range of conditions was investigated, considering both current weather and future climate projections, as well as five major crops cultivated in several European sites and using two different modelling solutions (the standard version of WOFOST and a version of the model improved for the simulation of the impact of extreme weather events). Model outputs were mainly influenced by parameters involved with storage organs development; nevertheless, in case limiting conditions were explored, simulations were influenced by parameters driving crop growth during early stages. Given leaf area index (LAI) data are those mostly used when crop models and remote sensing are integrated, the second activity targeted the quantification of the impact of subjectivity in LAI estimates from hemispherical images. Precision was determined via the application of the ISO 5725 validation protocol, thus leading to define repeatability and reproducibility limits. Results proved the reliability of LAI estimates from hemispherical images; the precision obtained was indeed comparable with that of other commercial instruments. The best results were obtained in case of high LAI and continuous canopy, further underlying the reliability of this method for intensive agricultural systems characterized by continuous and homogeneous canopies. Both the activities just presented aimed at defining a sound starting point for the coupling of crop models and remote sensing, providing useful information for the design of the case study. For this last activity, a high-resolution pre-operational system based on the WARM model and remotely sensed information was evaluated using observations from paddy rice fields during the seasons 2014,

2015 and 2016. The remotely sensed information, consisting in temporal series of LAI, were integrated in the model by automatically re-calibrating either parameters identified as the most influential or those strictly related with LAI dynamics. The system performances were compared with those obtained using the default parameterizations of the model. Results underlined the improvement in rice yield simulation after the integration of remotely sensed data, proving the reliability of the system. Overall, the simulation of rice yield was affected by a restrained RRMSE (13.8%), compared to the results obtained with the default model parameterizations (RRMSE = 15.7%). Moreover, the assimilation of remotely sensed information at high spatial resolution (30 m × 30 m) led to satisfactorily describe the within-field yield variability. The obtained results make the proposed system a valuable solution to provide high-resolution estimates of rice productivity. Nonetheless, weakness were highlighted, related with some the inconsistencies between observed crop state variables and crop reflectance properties. This, as well as the possibility to consider other models and crops, lays the basis for further studies.

Keywords

Sustainability, Crop modelling, Remote Sensing, Decision support system, Yield prediction

CONTENTS

Chapter 1

INTRODUCTION

1.1 Increasing agricultural productions while preserving natural resources

Starting from the Common Agricultural Policy (CAP) reform in the 1992, rising attention has been put on the sustainability of agricultural productions. This was dictated by a growing awareness of the environmental impacts caused by intensive agricultural systems and by the worries about the loss of environmental resources (Van der Werf and Petit, 2002). With the last CAP reform (2014-2020), the environmental objectives assumed further importance; a quota of direct payments has been tied to the compliance of environmental requirements and the 30% of the Rural Development programme was reserved to measures targeting the environmental preservation (Council of the European Community, 2013). To comply with this newly regulations, farmers have modified the agronomic management of crops by adopting practices focused on environmental sustainability, like the interruption of cereal mono-culture and mono-cropping with the insertion of cover crops targeting a mitigation of land degradation, a contribution to the conservation of soil water and nutrients reserves and, in case of legumes, nitrogen fixation into the soil (Gaudin et al., 2014). Other activities targeting environmental preservation are the minimum or no tillage practices; besides being energy saving, these practices, compared with intensive tillage, allow the preservation of soil's structural properties and water resources (Mupangwa et al., 2007). Emphasis has also been put on the limitation of pollution due to agro-chemicals. Strategies to modulate fertilization rates based on optical crop sensing has been also developed to increase nitrogen use efficiency (Raun et al., 2002). To reduce the amount of herbicides with a potentially leading to groundwater pollution, strategies to contain weeds growth such as higher crop seeds rate, reduced row spacing and incorporation into the soil of green manure and cover crops were adopted (Blackshaw et al., 2006). Since agriculture is, globally, the largest freshwater consumer and considering that only half of the distributed water is actually used by the crops (Turral et al., 2010), the recourse to efficient irrigation systems (Knox et al., 2012) and even the adoption of controlled water deficit (Du et al., 2010) represent other valuable practices targeting environmental sustainability.

Beside the fulfillment of sustainability requirements, agriculture is called to feed the rising global population which is projected to be about nine billion people by 2050. This strong demographic growth will be accompanied by a substantial increase in food demand (Tilman et al., 2002). The described scenario is a big challenge for the agricultural sector considering also the exacerbation of the competition for resources (i.e., land, water, energy) with other production sectors (Godfray et al., 2010). The goal of increasing food production under scenarios characterized by decreasing

resources while preserving the environment can be reached improving the management of on-farm resources (i.e., land, water, fertilizers, herbicide, pesticide) including energy inputs such as gas and oil (Fess et al., 2011). To achieve this aim, farmers and technicians have to increase the effort dedicated to cropping systems monitoring, this being a key assumption to optimize management practices. Decision support tools can support farmers in such activities, collecting and elaborating information from several domains of the agricultural system and producing synthetic data useful to optimize the agro-management (Sørensen et al., 2010).

1.2 Decision support tools in agriculture

In the last years, several kind of decision support tools were formalized, differing in structure, inputs needed and type of information spread. The most simple are based on empirical relationship between crop variables and the quantity of a certain input (e.g., canopy dimension and nitrogen fertilization rate). Besides those based on in situ measurements, often expensive in terms of labour and thus not applicable at large scale, the crop monitoring through sensors has been one of the most exploited technique. The main efforts have been directed towards the optimization of nitrogen fertilization, to reach the potential production while limiting nitrogen losses. Holland and Schepers (2010) and Solie et al. (2012) formalized two strategies to modulate nitrogen fertilization rate based on instruments for optical crop sensing. Although these instruments can be mounted on tractors, the high dependency on machinery availability and the need of reference value of crop reflectance for optimal nitrogen content limit their usefulness for operational purposes. Thanks to the continuous improvements in satellite technology and the possibility to equip airplanes with sensors, the remote sensing of environment has become one of the most popular technique to monitor agricultural systems. Wood et al. (2003) have found a correlation between an index of the photosynthetic surfaces (GAI, Green Area Index), estimated through airborne photography, and the fertilization rate that should be applied to gain the optimal GAI value. Through the adoption of vegetation indices (e.g., NDVI, PRI) and the monitoring of crop temperature during the growth cycle, Panigada et al. (2014) and Rossini et al. (2015), proposed strategies to detect water stress in cereal crops. Panda et al. (2014) showed the combined used of images from several satellite (LANDSAT, SPOT, NAIP) to retrieve information about the crop stomatal conductance, canopy temperature and leaf are index (LAI) dynamics. Lobell et al. (2015) proposed a method to perform yield forecasting based on crop monitoring from satellites. Other efficient instruments on which the formalization of decision support tools has been based are simulation models. These instruments are able to integrate the effects of different environmental

factors and management practices on crop growth and development (Basso et al., 2001), and can thus be adopted to support decision-making. For instance, crop models have been used to (i) optimize irrigation at farm level (García-Vila and Fereres, 2012); (ii) analyse the response of crops to different water and nitrogen availability (Singh et al., 2008); (iii) select the best management practices in specific environments (Morari et al., 2004) or even (iv) support the adaptation of crop management to climate change (Lehman et al., 2013).

Despite the great diffusion of remote sensing and crop modelling to support decision-making, both technologies are characterized by some constraints. One the one hand, even if remotely sensed data bring useful information about the spatial variability of crops, they are linked to the temporal resolution of satellite and even to the presence of clouds thus determining the temporal discontinuity of these kind of data (Liu and Weng., 2012). Moreover, remote sensing allows deriving vegetation indices, which are not variable with a specific biophysical meaning. On the other side, crop models provide outputs for simulation units assumed to be homogeneous in terms of inputs. This makes them unable to describe, e.g., intra-field heterogeneity (Batchelor et al., 2002). To overcome the intrinsic limitations of each technology, their coupling appears as a promising technique.

1.3 Integrating crop models and remote sensing

Thanks to the advances in computer technology and to the availability of remotely sensed information with increased spatial and temporal resolutions, the coupling between remote sensing and crop models has been subjected to an exponential growth during last years. Several studies were indeed performed covering a wide range of crops and locations (e.g., Jongschaap, 2006; Youping et al., 2008; Casa et al., 2012; Ines et al., 2013; Zhao et al,. 2013; Li et al., 2014). Different ways to include remotely sensed information into crop models were proposed; however, they can be grouped in the following categories: (i) calibration, which entails an automatic adjustment of model parameters or initial states to minimize the difference between simulated and exogenous state variable; (ii) forcing, which replaces the simulated variables with the observed ones (re-initialization) and (iii) updating, that consists in the continuous update of model state variables whenever an observation is available (Dorigo et al., 2007). Several crop variables have been sensed within monitoring activities; however, most studies focused on leaf area index (LAI), due to its direct influence on the canopy spectral reflectance. All the cited works deal with an improvement in crop monitoring along the growing season targeting the improvement in yield prediction. Despite the promising results obtained both in the monitoring of crop status and in the

prediction of yields, the main drawback of these works is the spatial resolution of the information provided. The outputs of the combination of crop model and remote sensing were at a district scale, thus being unsuitable to support the agro-management. The recent launch of satellites with an increased spatial resolution can allow the assimilation of remotely sensed data into crop models at a higher level of detail.

1.4 Objectives

The main goal of this research is the setup and evaluation of operational tools based on the integration of crop models and remote sensing for supporting decision-making in agriculture. While crop models allow describing, through a process based approach, the multiple interactions among agricultural systems components (e.g., soil, crop, weather, agro-management), the assimilation of remotely sensed information can allow describing the spatial variability of crop status. The work benefits from existing models – e.g., WARM (Confalonieri et al., 2009) and different versions of WOFOST (Van Diepen et al., 1989; Stella et al., 2014) – and software component (UNIMI.Forcing) which allows the assimilation of exogenous data in crop models. The latter mainly consist of LAI time series between crop establishment and canopy closure. Despite both technologies (i.e., simulation models and remote sensing) are continuously improved by the scientific community, their coupling still presents some limitations, due to different sources of uncertainty not properly managed. For these reasons, before the application of models and remote sensing in a study case, part of the research was targeted to:

- The identification of the most reliable technique to assimilate exogenous data among those available (forcing and recalibration). The former entails a simple substitution of the simulated LAI values with the correspondent values estimated by satellite, and then a re-initialization of all model state variable starting from the exogenous one and from the state at the previous time step. The second technique, instead, is based on an automatic recalibration of model parameter through a modified version of the downhill simplex optimization method (Nelder and Mead, 1965). In this case, parameter values are defined by optimizing an objective function between simulated and exogenous state variables.
- The increase of the knowledge on model structure and behaviour under a wide range of conditions to identify the parameters at which the model is most sensitive, which are those to be automatically recalibrated during optimization. This can be achieved via the adoption of sensitivity analysis techniques in a wide range of agro-climatic conditions.

- The evaluation of the reliability of LAI estimates using hemispherical photography. The processing of hemispherical images is a widespread indirect method to estimate LAI and to validate the radiative transfer model adopted to derive LAI values from crop reflectance. However, this indirect method for LAI estimates is based on a supervised segmentation method, that can be subject to user subjectivity.

The last part of the research was designed starting from the lesson learned from what above, and targeted the implementation of the case study, where the assimilation of exogenous LAI data from paddy rice fields let the WARM model to reproduce the within-field variability, thus providing information to support the agro-management practices planning.

1.5 Outline of the Thesis

Chapter 2 describes the formalization of a specific model (WOFOST-GTC) for rapeseed simulation. The model, derived from the WOFOST-GT2 model (Stella et al., 2014), benefit of a reduction of complexity substituting the AFGEN tables with functions driven by few parameters with a clear biological meaning. This activity aims at simplifying model calibration and limits the possibility of generating inconsistent parameterizations. Particular attention was put on the representation of photosynthetic surfaces within the vertical profile of rapeseed canopies, whose LAI is split into 20 horizontal layers using a beta function changing according to crop development. In particular, most photosynthetic tissues are located in the bottom layers during early stages, whereas during flowering they are evenly distributed within the canopy, and – during senescence – they are located in the upper layers. This improvement compared to the original WOFOST version led to increase model accuracy both for LAI and biomass simulation, as well as for final yield. Moreover, the new version of the model allows the simulation of quality of production (i.e., oil content in the seeds and its composition). Despite the improved description of canopy dynamics (crucial for the assimilation of exogenous LAI values), some constraints still persist. Not all the process driving crop growth are formalized; in particular the effect of frost injuries on LAI and biomass are not reproduced. In these cases, the inclusion of exogenous data can improve model performances re-initializing the simulation at the spring restart.

Chapter 3 shows the results of sensitivity analysis experiments applied to the model WOFOST. To analyze model behavior under a wide range of conditions, both current weather series and mid-term climate change scenarios were used at different European sites and for different crops. The effect of extreme weather events on crop growth and productivity was also considered (Villalobos

et al., 2015). This work aimed at deepening the knowledge of the model WOFOST through the identification of the most relevant parameters. This work enlarged the knowledge on model structure and allowed defining the procedure to select the parameters to be automatically re-calibrated during assimilation.

Chapter 4 presents the quantification of the impact of subjectivity when LAI is estimated using hemispherical photography and the widespread Can-Eye package. This is due to the need of specifying manually the thresholds for image segmentation. Four users processed hemispherical images, and repeatability and reproducibility limits were estimated. Hemispherical images were taken from a variety of tree canopies to cover a wide range of architectures. The best results were obtained for images constitutes by an high proportion of canopy (i.e., continuous and homogeneous canopies) whereas poorer results were obtained in case of sparse vegetation. In general, the low values of repeatability and reproducibility further demonstrated the reliability of hemispherical photography to estimate LAI values, in turn encouraging its adoption.

Chapter 5 presents the application, in an operational context, of a system based on the integration of the WARM rice model and of 30 m × 30 m resolution remote sensing data. The main goal of this part of the research was to analyze the within-field spatial variability to support the agro-management practices. The assimilation of remotely sensed LAI data into WARM was performed via recalibration of model parameters. The parameters under recalibration were selected via sensitivity analysis (maximum radiation use efficiency) or because strictly linked to LAI dynamics (initial and mid-tillering specific leaf area). The ability of the system to describe the within field variability was evaluated through the comparison with production maps generated at the harvest.

Chapter 6 draws the overall conclusions of the research. Emphasis is given to the importance of the achievements and to the identification of further researches.

Note

Chapter 2 is published in Field Crops Research. Chapter 3 is published to Ecological Modelling. Chapter 4 is submitted to Agricultural and Forest Meteorology and Chapter 5 will be submitted to Remote Sensing of Environment.

Chapter 2

WOFOST-GTC: A NEW MODEL FOR THE SIMULATION OF WINTER RAPESEED PRODUCTION AND OIL QUALITY

Carlo Gilardelli, Tommaso Stella, Nicolò Frasso, Giovanni Cappelli, Simone Bregaglio, Marcello E. Chiodini, Barbara Scaglia, Roberto Confalonieri

Published in: Field Crops Research (2016) 197, pp. 125-132.

2.1. Abstract

Rapeseed is one of the most important sources of vegetable oils, and its cultivation in Europe is expanding due to the economic incentives to grow energy crops. Given the unique characteristics of this crop, simulation studies targeting yield predictions and scenario analysis should be performed using specific models rather than using generic crop simulators adapted to rapeseed via calibration. This study presents a new model – WOFOST-GTC – which implements a dynamic representation of the rapeseed canopy architecture and includes modelling approaches to simulate oil content and composition. We reduced the number of model parameters to 35, compared to the 97 parameters of the original WOFOST model, from which it derives. WOFOST-GTC was developed using data collected in dedicated field experiments carried out in northern Italy in 2012-2013. The model ability to reproduce the underlying processes was evaluated using data collected in Europe between 1993 and 2013. In particular, dynamics involved with production and oil quality were evaluated on 7 and 18 datasets, respectively. The aboveground biomass and photosynthetic area index at different depths in the canopy were accurately simulated (R^2 = 0.86 and 0.78, respectively). Despite the lower complexity, WOFOST-GTC proved to be as accurate as the original WOFOST model. The simulation of the seed oil content (R^2 =0.76) and of the oleic (R^2=0.95), linoleic (R^2=0.88) and α-linolenic acid (R^2=0.95) fractions was accurate. Hence, we propose WOFOST-GTC as a suitable simulation model to analyse the rapeseed production and oil quality under different weather and management scenarios.

Keywords
Canopy architecture, canola, oil quality, WOFOST, WOFOST-GT.

2.2 Introduction

Rapeseed (Brassica napus L.) is the third most cultivated oleaginous crop worldwide, with approximately seven million hectares planted in the European Union (EU) in 2013 (FAO, 2014). Rapeseed cultivars have a diverse range of fatty acid compositions in the seed oil, and this characteristic makes the crop suitable for a broad range of uses, such as the production of biodiesel (Ramos et al., 2009), edible oils (Ursin et al., 2003), livestock feed (Bell et al., 2003) and industrial lubricants (Wagner et al., 2001). Currently, rapeseed represents the major source of raw material for European biodiesel production, and its importance will further increase due to the incentives promoted by the Renewable Energy Directive (2009/28/EC), which imposes requirements on the member states to derive at least 10% of the total energy for the transport sector from renewable resources in 2020.

In this context, the competition for land use between food and energy crops is emerging as a critical issue, and there is an increasing demand for tools for supporting the development of policies via the evaluation of alternative scenarios and management plans (Cappelli et al., 2015). The key role of crop models for this purpose is widely recognized because of their ability to simulate the non-linear responses of crops to management strategies and climatic conditions (De Carvalho Lopes and Steidle Neto, 2011).

Despite the importance of rapeseed and its unique morphological and physiological traits, modelling studies for this crop are usually performed by adapting generic crop simulators via calibrations, which force the model to mimic the rapeseed growth dynamics without the formalization of algorithms to simulate rapeseed-specific traits (e.g., Habekotté, 1997; Confalonieri et al., 2016). In recent years, the rising importance of this crop led to several attempts to adapt widely known crop system models to the simulation of winter rapeseed. Examples include CERES (Gabrielle et al., 1998), AquaCrop (Zeleke et al., 2011), DSSAT (Deligios et al., 2013) and APSIM (Zeleke et al., 2014). Among the main factors that make the rapeseed modelling particularly challenging is the complex canopy architecture and the differential contribution of plant organs to photosynthesis during the crop cycle (Müller et al., 2005). The aim of this study was to develop and evaluate the WOFOST-GTC, a new model for the simulation of rapeseed production and oil quality.

2.3 Materials and methods

2.3.1 WOFOST-GTC description

WOFOST-GTC is derived from WOFOST-GT/GT2 (Stella et al., 2014), which improved the canopy description and reduced the model complexity of the original WOFOST model (Van Diepen et al., 1989). Three main issues were addressed in the development of WOFOST-GTC: (i) the contribution of the different plant organs to photosynthesis during the crop cycle, (ii) the model simplification, and (iii) the simulation of seed oil content and composition. Other processes are based on the original WOFOST model (Van Diepen et al., 1989).

2.3.1.1 Representation of the canopy architecture dynamics

The vertical distribution of the photosynthetic area index (PAI, m2 m-2) is dynamic during the rapeseed cycle (Diepenbrock, 2000). From emergence to the differentiation of flower buds, the bottom leaves accounts for most of the PAI, whereas the PAI is homogeneously distributed along the vertical canopy profile during flowering. After pod formation, the basal leaves become senescent and the upper portion of the canopy intercepts most of the light (Müller et al., 2005). WOFOST-GTC simulates this temporal PAI pattern by splitting the canopy into 20 horizontal layers, each representing 5% of the total plant height. A Kumaraswamy cumulative distribution function (Kumaraswamy et al., 1980) was used to derive the fraction of the PAI in the different canopy layers (Eq. 1):

$$PAI_{\%,i} = 1 - \left(1 - x_i^{\alpha}\right)^{\beta} \quad [1]$$

where PAI%,i (0-1) is the cumulative fraction of the PAI allocated from the top of the canopy to the i-th canopy layer; x is the percentage of the canopy depth assigned to the i-th layer (which ranges from 0.05 in the top layer to 1 in the bottom layer); and α and β are the parameters of the distribution. The amount of PAI in each layer (PAIi, m2 m-2) is derived daily by allocating the PAItot according to the PAI%,i. The values of α and β in Eq. 1 determine the shape of the distribution and were derived as a function of the SUCROS-type development stage code (DVS; 0: emergence, 1: flowering, 2: maturity) according to the PAI dynamics observed in dedicated field trials.

2.3.1.2 Model simplification

The approach described by Stella et al. (2014) was used to replace the AFGEN (Arbitrary Function GENerator) tables of the WOFOST model with specific functions driven by a few parameters with a clear biological meaning. The AFGEN tables are sets of X, Y pairs, where Y is the parameter value

that corresponds to a certain X, and X is either the daily average air temperature or the DVS. The X, Y values are linearly interpolated every day to derive the parameter value to be used within the time step model. There are two main problems associated with the use of AFGEN tables. First, the large number of X, Y pairs for the same parameter corresponds to an equally large number of degrees of freedom during calibration, which increases the risk of an incoherent description of the underlying processes (Stella et al., 2014). Second, the AFGEN tables are not entirely compatible with advanced tools for sensitivity analysis and automatic calibration; such tools can only be applied by drastically reducing the number of X, Y pairs to minimize the risk of overlaps among parameter distributions for different values of X (Confalonieri, 2010).

The analysis of the literature and of the AFGEN tables available for rapeseed in the official WOFOST release (v. 7.1.7, implemented in the WOFOST Control Centre 2.1) allowed replacing the AFGEN tables by new functions driven by a few parameters with a clear biological meaning (i.e., measurable quantities), listed in Appendix B.

2.3.1.3 Oil content and composition in seeds

The main variables that determine the quality of the rapeseed oil are its accumulation in kernels and the fractions of oleic, linoleic and α–linolenic unsaturated fatty acids (Bhardwaj and Hamama, 2008). The data used for the development of the model derive from the studies by Baux et al. (2008; 2013), who monitored the fatty acid profiles of different rapeseed varieties from the beginning of grain filling to full maturity. The simulation of the effects of environmental conditions on the oil quality was described according to Walton (1999), who investigated the role of temperature and precipitation on the oil content and composition during ripening.

2.3.2 Experimental data and model evaluation

An experimental trial was performed during the 2012/13 crop season (Table 1; datasets 1 and 5) in two sites of northern Italy: Buscate (latitude 45° 32’ N, longitude 8° 48’ E) and Casorezzo (45° 31’ N, 8° 45’ E). Rapeseed (cultivar Excalibur) was sown on October 5 and 10 for datasets 1 and 5, respectively, and received 300 kg ha-1 of ammonium sulphate at the beginning of the spring as well as chemical treatments to keep the crop weed and pest free. Ideal agronomic and environmental conditions guaranteed nearly potential production levels. The aboveground biomass (AGB, kg ha-1) and the PAI were measured nine times during the season. The AGB was determined on 20-plant samples, whereas the PAI was estimated at different heights in the canopy with an Accupar LP-80 ceptometer (Decagon device Inc. Pullman, USA) to analyse the dynamic changes in the vertical distribution of photosynthetic tissues during the crop cycle. In

particular, the total PAI was measured in post-emergence and at three canopy depths (ground level, 1/3 and 2/3 of the maximum plant height) starting from stem elongation to the beginning of flowering. From flowering to maturity, an additional measurement was also taken below the inflorescence. After the beginning of the pod growth, the basal leaves became senescent and the PAI sampling at 1/3 of the plant height ceased. The relative abundance of oleic, linoleic and α-linolenic polyunsaturated fatty acids was determined with 200 siliquae harvested in each field. The extraction of the total fatty acids followed the method of Bhardwaj and Hamama (2008), whereas gas chromatography was carried out according to Haines et al. (2011).

The calibration of WOFOST-GTC to simulate the PAI and aboveground biomass dynamics was carried out with the experimental data collected in 2012-2013 in Buscate and Casorezzo as well as with literature data referring to five experimental trials carried out in Italy and France between 1994 and 2013 (Table 1). The performance of WOFOST-GTC for reproducing the AGB values for the datasets presented in Table 1 was compared with the performance of the original version of WOFOST.

The evaluation of the model performance for simulating the oil quality variables was carried out in 16 additional datasets collected in four European sites during the period from 1993 to 2013 (Appendix A). These datasets were divided into calibration and validation datasets, and the model performances were separately evaluated for each quality variable. The agreement between measured and simulated data was quantified using the normalized root mean square error (NRMSE, i.e., the ratio between RMSE and the range of observed values), the Nash and Sutcliffe modelling efficiency (NSE), and R2.

2.4 Result and discussion

2.4.1 Model development

Most of the PAI was concentrated in the basal region of the canopy after emergence and in the apical region during ripening, and it was more evenly distributed around the flowering stage (Fig. 1). During flowering, the uppermost five canopy layers did not contribute to photosynthesis; however, they intercepted the incoming radiation, in turn shading the underlying layers.

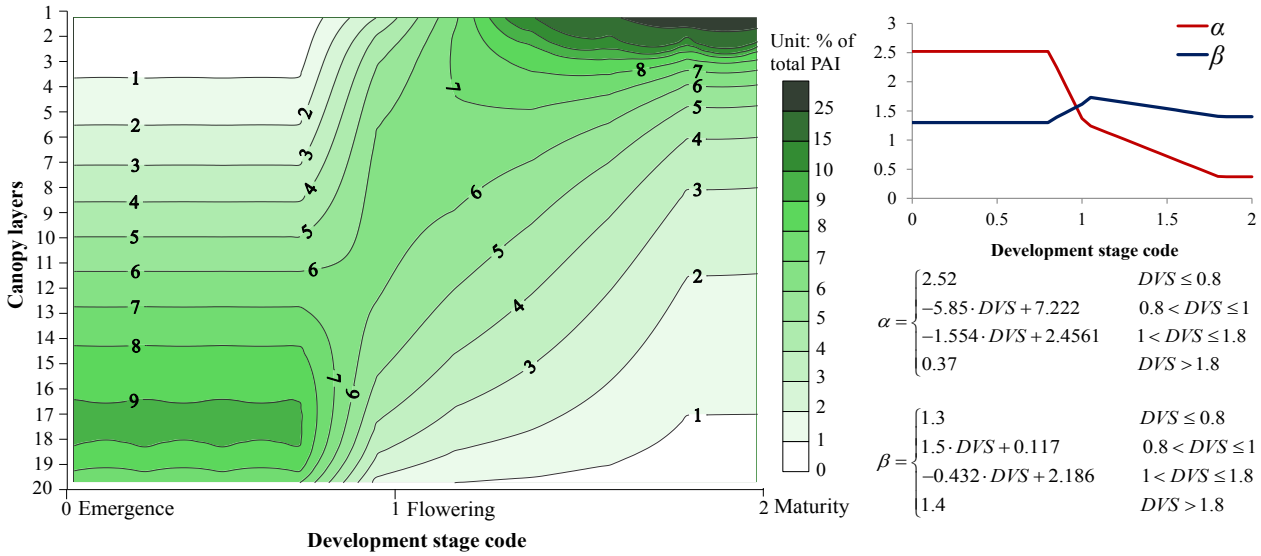

Figure 1. Changes in the relative distribution of the photosynthetic area index among the canopy layers as a function of developmental stage; layers 1 and 20 correspond to the apical and the basal part of the canopy, respectively. On the right, the functions for α and β used to parameterize Eq. 1 are shown.

The new functions developed to simulate physiological changes as a function of temperature or DVS are reported in Appendix B. Each function substitutes an AFGEN table of the original WOFOST model. The parameters that drove the new functions have a clear morphological or physiological meaning, which allows determining the values through a literature search or by direct measurement in the field. The development of new functions reduced the number of model parameters to 35 (there are 97 in the original WOFOST version).

The approaches implemented in WOFOST-GTC to reproduce the dynamics of oil accumulation and of the fractions of oleic, linoleic and α–linolenic acids are reported in Appendix C. The accumulation of oil in kernels was simulated using a sigmoid function from flowering to maturity, modulated by the effects of temperature and rainfall during ripening. The fractions of oleic and linoleic acid contents were determined as a function of the average minimum air temperature perceived by the crop during the post-pollination period. The fraction of α–linolenic acid content was estimated based on crop-specific parameters and the thermal time accumulated from the onset of flowering.

2.4.2 Model evaluation

2.4.1.1 Simulation of rapeseed growth dynamics and production

As an example, time trends of measured and simulated values of the AGB and total PAI for Buscate (dataset 1 in Table 1) are shown in Fig. 2, together with the simulated values of the biomass of the aerial organs. The simulated dynamics were consistent with measured data, with the exception of

the first observation after emergence, which was markedly underestimated by the model for both the PAI and AGB. This discrepancy was attributed to the lack of specific algorithms for frost damage: a vigorous growth was observed after emergence, but part of the biomass and a substantial amount of photosynthetic tissues were lost during winter (Fig. 2). Currently, the model does not account for this process; however, it can be parameterized to simulate lower biomass accumulation rates during autumn and dormancy – without any damage to plant tissues – in winter. Simulations results can, in this way, match the observed AGB and PAI values at the end of the winter and reliably reflect the growth dynamics in the remaining part of the crop cycle.

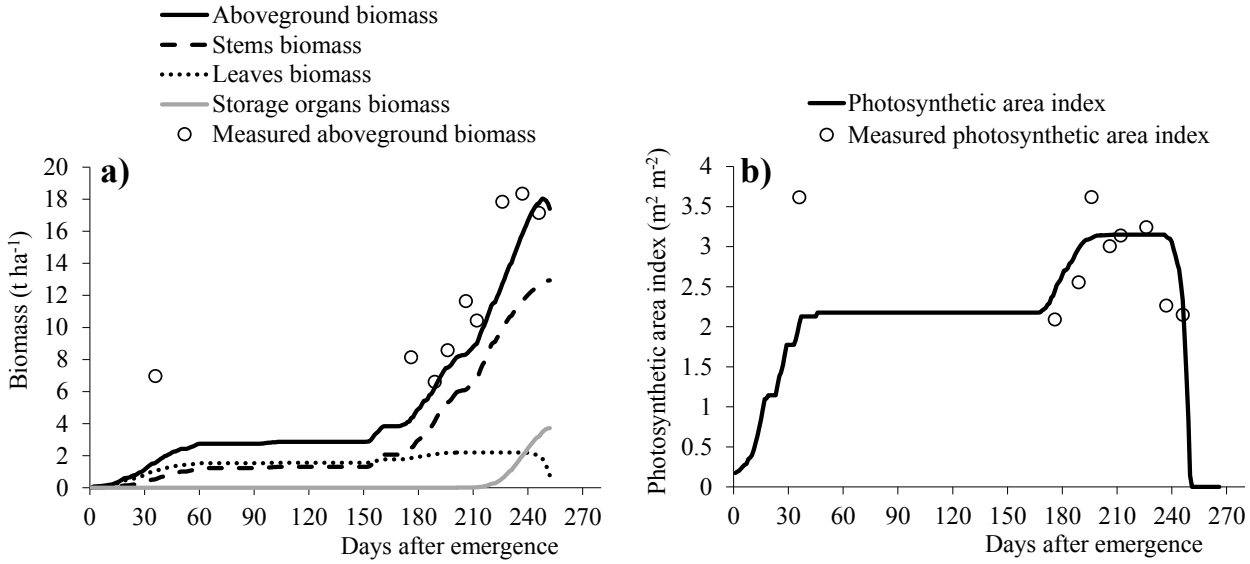

Figure 2. a) Aboveground biomass (AGB in t ha^{-1}). b) Photosynthetic area index (PAI in m^2 m^{-2}). Both figures are simulations based on data from Buscate (dataset 1) and are compared with observations. In (a): simulated aboveground biomass is indicated with continuous line; stems, leaves and storage organ biomass are indicated with dashed, dotted and grey lines, respectively; measured aboveground biomass is indicated with empty circles. In (b): simulated photosynthetic area index is indicated with continuous line; measured photosynthetic area index is indicated with empty circles.

The new algorithm used to simulate the PAI dynamics led to a satisfactory simulation of the distribution of photosynthetic tissues along the vertical canopy profile throughout the crop cycle. As an example, Fig. 3 shows the measured and simulated PAI values of Casorezzo (dataset 5) at four different canopy depths: ground level, 1/3 of the canopy height, 2/3 of canopy height, and immediately below the inflorescence. The best results were obtained for the simulation of the PAI in the top layers (NRMSE= 24%). Thus, this outcome allowed a realistic estimation of light interception in the flowering stage and, in turn, of the photosynthetic rates during grain filling, when the pods represent the primary organs of CO2 assimilation (Diepenbrock, 2000).

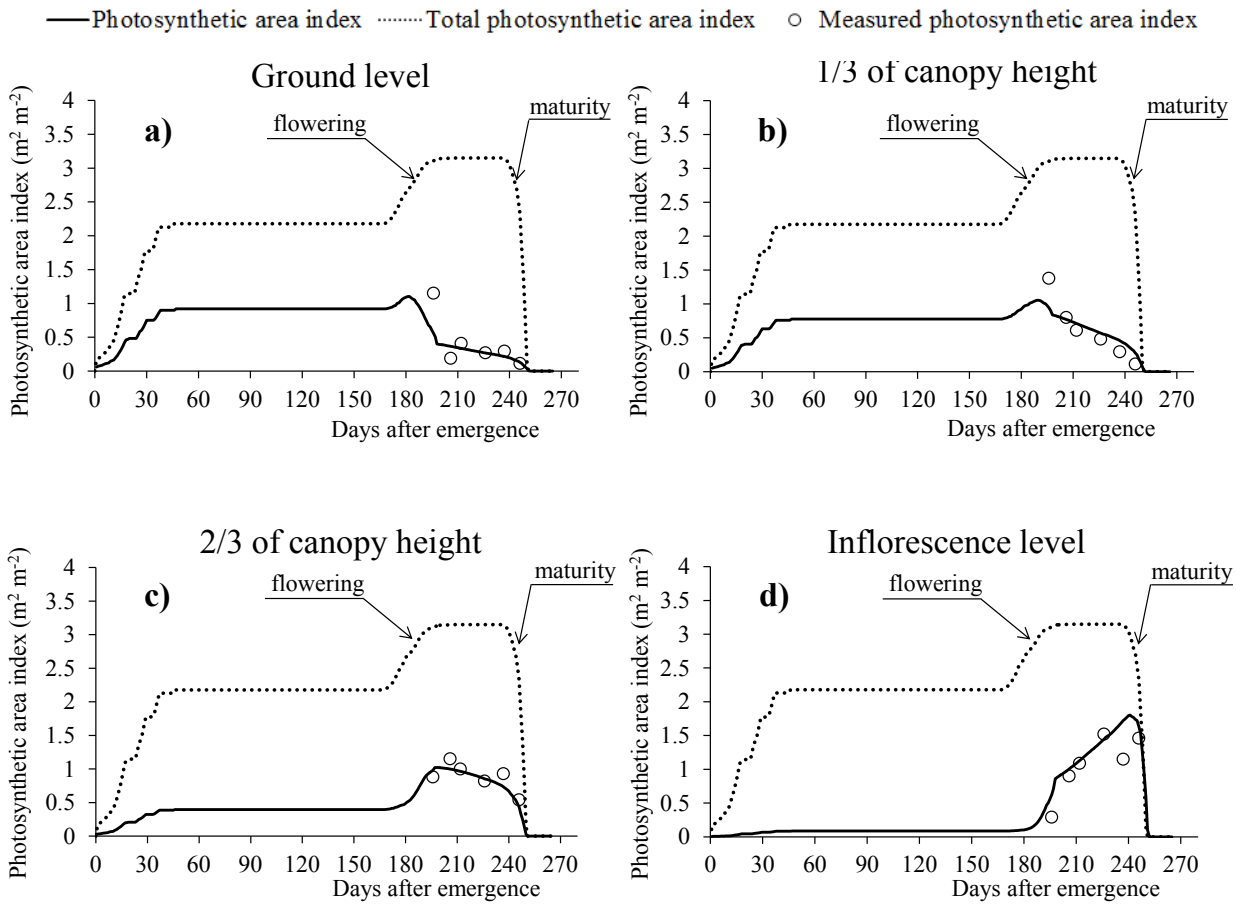

Figure 3. Measured and simulated photosynthetic area index (PAI) values for Casorezzo (dataset 5) at different canopy depths. The PAI refers to (a) ground level, (b) 1/3 of the canopy height, (c) 2/3 of canopy height, (d) immediately below the inflorescence. Simulated photosynthetic area index in each canopy depth is indicated with continuous line; total photosynthetic area index is indicated with dotted line; measured photosynthetic area index in each canopy depth is indicated with empty circles.

The indices of agreement between measured and simulated AGB values are shown in Table 1. Within the calibration datasets, WOFOST-GTC demonstrated a greater accuracy in simulating the AGB data (average NSE = 0.59, NRMSE = 22.2%) compared to WOFOST (average NSE = -0.09, NRMSE = 34.4%). The new version of the model led to a higher correlation between measured and simulated values for the calibration datasets (average R2 = 0.94 versus 0.83 achieved by WOFOST). WOFOST-GTC performed slightly worse in the evaluation datasets. The model confirmed its higher accuracy (NRMSE = 22.6%) compared to the original WOFOST (NRMSE = 27.3%), although the two models achieved similar values for the other agreement metrics. Both models failed to properly reproduce the AGB dynamic in dataset 7 (Legnaro, 2008/09, cultivar PR45D01), which was characterized by a cold spring that resulted in low growth rates. This outcome supports the need to further investigate the temperature-dependent growth dynamics – especially after the winter dormancy – to improve the model representation. The lower number of parameters of WOFOST-GTC compared to WOFOST and its higher accuracy led to a value of Akaike Information Criterion

(Akaike, 1974) that was decidedly better than the one achieved by WOFOST (210.97 versus 596.24), which highlights an improved trade-off between model performance and complexity.

Table 1. Performances of WOFOST (W) and WOFOST_GTC (GTC) for reproducing the aboveground biomass in calibration and evaluation. NRMSE: normalized root mean square error (optimum and minimum = 0; maximum = +100%); NSE: modelling efficiency (optimum and maximum = 1; minimum = -∞); R^2: coefficient of determination. a: this study; b: Gabrielle et al. 1998; c: Rossato, 2012; d: Prando, 2011.

ID	Site	Cultivar	Cropping season	Source	NRMSE		NSE		R^2	
					W	GTC	W	GTC	W	GTC
					Calibration					
1	Buscate	Excalibur	2012/13	a	47.6	35.4	0.89	0.20	0.94	0.88
2	Chalons	Goéaland	1994/95	b	11.6	13.1	-0.56	0.86	0.79	0.95
3	Legnaro	Catalina	2011/12	c	52.1	28.9	-0.78	0.45	0.86	0.99
4	Legnaro	Excalibur	2008/09	d	26.3	11.5	0.1	0.85	0.72	0.93
Average					*34.4*	*22.2*	*-0.09*	*0.59*	*0.83*	*0.94*
					Evaluation					
5	Casorezzo	Excalibur	2012/13	a	27.9	17.4	0.39	0.24	0.99	0.96
6	Legnaro	Viking	2008/09	d	19.1	23.3	0.53	0.27	0.75	0.75
7	Legnaro	PR45D01	2008/09	d	34.8	27.2	-0.44	-0.08	0.86	0.88
Average					*27.3*	*22.6*	*0.16*	*0.14*	*0.87*	*0.86*

The comparison between simulated and observed yields (Table 2) resulted in minor differences, with absolute deviations ranging from 0.09 to 0.65 t ha-1 (NRMSE = 0.18). WOFOST_GTC succeeded in reproducing the inter-annual variability of measured yields as confirmed by the values of the agreement metrics (NSE = 0.58 and R2 = 0.75, $p < 0.01$). This lays the basis for an accurate prediction of seed oil content and fatty acids fractions, which are respectively expressed as percentage of grain dry matter and of the total seed oil concentration.

Table 2. Comparison between observed and simulated yield

Site	Cultivar	Cropping season	Observed yield [t ha^{-1}]	Simulated yield [t ha^{-1}]
Buscate	Excalibur	2012/2013	3.36	3.56
Chalons	Goéaland	1994/1995	4.87	5.54
Legnaro	Catalina	2011/2012	3.85	3.38
Legnaro	Excalibur	2008/2009	3.64	3.46
Legnaro	Viking	2008/2009	3.34	3.46
Legnaro	PR45D01	2008/2009	3.37	3.46
Changins	Splendor	2004/2005	2.77*	3.42
Changins	Splendor	2005/2006	3.02*	3.13
NRMSE		NSE		R^2
0.18		0.58		0.75 ($p < 0.01$)

*mean yield in different experiments carried out in the same cropping season, with fixed sowing date.

2.4.1.2 Simulation of rapeseed quality

The comparison between measured and simulated rapeseed oil quality variables (i.e., seed oil content and oleic, linoleic and α-linolenic acid fractions) is presented as scatterplots in Figure 4. WOFOST-GTC succeeded in reproducing both the seed oil content and composition, with better results achieved in the calibration (average NRMSE = 4.16%, NSE = 0.87 and R2 = 0.94) than in the evaluation datasets (average NRMSE = 6.5%, NSE = 0.83 and R2 = 0.85). The simulation of the total seed oil content denoted a slight overestimation when the measured content was low (below 44%). The best performances were achieved for the oleic (average NRMSE = 2.62%, NSE = 0.95 and R2 = 0.96) and α-linolenic (average NRMSE = 8.15%, NSE = 0.95 and R2 = 0.96) acid contents. This result proved the ability of WOFOST-GTC for modulating the response according to the weather conditions experienced by the crop during the ripening phase. The lower accuracy for reproducing the fraction of linoleic acid content (average NRMSE = 7.12%, NSE = 0.86 and R2 = 0.88) could partly be due to the lower desaturation in high-oleic low-linolenic varieties (i.e., Splendor), which are known to be less sensitive to temperature in the critical period (Baux et al., 2013).

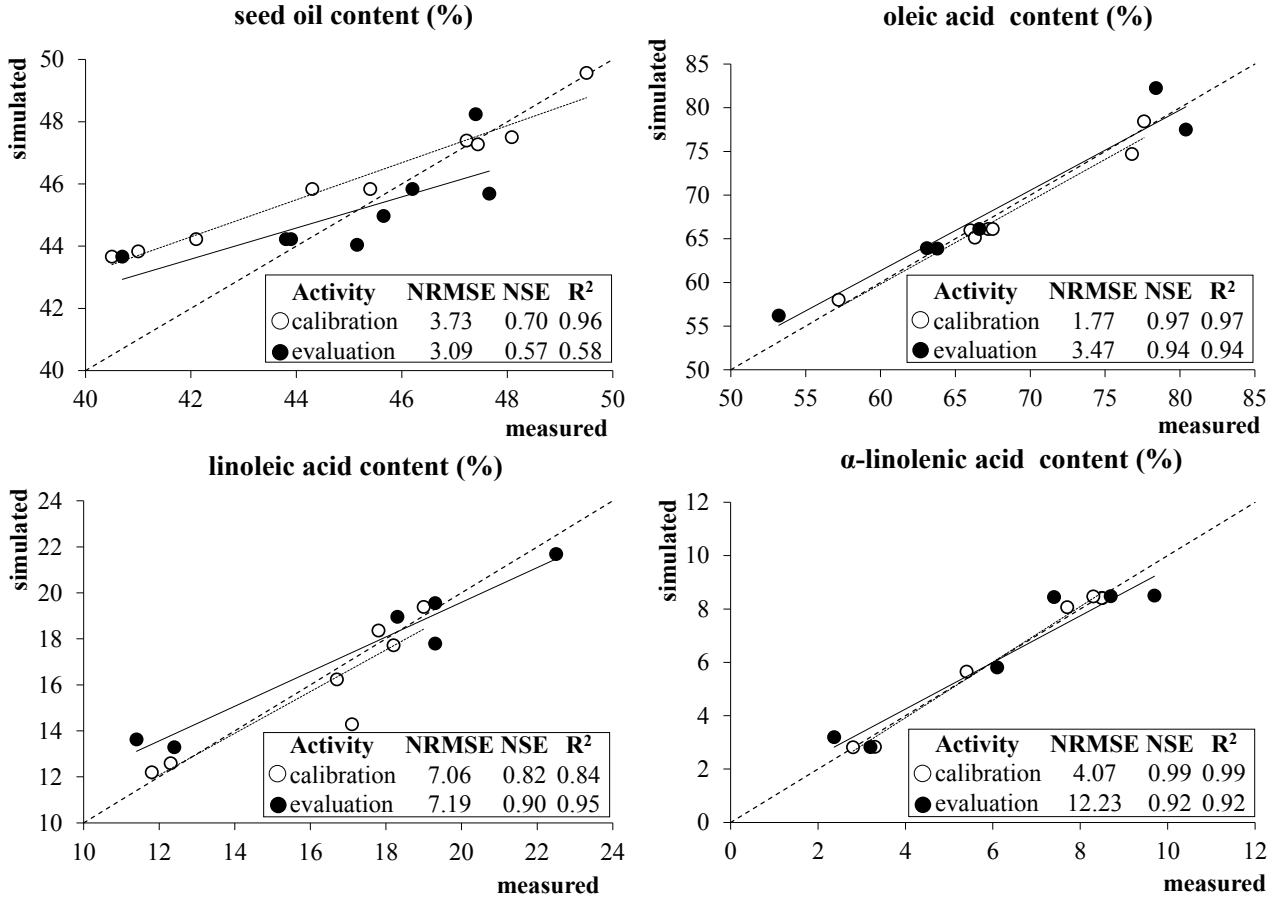

Figure 4. Comparison between measured and simulated seed oil content (% of grain dry matter) and oleic (% of total seed oil content), linoleic (% of total seed oil content), and α-linolenic (% of total seed oil

content) acid fractions. Dotted and solid lines refer to calibration and evaluation, respectively. Dashed lines indicate perfect agreement between measured and simulated values (1:1).

2.5 Conclusion

The development of the WOFOST-GTC model aimed to improve the accuracy to simulate the unique characteristics of rapeseed while reducing the model complexity compared to the original version of WOFOST. The new dynamic representation of the vertical distribution of photosynthetic tissues during the phenological development increases the coherence with the underlying system and allowed improving the simulation of biomass accumulation. The significant reduction of the number of parameters enhances the model usability, whereas the inclusion of approaches to estimate the oil quality favours the application of WOFOST-GTC to support the optimization of crop system performances under different agro-climatic scenarios. Nevertheless, approaches for the important processes that affect rapeseed growth dynamics, such as frost damage to vegetative tissues during winter, still have to be developed and included in the model to further improve its ability to simulate the spatial and temporal variability of crop production. WOFOST-GTC enlarges the family of WOFOST-GT models by providing approaches for the cultivation of rapeseed in addition to those already available for cereals (Stella et al., 2014). WOFOST-GT models are available – in a complete software development kit that includes the documentation of codes and algorithms as well as a number of sample applications – in the software library CropML (http://www.cassandralab.com/components/1).

Acknowledgements

This study received financial support from the EC Seven Framework Programme (KBBE.2013.1.4-09) under Grant Agreement No. 613817.2013-2016 (MODEXTREME).

2.6 Appendices

Appendix A. Information related to the datasets used to calibrate and evaluate the model performances: site (latitude and longitude), cultivar, flowering date, activity (C=calibration, V=validation), available variables (acronyms are reported below the table and in the literature reference).

Site	Year	Cultivar	Flowering date	Activity	Available variables	Reference
Italy: [*] latitude 45° 32' N, longitude 8° 48' E; [§] latitude 45° 31' N, longitude 8° 45' E						
Buscate[*]	2012/2013	Excalibur	26/04	C	Oil, OAC, LAC, αLAC	-
Casorezzo[§]	2012/2013	Excalibur	02/05	V	Oil, OAC, LAC, αLAC	-
Switzerland: latitude 46° 24' N, longitude N, 6° 14' E						
Changins	2004/2005	Splendor	30/04	C	Oil, OAC, LAC, αLAC	1
			28/04	C	Oil, OAC, LAC, αLAC	1
			30/04	V	Oil	1
	2005/2006	Splendor	27/04	C	Oil	1
			04/05	V	Oil, OAC, LAC, αLAC	1
			27/04	C	Oil	1
			04/05	V	Oil	1
			04/05	C	Oil	1
			27/04	V	Oil, OAC, LAC, αLAC	1
Poland: latitude 52° 26' N, longitude 16° 54' E						
Poznan	1993/1994	PN 3756/93	01/05	C	Oil, OAC, LAC, αLAC	2
	1995/1996		28/04	V	Oil, OAC, LAC, αLAC	2
	1996/1997		20/4	C	OAC, LAC, αLAC	2
	1997/1998		12/4	C	Oil, OAC, LAC, αLAC	2
	1998/1999		26/4	C	Oil, OAC, LAC, αLAC	2
	1999/2000		01/05	V	Oil, OAC, LAC, αLAC	2
	2000/2001		01/05	V	Oil, OAC, LAC, αLAC	2

Oil (%): oil content, as % of the seed dry matter; OAC (%): oleic acid content, as % of the total oil content; LAC (%): linoleic acid content, as % of the total oil content; αLAC (%), α-linolenic acid content, as % of the total oil content. 1: Baux, A., Colbach, N., Pellet, D., 2011. Crop management for optimal low-linolenic rapeseed oil production - Field experiments and modelling. Europ. J. Agronomy 35, 144-153; 2: Spasibionek, S., 2006. New mutants of winter rapeseed (*Brassica napus* L.) with changed fatty acid composition. Plant Breeding 125, 259-267.

Appendix B. Functions implemented in WOFOST-GTC to substitute the related AFGEN tables.

Process	AFGEN table [X units, Y units]	WOFOST-GTC function
Development	DTSM [°C, °C-day]	$\left[(T-T_b)/(T_0-T_b)\cdot\left[(T_c-T)/(T_c-T_0)\right]^{\frac{T_c-T_o}{T_o-T_b}}\right]^{1.2}$ *if* $T_b<T<T_c$; 0 *elsewhere*
Photosynthesis	EFF [°C, kg ha^{-1} h^{-1} J^{-1} m^2 s]	0.5
	KDIF [-, -]	0.54
	TMNF [°C, -]	0 *if* $T_{\min}<0$; $0.\overline{33}\cdot T_{\min}$ *if* $0\le T_{\min}<3$; 1 *if* $T_{\min}\ge 3$
	TMPF [°C, -]	$(T-T_b)/(T_0-T_b)\cdot\left[(T_c-T)/(T_c-T_0)\right]^{\frac{T_c-T_o}{T_o-T_b}}$ *if* $T_b<T<T_c$; 0 *elsewhere*
	AMAX [-, kg ha^{-1} h^{-1}]	$AMAX_{ini}$ *if* $DVS<1.2$; $m\cdot DVS+q$ *where* $m=-AMAX_{ini}/0.8$; $q=-m\cdot 2$ *elsewhere*
Respiration	RFSE [-, -]	1
Biomass partitioning	FR [-, kg kg^{-1}]	0.2 *if* $DVS\le 0.3$; $-0.2857\cdot DVS+0.2857$ *if* $0.3<DVS\le 1$; 0 *elsewhere*
	FO [-, kg kg^{-1}]	$\dfrac{FO_{mat}}{\left(1+0.7^{\frac{-20\cdot DVS-28}{1.45}}\right)}$
	FL [-, kg kg^{-1}]	FL_{em} *if* $DVS\le 0.2$; $DVS^2\cdot FL_{em}-(2.4\cdot DVS\cdot FL_{em})+1.44\cdot FL_{em}$ *if* $0.2<DVS<1.2$; 0 *elsewhere*
	SLA [-, ha kg^{-1}]	$SLA=DVS\cdot m+SLA_{em}$; $m=-0.1667\cdot SLA_{em}+0.0002167$
Senescence	RDRS [-, kg kg^{-1} day^{-1}]	0 *if* $DVS\le 1$; $0.025\cdot DVS-0.005$ *if* $1<DVS<1.4$; $0.0167\cdot DVS+0.0067$ *elsewhere*
	RDRR [-, kg kg^{-1} day^{-1}]	0 *if* $DVS\le 1.5$; 0.02 *elsewhere*

T: average daily temperature; DVS: development stage code; DTSM: daily increase in temperature sum. Cardinal temperatures for development: T_b = base, T_o = optimum, T_c = critical; EFF: light use efficiency of a single leaf; KDIF: extinction coefficient for diffuse visible light; TMNF: reduction factor of gross assimilation rate as function of the minimum temperature (Tmin); TMPF: reduction factor of AMAX as function of the average temperature. Cardinal temperatures for growth: T_b = base, T_o = optimum, T_c = critical; AMAX: maximum leaf CO_2 assimilation rate. $AMAX_{ini}$ = AMAX before flowering; RFSE: reduction factor of respiration for senescence; FR: fraction of the total dry matter increase to roots; FO: fraction of the aboveground dry matter increase to the storage organs; FO_{mat} = partitioning to storage organs at maturity; FL: fraction of aboveground dry matter increase to leaves; FL_{em} = partitioning to leaves at emergence; SLA: specific leaf area; SLA_{em} = SLA at emergence; RDRS: relative death rate of stems; RDRR: relative death rate of roots.

Appendix C. Equations implemented in WOFOST-GTC to simulate the oil content and composition.

Process	Equations
Oil accumulation [%]	$\left(\frac{Oil_{\max}}{1+\exp\left(-0.01603\cdot GDD_{flo}+\left(\frac{0.75\cdot GDD_{mat}}{100}\right)\right)}\right)\cdot MIN\left(RainF, TavgF\right)$ $RainF = 0.6\ if\ rain \le 12.5;\ 0.0027\cdot rain + 0.4667\ if\ < 12.5 < rain < 200;\ 1\ if\ rain \ge 200$ $TavgF = 1\ if\ Tavg \le 10.5;\ -0.0276\cdot Tavg + 1.2897\ if\ 10.5 < Tavg \le 25;\ 0.6\ if\ Tavg > 25$
Oleic acid content [%]	$\left[-0.0007\cdot\left(\sum_{DAF_{ini}}^{DAF_{end}} T_{\min}\right)^2 + 0.4271\cdot\left(\sum_{DAF_{ini}}^{DAF_{end}} T_{\min}\right) + 1.8971\right]\cdot d$; $d = 0.0151\cdot OAC_{\max} - 0.0104$
Linoleic acid content [%]	$\left[-0.047\cdot\left(\sum_{DAF_{ini}}^{DAF_{end}} T_{\min}\right) + 13.8542\right]\cdot a$; $a = 0.0835\cdot LAC_{\max} - 0.0003$
α-linolenic acid content [%]	$\alpha LAC_{\min} + 150\cdot\exp\left(-b\cdot GDD_{flo}\right)$; $b = c\cdot\ln\left(GDD_{th}\right) - d$; $c, d = f\left(\alpha LAC_{\max}\right)$

Oil_{max} = maximum oil content (%); GDD_{flo} = GDD from the onset of flowering (°C day^{-1}); GDD_{mat} = GDD to reach maturity (°C day^{-1}); rain = cumulated rainfall (mm) and T_{avg} = average air temperature (°C) from flowering; DAF_{ini}, DAF_{end} = number of days defining the start and end of the crop sensitivity period after flowering; T_{min} = minimum air temperature (°C); OAC_{max} = maximum oleic acid content (%); LAC_{max} = maximum linoleic acid content (%); αLAC_{min}, αLAC_{max} = minimum and maximum of the α-linolenic acid content (%); GDD_{th} = GDD threshold to trigger the decline in the relative content of α-linolenic acid.

Appendix D. Parameters values after calibration to simulate winter rapeseed production and oil quality.

Process	Parameter	Value
DTSM: daily increase in temperature sum as function of average temperature	T_o	23 [°C]
	T_b	3 [°C]
	T_c	30 [°C]
TMPF: reduction factor of AMAX as function of average temperature	T_o	20 [°C]
	T_b	3 [°C]
	T_c	35 [°C]
AMAX: maximum leaf CO_2 assimilation as function of development stage code (DVS)	$AMAX_{ini}$	41 [kg ha^{-1} d^{-1}]
FO: fraction of above ground dry matter to storage organ as function of development stage code (DVS)	FO_{mat}	0.6 [kg kg^{-1}]
FL: fraction of above ground dry matter to leaves as function of development stage code (DVS)	Fl_{em}	0.65 [kg kg^{-1}]
SLA: specific leaf area as function of development stage code (DVS)	SLA_{em}	18 [m^2 kg^{-1}]
Oil accumulation [%]	Oil_{max}	50[%]
	GDD_{mat}	1200 [°C d^{-1}]
Oleic acid content [%]	DAF_{ini}	18 [d]
	DAF_{end}	54 [d]
	AOC_{max}*	66.1 (P, E); 85.2 (S) [%]
Linoleic acid content [%]	DAF_{ini}	54 [d]
	DAF_{end}	65 [d]
	LAC_{max}	26 [%]
α-linolenic acid content [%]	αLAC_{min}*	7.7 (P); 5.0 (E), 2.4 (S) [%]
	GDD_{th}	568 [°C d^{-1}]
	αLAC_{max}	11.3 (P); 7.7 (E), 8.2 (S) [%]

*: variety-specific parameters values. P=PN 3756/93; E=Excalibur; S=Splendor

Chapter 3

SENSITIVITY OF WOFOST-BASED MODELLING SOLUTIONS TO CROP PARAMETERS UNDER CLIMATE CHANGE

Carlo Gilardelli, Roberto Confalonieri, Giovanni Alessandro Cappelli, Gianni Bellocchi

Published in: Ecological Modelling (2018) 368, pp. 1-14.

3.1 Abstract

The formalization of novel equations explicitly modelling the impact of extreme weather events into the crop model WOFOST (EMS: existing modelling solution; MMS: modified modelling solution) is proposed as a way to reduce the uncertainty in estimations of crop yield. A sensitivity analysis (SA) was performed to assess the effect of changing parameters values on the yield simulated by the model (both EMS and MMS) for different crops (winter and durum wheat, winter barley, maize, sunflower) grown under a variety of conditions (including future climate realisations) in Europe. A two-step SA was performed using global techniques: the Morris screening method for qualitative ranking of parameters was first used, followed by the eFAST variance-based method, which attributes portions of variance in the model output to each parameter.

The results showed that the parameters related to the partitioning of assimilates to storage organs (FOTB) and to the conversion efficiency of photosynthates into storage organs (CVO) generally affected considerably the simulated yield (also underlying tight correlation with this output), whereas the parameters involved with respiration rate (Q10) or specific leaf area (SLA) became influential in case of unfavourable weather conditions. Major differences between EMS and MMS (which includes a component simulating the impact of extreme weather events) emerged in extreme cases of crop failure triggered by markedly negative minimum temperatures. With few exceptions, the two SA methods revealed the same parameter ranking. We argue that the SA performed in this study can be useful in the design of crop modelling studies and in the implementation of crop yield forecasting systems in Europe.

Keywords

Climate scenarios; Crop parameters; Crop yield; e-FAST method; Extreme weather events; Morris' method; Sensitivity analysis; WOFOST.

3.2 Introduction

Crop models mathematically represent the complex interactions between plant, weather, soil and agricultural practices. They play an important role in understanding and quantifying the relationships, or trade-offs, between crop management and environment on one side, and cropping systems productivity on the other. Crop models have evolved over time, increasing in complexity to meet the increasingly intricate challenges facing agriculture (e.g. Donatelli and Confalonieri, 2011). For instance, the global carbon balance has become an issue of great societal concern in the last decades, when the global emission of CO2 has continued to increase together with its impact on climate (IPCC, 2013). This has required modelling efforts, for instance, to represent plant responses to CO2 levels (e.g. Ethier and Livingston, 2004) and thus make crop models responsive to changing climate conditions (Asseng et al., 2013; Bassu et al., 2014; Li et al., 2014). Nowadays, crop models are largely used to understand and anticipate the impacts of climate change on agricultural production (e.g. Ewert et al., 2005; Falloon and Beets, 2010; White et al., 2011; Supit et al., 2012; Nelson et al., 2014), to support the implementation of adaptation strategies (e.g. Tingem et al., 2009; Fernandes et al., 2012; Perego et al., 2014; Cappelli et al., 2015), and to design future crop ideotypes (e.g. Paleari et al., 2017).

However, robust simulation models are needed for diagnosing and prognosing the impacts of environmental factors on the crop production systems and, as a matter of fact, some modelling studies have not been completely successful in addressing the impact of extreme weather events on crop production (van der Velde et al., 2012; Zinyengere et al., 2014). Extreme events such as heat waves, cold shocks, droughts and frost affect directly and indirectly cropping systems by altering physiology and behaviour of plants, with impacts on the productivity as well as the seasonality and quality of crop production (e.g. Lesk et al., 2016). Moreover, the additional heat that is generated from ongoing temperature rise has increased the chances for severe heat waves, drought, and other forms of extreme weather (Field et al., 2012). Suggestions have been put forward that most of the existing crop models need an overhaul or an update as they often fail to correctly describe how crops respond to the impact brought about by extreme weather events (Rötter et al., 2011).

Formalizing the biophysical interactions between the crop and its environment has required the development of customized modelling solutions (Luo et al., 2013) characterized by a large set of interdependent equations representing specific sub-domains of the system. Accounting for such complex interactions has inevitably increased the number of input factors in crop models

(variables and parameters) and the uncertainties associated with parameter values and their distributional assumptions, driving variables (climate, soil and management) and model structure (e.g. Gabrielle et al., 2006). The structure of crop models is generally too complex to easily shed light on the relationship between input factors and output variables, even more so the models are continuously improved with novel approaches. Parameter estimation, in particular, is a key challenge in model development, in light of the crucial role in determining the quality of model predictions (Richter and Sondgerath, 1990). There is therefore a need to better understand the behaviour of crop models under a wide range of conditions, also by identifying the parameters that have the greatest influence on outputs (Jacquez and Perry, 1990; Brun et al., 2001; Haag, 2006).

Sensitivity analysis (SA) is the main tool for a comprehensive evaluation of complex models (e.g. Rabitz, 1989; Omlin et al., 2001). It assesses the changes in the model outputs due to changes in the values of input factors (the latter being generated by sampling from inputs' distributional range). As a result, SA provides a valuable method to identify properties that characterize the relationships between model outputs and input parameters and enhance the understanding of the system under study (Saltelli et al., 2000). The distinction – under specific conditions of application (Stearns, 1992) – between influential (relevant) and non-influential parameters is generally based on SA results (Cariboni et al., 2007; Confalonieri et al., 2009a). By ranking model parameters based on their relevance from the most to the least important (Cryer and Havens, 1999), SA offers guidance to the design of experimental programs as well as to more efficient model development and calibration. SA can be implemented either locally to examine the effect of minor variations of the parameter values on model results (Brun et al., 2001), or globally to consider the entire range of parameter values (Xu and Gertner, 2007; Confalonieri et al., 2010a). The latter is generally based on differential analysis through the use of Taylor series (e.g. Pastres and Ciavatta, 2005) and Monte Carlo methods (e.g. Annan, 2001). In particular, there is a challenge in ensuring robust modelling approaches under changing climate conditions, because the implicit assumption that well-designed and calibrated models under current conditions will remain valid under future climate realizations can be an unrealistic one. This is why the importance of improving the understanding of plant responses to the interactive effects of higher temperature and altered patterns of precipitation has been highlighted (e.g. Wang et al., 2012).

This study focused on the generic crop simulator WOFOST (van Diepen et al., 1989), successfully used since years to reproduce growth and development of a variety of crops (de Wit et al., 2012;

Boogaard et al., 2013), to forecast crop yields (https://ec.europa.eu/jrc/en/mars), and within model intercomparison and ensemble studies (e.g. Todorovic et al., 2008; Palosuo et al., 2011; Bassu et al., 2014). In this study, we have performed a wide range of SA experiments on WOFOST using two versions of the model: an implementation referred to as existing modelling solution (EMS) and an improved model referred to as the modified modelling solution (MMS), with the latter including a software component (coupled to EMS) that explicitly takes into consideration the impacts of extreme weather events such as high and low temperatures, water deficit and frost (Villalobos et al., 2015). For both modelling solutions, SA was performed for five crops at eight sites representative of contrasting conditions in Europe (Italy, Spain, Switzerland and Ukraine) using two SA methods, and under current and altered weather conditions.

3.3 Materials and methods

3.3.1 WOFOST-based modelling solutions

WOFOST (van Diepen et al., 1989) adopts a gross photosynthesis approach to calculate net carbon fixation, explicitly considering phenological development, light interception, gross CO2 assimilation, transpiration, growth and maintenance respiration. Crop development is reproduced as a temperature-driven process, optionally accounting for photoperiod. Instantaneous gross CO2 assimilation (estimated at three moments in the day for three depths into the canopy of plant leaves) is computed on the basis of intercepted solar radiation and of a photosynthesis-light response at leaf level. Light interception depends on total incoming radiation, as modulated by photosynthetic leaf area and leaf angle distribution. Assimilates are partitioned to the various organs according to partitioning factors, computed as a function of plant development stage: a fraction of assimilates is allocated to roots first, and then the remainder is split over the above-ground organs (including below ground storage organs such as tubers). The emission of LAI units is driven by temperature in the early stages and it depends on specific leaf area and leaf-partitioned biomass later. Dead LAI units (i.e. leaves no more photosynthetically active) are quantified as a function of self-shading and senescence of old leaves. The model simulates both potential and water-limited production levels, providing information on crop water use, biomass growth and yield. Potential evapotranspiration is calculated via the Penman equation (Frere and Popov, 1979), and water stress is represented by the ratio of actual to potential transpiration. Crop water use is calculated separately for: crop canopy (transpiration), bare soil surface (soil evaporation), and soil surface with ponding (water evaporation).

The capability of the standard WOFOST version (EMS) was enhanced (MMS) thanks to a dedicated component for the impact of extreme weather events (Villalobos et al., 2015; Movedi et al., 2016). In particular, the effects of severe cold and high temperatures, frost and extreme water deficit on crop yields were accounted for by modulating the harvest index (HI) and LAI (only for frost) according to stress-related response functions (0 = maximum reduction; 1 = no effect) computed at a daily time step. These variations are mediated by the time of occurrence of an extreme event, the environmental conditions, and the crop-specific susceptibility. The decline of crop yield can even lead to crop failure in the case of severe extreme weather conditions. Two development phases are identified where crops are most sensitive to weather extremes: (i) around anthesis (+/- 1 week from anthesis) with main effects on pollen viability, fertilization, and grain formation, and (ii) from anthesis to physiological maturity, with impacts related to rates of grain filling. For temperature-related damages, crop temperature is estimated (solving the surface energy balance equation) and used. The algorithms used to quantify the impact of weather extremes are fully documented in Appendix A.

3.3.2 Sensitivity analysis methods

The Morris screening method (Morris, 1991) as modified by Campolongo et al. (2007) was first applied to rank model parameters according to their influence on crop yield. Then, the extended version (eFAST, Saltelli et al., 1999) of the Fourier Amplitude Sensitivity Test method (FAST, Cukier et al., 1973) was applied to quantify the portion of the output variation due to changes in each parameter.

For the Morris method, the number of model runs for each SA experiment is equal to the number of trajectories (r) multiplied by (n+1), with n being the number of parameters analysed. According to Confalonieri et al. (2010a), r was set equal to 5. The number of model runs (C) needed to complete a numerical experiment of SA with the eFAST method is equal to $C = n\ N_s$ with n being the number of parameters and N_s being the sample size. We obtained the convergence of sensitivity indices with $N_s = 330$, which is above the minimum value of 128 indicated by Wang et al. (2013), and represents a balanced solution between computational cost and the ability to explore the full parameter space.

The parameters related to light interception, gross photosynthesis, respiration, partitioning of photosynthates, leaf area expansion and senescence were subject to SA. Phenology-related parameters were not considered since they are limited in number and they are all potentially subject to local calibration (Confalonieri et al., 2010a). In WOFOST, a high number of parameters

are organized in AFGEN (Arbitrary Function GENerator) tables, which describe the linear dependence of parameters (dependent variables) on average air temperature (Tavg) or development stage (DVS) (independent variables). The number of pairs (DVS, parameter value; Tavg, value), which constitute AFGEN tables, was reduced in order to avoid parameter distributions' overlap during samples generation (Confalonieri, 2010). Considering the relatively small number of parameters investigated (at most 31), all of them were analysed using both Morris and the eFAST methods. This allowed us to fully compare the results obtained with both SA methods.

3.3.3 Sensitivity analysis experiments

SA experiments were performed on five crops, i.e. winter wheat (Triticum aestivum L), durum wheat (Triticum durum Desf.), winter barley (Hordeum vulgare L), maize (Zea mays L.) and sunflower (Helianthus annuus L.), grown in eight experimental sites located in four European countries (Table 1). Parameters' description, distribution and related sources of information are presented in Appendices B, C and D.

Water-limited crop production was simulated, assuming unlimited nutrient supply and crops free from pests, diseases and weeds. Sowing and harvest dates were derived from local conventional farming practices.

Table 1. Location of the sites (with the relative crops) where sensitivity analysis was performed.

Country	Site	Latitude N (°)	Longitude E (°)	Elevation (m a.s.l.)	Crops
Spain	Cordoba	37.85	-4.80	100	Winter wheat, sunflower
	Granada	37.15	-3.00	650	Winter barley
Italy	Foggia	41.45	15.50	89	Durum wheat
Switzerland	Changins	46.40	6.23	455	Winter wheat; maize
	Ellighausen	47.60	9.13	508	Winter wheat; maize
	Reckenholz	47.43	8.52	444	Winter wheat; maize
	Therwil	47.50	7.54	316	Winter wheat; maize
Ukraine	Mironivka	49.66	31.00	155	Winter wheat; maize

Daily downscaled weather data (0.25° spatial resolution) for current climate conditions and future climate projections were used. Synthetic weather series were generated using two climate models

– ICHEC-EC-EARTH KNMI-RACMO22E (van Meijgaard et a., 2008) and CNRM-CERFACS-CNRM-CM5 SMHI-RCA4 (Voldoire et al., 2013) – for the emission pathway scenario RCP8.5 (radiative forcing up to 8.5 W m-2 in 2100), which is the most extreme among those provided by the IPCC's Fifth Assessment Report (Moss et al., 2010; van Vuuren et al., 2011). Time slices of near past (1981-2010, with the exception of Spain, 1987-1999 and Switzerland, 1981-2014) and medium future (2041-2060) were considered. Fox Maule and Christensen (2015) describe the methods used in processing and post-processing the GCM/RCM outputs used in the generation of weather scenarios. The above methodology produced bias-corrected daily series of surface air temperature (minimum and maximum) and rainfall (different lengths of near-past time slices correspond to the varying observational data series used for bias-correction in different countries). Other variables needed to run the modelling solutions, such as global solar radiation, relative humidity and wind speed, were derived according to Duveiller et al. (2017). The beneficial effect of increasing CO2 concentration on carbon assimilation rates was not considered in this study. The main reason for this choice is that the study was performed within a project (EU-FP7 MODEXTREME; http://modextreme.org) that targeted the WOFOST-based platform adopted by the European Commission to perform yield forecasts, which in its current version does not consider the effects of increasing atmospheric CO2 concentration on crop productivity. Moreover, the effect of increasing CO2 concentration on carbon assimilation rates in the presence of more frequent and intense extreme weather events is still controversial. This was highlighted by Long et al. (2006) and has been confirmed by two recent studies (Obermeier et al., 2016; Novak, 2017) demonstrating that CO2 fertilization effects decline or even disappear as weather becomes drier and warmer.

For each combination crop × site, nine contrasting years were considered, three of them belonging to historical series and six belonging to projected weather series centred on 2050 at all sites. The nine years were selected to be sufficiently contrasting in terms of coldest-wettest, warmest-driest and average conditions, as represented by yearly-based agro-climatic indicators (Peterson et al., 2001; Barnett et al., 2006).

The range of climatic conditions represented by each scenario and time slice is shown in Fig. 1 by means of indicators of aridity and heat wave frequency. The possibility to discriminate between thermo-pluviometric conditions associated with aridity (b, De Martonne, 1942) gradients in the eight sites is given by the range published by Diodato and Ceccarelli (2004): $b<5$: extreme aridity; $5\leq b<14$: aridity; $15\leq b<19$: semi-aridity; $20\leq b<29$: sub-humidity; $30\leq b<59$: humidity; $b>59$: strong

humidity. For identifying the frequency of heat wave (hw) days within a year in each site, we summarized the number of consecutive days (at least seven) when the maximum air temperature was higher than the average summer (June, July and August) maximum air temperature of all the available years (baseline) +3 °C (Confalonieri et al., 2010b after Barnett et al., 2006). The range limits in this study were given by the minimum and the maximum numbers of the hw days of all sites and conditions (after Sándor et al., 2016): hw≤14: extremely moderate frequency; 14<hw≤28: very moderate frequency; 28<hw≤42: moderate frequency; 42<hw≤56: high frequency; 56<hw≤70: very high frequency; hw>70: extremely high frequency.

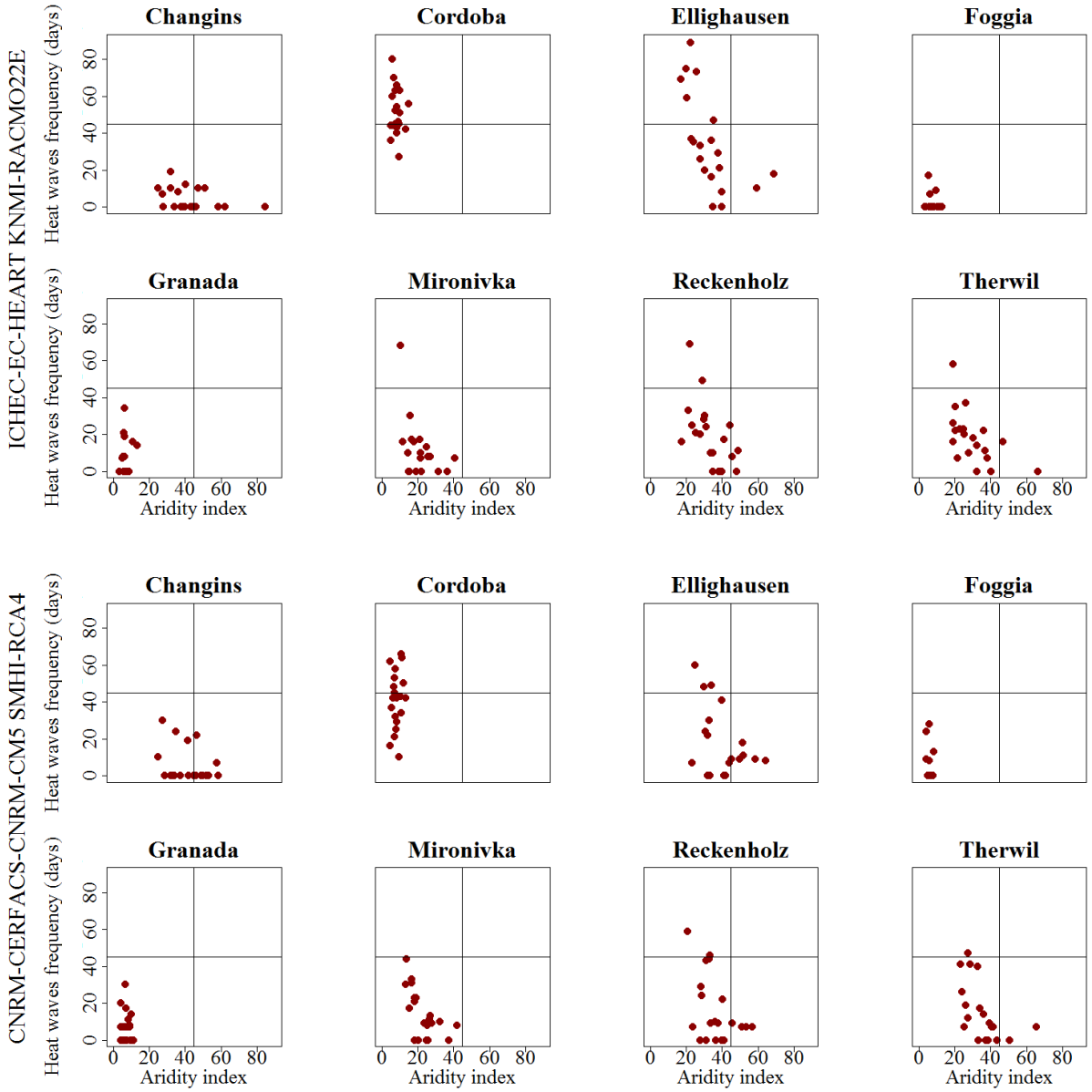

Figure 1. De Martonne-Gottmann aridity index and heat wave days frequency calculated for each year of four weather scenarios and two periods, in a reference pixel for each study site.

3.4 Result and discussion

3.4.1 Sensitivity analysis results (eFAST method)

Figure 2 shows the crop-specific variations of total sensitivity indices achieved by the top 10 ranked parameters across sites, years and modelling solutions considered.

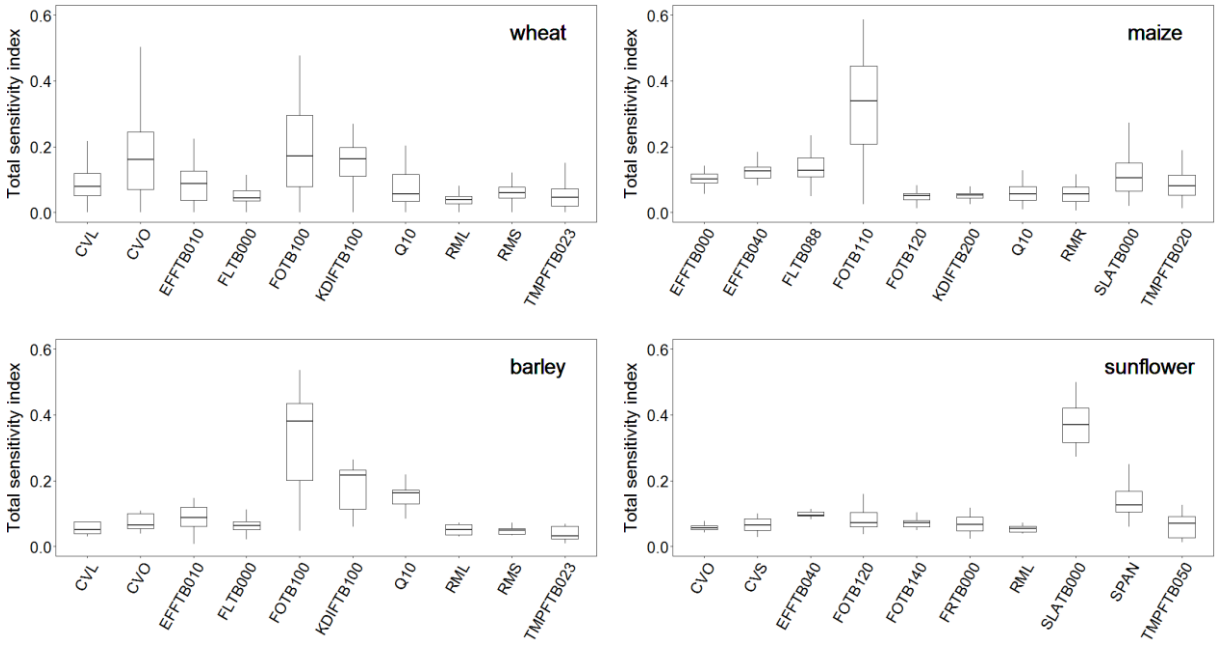

Figure 2. Distributions of total sensitivity indices for each simulated crop. Results from durum and winter wheat simulations were processed together since the same parameterization was operatively used within the simulation experiment.

The parameter involved with partitioning to storage organs (FOTB100 for wheat and barley and FOTB110 for maize) remerged as the most influential in yield simulations and the most sensitive to variations in the conditions explored (0.06<Total sensitivity index<0.59, median=0.27). Conversely, the simulations of sunflower yield revealed the predominance of leaf dynamics- (SLATB000 and SPAN) versus photosynthesis- related parameters; the narrow range of variation of the total sensitivity index for both parameters denoted the primary role of temperature in limiting the leaf biomass conversion into leaf area at early crop stages regardless the site and year considered.

Focusing on winter wheat simulations in the Swiss sites, several influential parameters were identified. Parameters related with life span at 35 °C (SPAN), partitioning to storage organs at flowering (FOTB100), conversion efficiency into storage organs (CVO), extinction coefficient for diffuse light at flowering (KDIFTB100) and conversion efficiency into leaves (CVL) are distinctly identifiable by high values of the eFAST total sensitivity index (Fig. 3 and supplementary material from Fig. S1 to Fig. S3).

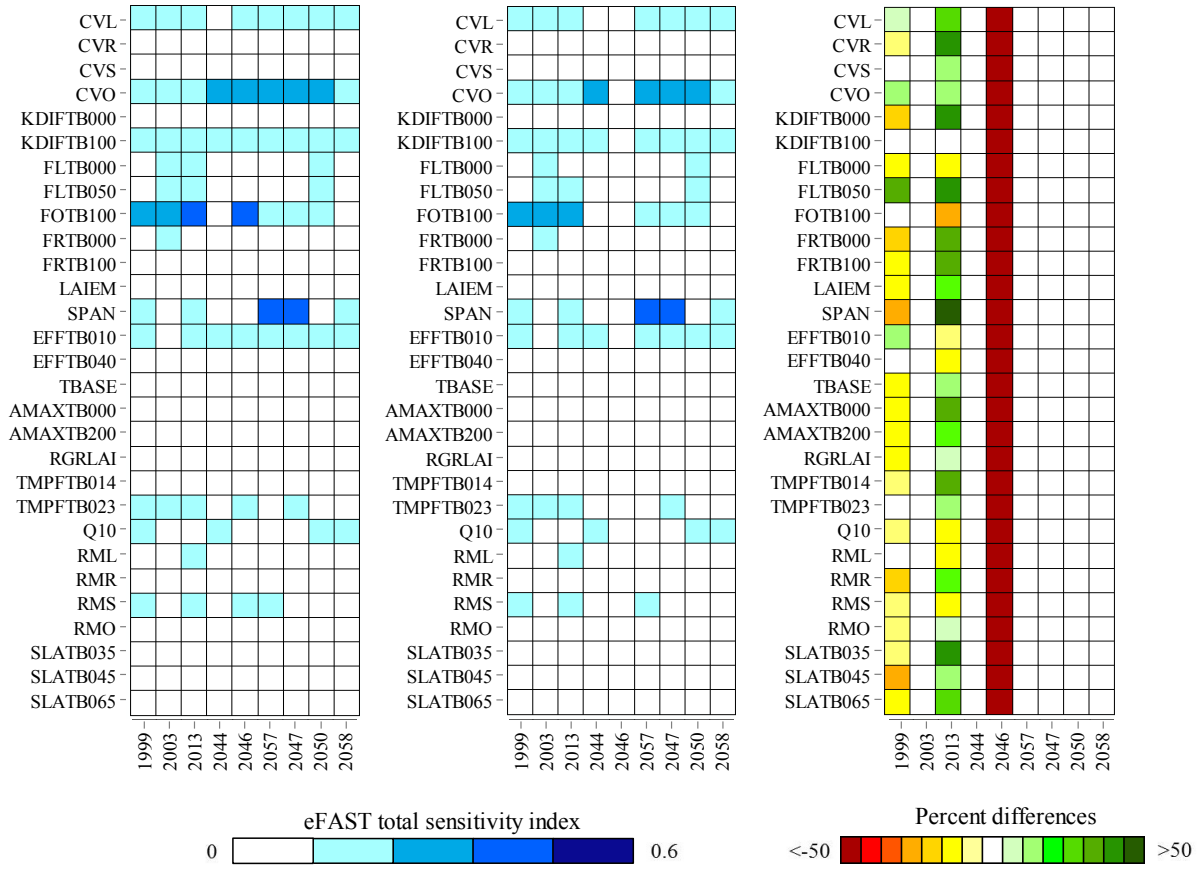

Figure 3. eFAST total sensitivity index for winter wheat yield simulated with WOFOST at selected years in Switzerland (Changins site). Left panel = EMS (existing modelling solution); central panel = MMS (modified modelling solution); right panel = percent differences between the two modelling solutions.

Certain balance in parameters ranking (i.e. the model is sensitive to several parameters) can be explained by the restrained meteorological variability which characterizes all the Swiss sites. Indeed, during the wheat cycle, temperatures rarely exceed 30 °C or drop below -8 °C. Moreover, water availability was always more than sufficient also in the years selected to represent warmest and driest conditions (>650 mm year-1 evenly distributed throughout the crop cycle). Substantial differences between modelling solutions emerged in three years out of nine, with MMS determining crop failure in the coldest and wettest year at all the Swiss sites due to the simulated effect of markedly negative minimum temperatures. These unexpected results underline the need to further adapt the component accounting for extreme weather events, which indicates very harmful impacts (i.e. crop failure) from a single day with minimum temperature below the threshold value for no damage at a time before hardening. A plausible solution to limit the frequency of frost shocks from single events could be the modulation of the crop response to temperature changes also considering the number of multiple consecutive days with extreme minimum temperature over the critical period (i.e. before hardening; Barlow et al., 2015).

The simulation of winter wheat in Mediterranean countries (Italy, supplementary material, Fig. S4; Spain, supplementary material, Fig. S5) provided quite different results. With few exceptions, FOTB100 was indicated as the most influential. In Spain, the parameter related with the relative increase in respiration rate per 10 °C (Q10) had the highest total sensitivity index in the warmest and driest growing seasons. In these years, due to high average temperatures and water scarcity, respiration rates are the factors that most affected crop growth and production (Tester and Langridge, 2010). In the other years, characterized by high amounts of rainfall and low average temperatures, CVO was instead the most influential. In these cases, the sub-optimal conditions led to a decrease in the partitioning to storage organs (Daniel and Triboi, 2002) and made CVO assuming the highest relevance.

Also in the Ukrainian site, CVO achieved high total sensitivity indices, with the exception of the years referring to the baseline time frame (i.e., 2004, 2005 2007; supplementary material, Fig. S6). For these years, the parameter accounting for light use efficiency of single leaves at 10 °C (EFFTB010) emerged as the most influential. Indeed, the conditions for growing wheat in this country are less favourable owing to low levels of solar radiation. Moreover, for this site, the component accounting for extreme weather events determined crop failure in several years due to low minimum temperatures in winter (till -25 °C).

In a recent study, Ma et al. (2013) established, through the same sensitivity analysis technique, that AMAXTB130, SPAN and CVO are the most influential parameters when simulating winter wheat with WOFOST in the Hebei province of China. These information were profitably used by Huang et al. (2015 and 2016) to calibrate WOFOST for the simulation of winter wheat in the same location and to identify the parameters to being re-initialized or re-calibrated to include in WOFOST remotely sensed data. The specific explored pedoclimatic conditions and the diverse varieties and crop management simulated led to different rankings among the parameters in the two studies, underlying the importance of performing sensitivity analyses before running models in a given operative context. Herein, the subset of WOFOST parameters to focus on was established according to the findings from previous studies carried out in European environments (van Diepen te al. (1988); Marletto et al. (2005); Priesack et al. (2006); Richter et al. (2010); Biernath et al. (2011); Rötter et al. (2011); Stella et al. (2014)) while the limited number of points used in the AFGEN tables (E.g. AMAXTB 100 and 130 were not considered) aimed at reducing possible overlaps between the distributions assigned to parameters.

The ranking of parameters for maize simulations in Switzerland was the same at each site (supplementary material, from Fig. S7 to Fig. S10). The high values of the total sensitivity index associated with the parameter related with partitioning to storage organs right after flowering (FOTB110) underlined the key role of this parameter in simulating maize yield. This was not the case for maize simulations performed in Ukraine under the warmest and driest climate conditions, where yields were mostly influenced by specific leaf area at emergence (SLATB000; supplementary material, Fig. S11). These years were characterized by a scarcity of water supply if compared with the others (on average 360 mm against 832 mm). This condition limited maize growth and made the simulation mostly influenced by the parameters related with the simulation of the early crop establishment (Subedi and Ma, 2009) rather than by those related with crop productivity at full canopy. The same rationale can be applied to the results achieved with sunflower simulation in Spain (Cordoba site; supplementary material, Fig. S12). SLATB000 achieved the highest total sensitivity indices (up to three times higher than the second-ranked parameter) in all selected years and with both modelling solutions. In this case, sunflower production was limited by high temperatures, which caused a reduction in the CO2 assimilation rate. This made SLATB000 the most influential parameter for sunflower yield simulation. The primary role of high temperatures in limiting crop growth and productivity is further underlined by the results achieved for the parameter SPAN (i.e. Life span of leaves growing at 35 °C), which denoted a higher value of total sensitivity index with the MMS rather than with the EMS.

The results of winter barley simulations in Spain (Granada site; supplementary material, Fig. S13) identified FOTB100, extinction coefficient for diffuse light at flowering (KDIFTB100) and Q10 as the most influential parameters. Only in the coldest and wettest year of the baseline time frame (i.e. 1996), the parameters' ranking was slightly different. A reduction in the total sensitivity index achieved by FOTB100 was counterbalanced by an increased total sensitivity index for CVO. For this year, indeed, the high amount of rainfall and the low average temperatures determined a limited influence of the partitioning to storage organs in the simulation of crop yield (as already discussed for winter wheat simulations in Spain), which was mostly influenced by CVO.

3.4.2 Comparison between sensitivity analysis methods

The results obtained with the SA methods of Morris and eFAST were compared (Fig. 4 and 5 and supplementary material from Fig. S14 to Fig. S25) in terms of how they ranked parameters. In particular, the Savage Scores (Savage, 1956; Eq. 1) were used to compare the parameters'

sensitivity metrics achieved with the two methods, thus emphasising the ranking of the most influential parameters.

$$SV_{k,n} = \sum_{i=k}^{n} \frac{1}{i} \quad [1]$$

where SVk,n is the Savage Score for the k-ranked parameter of a set of n parameters.

For the eFAST method the Savage Scores were computed considering the total sensitivity index, whereas for the Morris method we focused on μ*, which provides an indication of the overall influence of each parameter on the output.

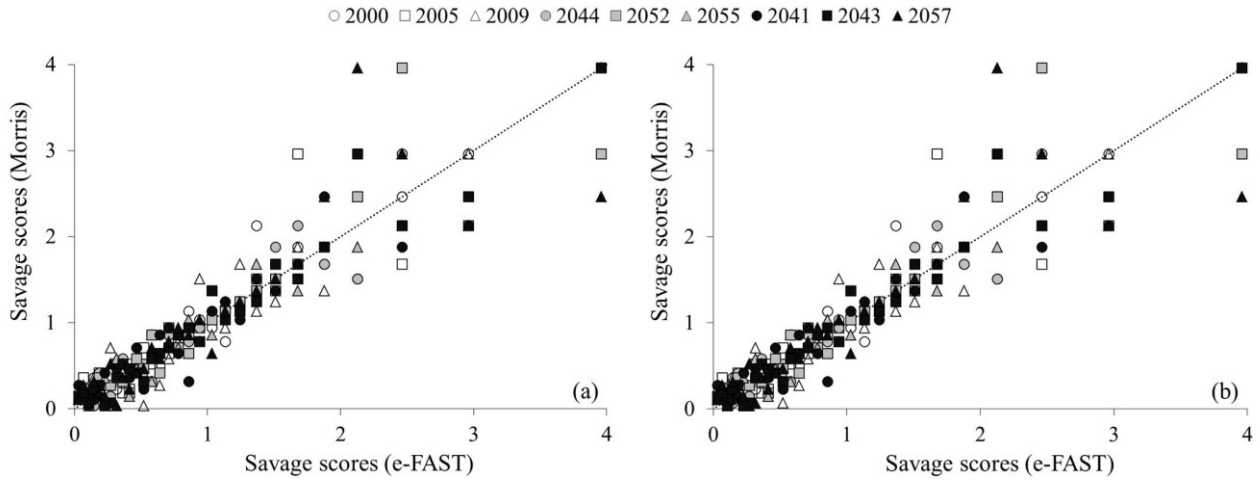

Figure 4. Comparison between results obtained with the Morris and eFAST sensitivity analysis methods for with winter wheat simulation in Italy (Foggia site). a) = Savage Scores for the EMS (existing modelling solution); b) = Savage Scores for the MMS (modified modelling solution); dotted line = 1:1 line.

The two methods provided similar parameter rankings, being the linear regression between Savage Scores calculated for the two methods significant ($p < 0.001$), with R2 ranging from 0.61 to 0.98 considering all the values). Furthermore, the ranking calculated based on the two methods for each combination crop × site was the same for the two modelling solutions (EMS, Fig. 4a; MMS, Fig. 4b). Major differences between the two modelling solutions arose when the component simulating the impact of extreme weather events determined crop failure; in these cases, the correlation between parameter rankings was higher for the MMS. An example is provided by winter wheat simulations in the Ukrainian site (Fig. 5), where the complete yield losses in the coldest years were explained solely by variations in parameters involved with the effect of extreme negative temperatures on HI (all other parameters were not relevant). In the same years, results achieved for EMS led to major discrepancies in the ranking of model parameters (Fig. 5a), meaning that several parameters related to yield formation played a key role in explaining yield responses at suboptimal temperature for growth.

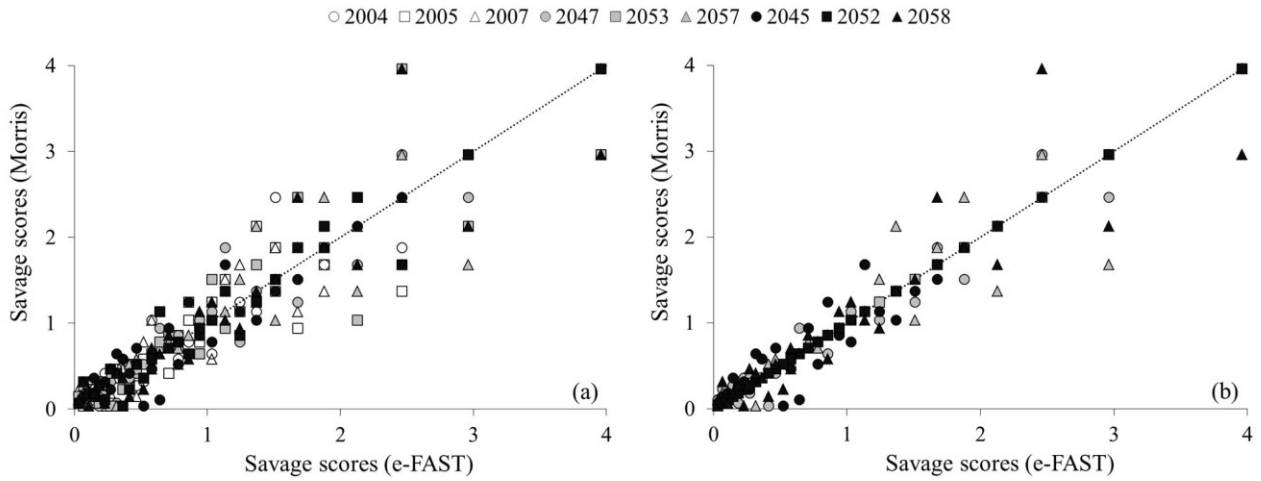

Figure 5. Comparison between results obtained with the Morris and eFAST sensitivity analysis methods for winter wheat simulation in Ukraine (Mironivka site). a) = Savage Scores for the EMS (existing modelling solution); b) = Savage Scores for the MMS (modified modelling solution); dotted line = 1:1 line.

3.5 Conclusions

The results of this sensitivity study increase the knowledge about the behaviour of the crop model WOFOST in the simulation of the yield of different crops across several European sites under current conditions and projected scenarios of climate change. The simulated crop yield was mostly influenced by parameters related with storage organs. Indeed, although with some exceptions, the parameters involved in partitioning to storage organs around flowering (FOTB100 – FOTB110) and conversion efficiency into storage organs (CVO) had the highest total sensitivity indices. Nevertheless, for sunflower simulations in Spain and maize in Ukraine, results were mainly influenced by specific leaf area at emergence (SLATB000), underlying the importance of early crop establishment in case of sub-optimal growth conditions. Some differences were observed between the results obtained for the two modelling solutions assessed in this study (i.e. EMS and MMS) in terms of both total sensitivity metrics and parameters' ranking, especially when the simulated impact of extreme weather events determined crop failure. The two SA methods (i.e. Morris and eFAST) provided similar parameters' rankings. This confirms the usefulness of the Morris method (which is less demanding in terms of computational time) for identifying the most influential parameters, and its suitability for screening purposes before the application of variance-based methods (computationally-expensive) in 2-step SA designs.

These results also indicate the need to further improve the component simulating the impacts of extreme weather events, owing to its tendency to sometimes overestimate the impact of weather extremes.

The SA experiments led to identify the most influential parameters for the simulation of several crops across European sites, spreading useful information to achieve the best trade-off between parameterization effort and reliability of model estimates. The coupling of the WOFOST model with the component simulating the impacts of extreme weather events and its application under climate change scenarios lays the basis to improve the in-season crop growth monitoring and yield forecasting capabilities at EU level in the short and medium term. Indeed, the crop yield forecasting system of the European Commission lacks a dedicated module to consider the effects of climatic shocks or extreme events on yield formation. This limit could even be exacerbated in the near future due to the likely increase in the frequency of climatic extremes due to climate change (EEA, 2017). The development of an early forecasting and warning system more adherent to real conditions can thus be a valuable support to multiple stakeholders of the agricultural sector in ensuring citizens health protection, crop needs and environment preservation according to local priorities and national/European regulations. As noted, details about the effect of increasing atmospheric CO2 concentration go beyond the aim of this study. However, as a natural evolution of what has already been presented, dedicated routines can be arranged and implemented with the purpose of testing CO2 effects within the European Commission (Crop Growth Monitoring System; https://ec.europa.eu/jrc/en/mars) version of WOFOST.

Acknowledgements

The research leading to these results has received funding from the European Community's Seven Framework Programme-FP7 (KBBE.2013.1.4-09) under Grant Agreement No. 613817.2013-2016. MODelling vegetation response to EXTREMe Events (MODEXTREME, http://modextreme.org).

The authors are indebted to Francisco J. Villalobos (University of Cordoba, Spain) and Luca Testi (Spanish National Research Council, Cordoba, Spain), through whose efforts plant processes were modelled to account for the impact of extreme weather events. We also acknowledge the colleagues who provided data from field trials in Italy (Domenico Ventrella, Council for Agricultural Research and Agricultural Economic Analysis), Spain (Luca Testi, Spanish National Research Council), Switzerland (Pierluigi Calanca, Agroscope Swiss Confederation's centre of excellence for agricultural research) and Ukraine (Oleksii A. Kryvobok, Ukrainian Scientific and Research Institute for Hydrometeorology).

3.6 Appendices

Appendix A. Key processes and modelling approaches for the impact of extreme events

General framework

For each day around anthesis, the overall value of the response function to temperature (as driven by mean crop temperature) and water stress is calculated using the following equation:

$$F = \frac{1}{day}\sum_{i}^{day} min(F_T, F_W) \quad [2]$$

where F (-) is the response function to crop temperature and water stress; FT (-) is the response function to average crop temperature; F_W (-) is response function to extreme water stress.

In addition, the effect of frost (function of minimum crop temperature) and extreme heat (function of maximum crop temperature) are computed as:

$$\mathrm{F_A} = \mathrm{F} \cdot \prod_{1}^{\mathrm{day}} \min(\mathrm{F_F}, \mathrm{F_H}) \quad [3]$$

where F_A (-) is overall response function to stresses; F_F (-) is the response function to frost; F_H (-) is the response function to extreme heat. Then, the actual maximum HI that might be attained after anthesis is completed (HI_{AA}, -) is computed as:

$$\mathrm{HI_{AA}} = \mathrm{F_A} \cdot \mathrm{HI_{max}} \quad [4]$$

where HImax (-) is the potential HI for the specific species.

From anthesis to maturity, the component assumes that the HI increases linearly from zero to HI_{AA}, so the final HI is computed according to Eq. 5:

$$\mathrm{HI} = \frac{\mathrm{HI_{AA}}}{\mathrm{d_{PA}}} \cdot \mathrm{t} \quad [5]$$

where HI (-) is the final HI; d_{PA} (d) is duration of the phase expressed as calendar days; t (d) is the time after anthesis expressed as calendar days.

Any frost or heat event occurring during this period (e.g. at time t1) has an impact calculated according to Eq. 6:

$$\mathrm{HI} = \mathrm{HI_{AA}} \cdot \left[(1 - \mathrm{F_A}) \cdot \frac{\mathrm{t_1}}{\mathrm{d_{PA}}} + \mathrm{F_A}\right] \quad [6]$$

Response to extreme water stress

The extreme water stress can be expressed as the cumulative reduction in transpiration since transpiration becomes limited. This limitation starts when the water content in the soil is equivalent to the concept of allowable depletion (Eq. 7), which is the fraction of plant available water that can be extracted by the crop without negative effects on transpiration, assimilation or growth.

$$AD = 0.04 \cdot AD_5 \cdot (5 - ET_0) \quad [7]$$

where AD (mm) is the allowable depletion (0.1<AD<0.8); AD_5 (-) is a crop-specific parameter that increases or decreases *AD* (reference values: 0.55 for winter/durum wheat, winter barley, maize; 0.45 for sunflower); ET_0 (mm) is the reference evapotranspiration.

For a given value of relative transpiration (i.e., actual to reference evapotranspiration ratio), the cumulative reduction in crop transpiration (f_R) since the onset of water deficit is:

$$f_R = (1 - r)^2 \cdot (1 - AD) \quad [8]$$

where r (-) is the relative transpiration.

So the fraction of unreduced transpiration (f_E, -) is equal to:

$$f_E = 1 - (1 - r)^2 \cdot (1 - AD) \quad [9]$$

The response function to severe water stress is thus computed according to Eq. 10 and is set to one when it exceeds the crop-dependent parameter f_{Ecrit} (reference value: 0.7 for winter/durum wheat, winter barley, maize; 0.8 for sunflower):

$$F_w = \frac{f_E}{f_{Ecrit}} \quad [10]$$

Response to heat

The response to heat (i.e. F_H; Eq. 11) is computed as a function of maximum canopy temperature (Tmax) and is equal to one when maximum crop temperature does not exceed a minimum damage threshold (T_{XC}). For high values, F_H decreases linearly to zero when an upper limit canopy temperature is reached (T_{X0}, °C):

$$F_H = \begin{cases} 1 & T_{max} \leq T_{XC} \\ \frac{(T_{max} - T_{X0})}{(T_{XC} - T_{X0})} & T_{XC} < T_{max} < T_{X0} \\ 0 & T_{max} \geq T_0 \end{cases} \quad [11]$$

where T_{max} (°C) is the daily maximum canopy temperature; T_{XC} (°C) is the temperature below which no heat stress occurs during reproductive phase; T_{X0} (°C) is the critical temperature at which the effect of heat stress on HI is maximum.

Response to frost

The simulation of the crop response to frost is described using two distinct equations accounting for the impacts on harvest index (F_{F1}, Eq. 12), and LAI (F_{F2}), as:.

$$F_{F1} = \begin{cases} 0 & T_{min} \leq T_{100} \\ \frac{(T_{min} - T_{100})}{(T_0 - T_{100})} & T_{100} < T_{min} < T_0 \\ 1 & T_{min} \geq T_0 \end{cases} \quad [12]$$

where T_{min} (°C) is the minimum daily canopy temperature; T_0 (°C) is the critical temperature below which flower/grains number begins to reduce; T_{100} (°C) is the critical temperature at which flowers/grain number is zero [°C]. The algorithm computing the frost impact on photosynthetic tissues (F_{F2}) is formally the same as the one used for *HI*, but the critical killing temperatures are referred to the number of dead leaves (as fraction of total LAI) instead of the number of flowers/grains.

Calculation of maximum canopy temperature

The maximum canopy temperature ($\mathrm{T_{max}}$; °C) is computed as:

$$\mathrm{T_{max}} = \mathrm{T_a} + [(1 - \mathrm{f_G}) \cdot \mathrm{R_n} - \mathrm{LE}] \cdot \frac{\mathrm{r_{aH}}}{\rho \cdot \mathrm{C_p}} \quad [13]$$

where $\mathrm{T_a}$ (°C) is the maximum daily air temperature; $\mathrm{f_G}$ (-) is the fraction of net radiation invested in soil heat flux (assumed equal to 0.1 during daytime); $\mathrm{R_n}$ (W m-2) is the net solar radiation; LE (W m-2) is the latent heat flux; $\mathrm{r_{aH}}$ (s m-1) is the aerodynamic resistance; ρ (kg m-3) is the air density; $\mathrm{C_p}$ [J kg-1 °C-1] is the specific heat of air.

Calculation of minimum canopy temperature

The minimum canopy temperature ($\mathrm{T_{min}}$) is computed as:

$$\mathrm{T_{min}} = \frac{(1-\mathrm{f_G}) \cdot [-\varepsilon_v a + \varepsilon_a a + \varepsilon_a b \mathrm{T_{aw}}] \cdot \mathrm{r_a} \gamma^* + \rho \mathrm{C_p} [\mathrm{T_a}(\Delta + \gamma^*) - \mathrm{D}]}{\rho \mathrm{C_p} \cdot (\Delta + \gamma^*) + (1-\mathrm{f_G}) \gamma^* \mathrm{r_a} \varepsilon_v b} \quad [14]$$

where: γ (0.067 kPa K^{-1}) is the psychrometric constant; γ^* (kPa K^{-1}) is equal to γ (1+rc/ra); D (kPa) is the vapor pressure deficit; T_{aw} (°C) is the air temperature measured at weather station; Δ [kPa K^{-1}] is the slope of saturation vapor pressure versus temperature; Δ′ (kPa K^{-2}) is the slope of Δ versus temperature; rc (s m^{-1}) is the canopy resistance [700 s m^{-1} for dry canopies, 0 s m^{-1} for wet canopies]; ra (s m^{-1}) is the aerodynamic resistance at a reference crop height of 0.12 m and at a standardized height for temperature, wind speed and humidity measurement (2 m above soil surface); ε_v and ε_a (-) are the emissivity of vegetation and of the atmosphere; a and b are coefficients of the linear form of the Stefan-Boltzmann equation.

Appendix B. WOFOST parameters used for winter wheat and winter barley and statistical settings used for sensitivity analysis (SA). Parameters with the field "Value" populated were not used for SA. For TSUM1 and TSUM2, first value refers to wheat, the second to barley.

Parameter	Units	Value	Mean	Stand. dev.	Source[d]
Base temperature for emergence (TBASEM)	°C	0			1
Maximum effective temperature for (TEFFMX)	°C	30			1
Thermal sums to reach emergence (TSUMEM)	°C-d	50			1
Daily increase in temperature sums (DTSMTB) at Tavg[a]=0	°C;°C-d	0			1
at Tavg=10		10			1
at Tavg=18		20			1
at Tavg=24		24			1
at Tavg=28		21			1
at Tavg=30		13			1
at Tavg=31		0			1
Thermal sums from emergence to anthesis (TSUM1)	°C-d	1700			1
Thermal sums from anthesis to maturity (TSUM2)	°C-d	850			1
Leaf area index at emergence (LAIEM)	ha ha^{-1}		0.137	0.0068	1
Maximum relative increase in leaf area index (RGRLAI)	ha ha^{-1} $°C^{-1}$ d^{-1}		0.01	0.0004	2, 3
Specific leaf area (SLATB) at DVS[b]=0	-; ha kg^{-1}	0.002			2, 3
at DVS=0.35			0.022	0.0001	1
at DVS=0.45			0.002	0.0001	2, 3
at DVS=0.65			0.002	0.0001	1
at DVS=2.00		0.002			1
Specific pod area (SPA)	ha kg^{-1}	0			1
Specific stem area (SSATB) at DVS=0	ha kg^{-1}	0			1
at DVS=2		0			1
Life span of leaves growing at 35°C (SPAN)	d		35	1.75	2, 4
Base temperature for leaf aging (TBASE)	°C		0	0.05	3, 5, 6
Extinction coefficient for diffuse light (KDIFTB) at DVS=0	-;-		0.4	0.03	2, 3

at DVS=0.65		0.4			1
at DVS=1			0.6	0.03	2, 3
at DVS=2		0.65			1
Light use efficiency single leaf (EFFTB) at Tavg=0	kg ha^{-1} h^{-1} J^{-1} m^2 s	0.6			1
at Tavg=10			0.6	0.03	2, 5, 7
at Tavg=40			0.6	0.03	2, 5, 7
Maximum CO_2 assimilation rate (AMAXTB) at DVS=0	-;kg ha^{-1} h^{-1}		36	1.79	3
at DVS=2			23	0.22	2, 3
Reduction factor of AMAX (TMPFTB) at Tavg=0	°C;-	0			1
at Tavg=12		0.7			1
at Tavg=14			0.92	0.05	3
at Tavg=23			1	0.05	3
at Tavg=28		0.9			1
at Tavg=31		0.6			1
at Tavg=33		0			1
Reduction factor of AMAX (TMNFTB) at $Tmin^c$=0	°C;-	0			1
at Tmin=3		1			1
Efficiency of conversion into leaves (CVL)	kg ka^{-1}		0.685	0.034	2, 4
Efficiency of conversion into storage organs (CVO)	kg ka^{-1}		0.709	0.035	2, 4
Efficiency of conversion into roots (CVR)	kg ka^{-1}		0.694	0.035	2, 4
Efficiency of conversion into stems (CVS)	kg ka^{-1}		0.662	0.033	2, 4
Rel. incr. in respiration rate per 10°C (Q10)	-		2	0.1	2, 3, 4
Rel. maintenance respiration rate for leaves (RML)	kg kg^{-1} d^{-1}		0.03	0.001	2, 4
Rel. maintenance respiration rate for storage organs (RMO)	kg kg^{-1} d^{-1}		0.01	0.0005	2, 4
Rel. maintenance respiration rate for roots (RMR)	kg kg^{-1} d^{-1}		0.015	0.0007	2, 4
Rel. maintenance respiration rate for stems (RMS)	kg kg^{-1} d^{-1}		0.015	0.0007	2, 4
Reduction factor for senescence (RFSETB) at DVS=0	-;-	1			1
at DVS=2		1			1

Partitioning to roots (FRTB) at DVS=0	-;kg kg^{-1}		0.5	0.025	2, 3, 8
at DVS=1			0.02	0.001	2, 3, 8
at DVS=1.2		0			1
Partitioning to leaves (FLTB) at DVS=0	-;kg kg^{-1}		0.65	0.032	2, 3, 8
at DVS=0.5			0.5	0.025	2, 3, 8
at DVS=0.85		0.1			1
at DVS=1		0.01			1
at DVS=2		0			1
Partitioning to storage organs (FOTB) at DVS=0	-;kg kg^{-1}	0			1
at DVS=0.75		0			1
at DVS=0.82			0	0.01	2, 3, 8
at DVS=1			1	0.059	2, 3, 8
at DVS=1.22		1			1
at DVS=2		1			
Partitioning to stems (FSTB) (function of DVS)	-;kg kg^{-1}	Derived as 1 – (FLTB + FOTB)			
Relative death rate of roots (RDRRTB) at DVS=0	-;kg kg^{-1} d^{-1}	0			1
at DVS=1.5		0			1
at DVS=1.5001		0.02			1
at DVS=2		0.02			1
Relative death rate of stems (RDRSTB) at DVS=0	-;kg kg^{-1} d^{-1}	0			1
at DVS=1.5		0			1
at DVS=1.5001		0.02			1
at DVS=2		0.02			1

[a] mean air daily temperature

[b] development stage code (0: emergence; 1: flowering; 2: maturity)

[c] minimum air daily temperature

[d] 1: adapted from Stella et al. (2014); 2: van Diepen et al. (1988); 3: Richter te al. (2010); 4: Arora and Gajri (1998); 5: Marletto et al. (2005); 6: Priesack et al. (2006); 7: Biernath et al. (2011); 8: Rötter et al. (2011)

Appendix C. WOFOST parameters used for maize and statistical settings used for sensitivity analysis (SA). Parameters with the field "Value" populated were not used for SA.

Parameter	Units	Value	Mean	Stand. dev.	Source[d]
Base temperature for emergence (TBASEM)	°C	10			1
Maximum effective temperature for (TEFFMX)	°C	30			1
Thermal sums to reach emergence (TSUMEM)	°C-d	40			1
Daily increase in temperature sums (DTSMTB) at Tavg[a]=0	°C;°C-d	0			1
at Tavg=8		10			1
at Tavg=30		23			1
at Tavg=35		23			1
Thermal sums from emergence to anthesis (TSUM1)	°C-d	1600			1
Thermal sums from anthesis to maturity (TSUM2)	°C-d	1100			1
Leaf area index at emergence (LAIEM)	ha ha^{-1}		0.372	0.0157	1, 2
Maximum relative increase in leaf area index (RGRLAI)	ha ha^{-1} $°C^{-1}$ d^{-1}		0.03	0.0145	1, 2
Specific leaf area (SLATB) at DVS[b]=0	-; ha kg^{-1}		0.003	0.0064	3
at DVS=0.5			0.002	0.0001	3
at DVS=0.78		0.001			3
at DVS=2.00		0.001			3
Specific pod area (SPA)	ha kg^{-1}	0			3
Specific stem area (SSATB) at DVS=0	ha kg^{-1}	0			3
at DVS=2		0			3
Life span of leaves growing at 35°C (SPAN)	d		36.5	1	1, 2, 3
Base temperature for leaf aging (TBASE)	°C		9	1.41	1, 2, 3
Extinction coefficient for diffuse light (KDIFTB) at DVS=0	-;-		0.6	0.03	2, 3
at DVS=2			0.6	0.03	2, 3
Light use efficiency single leaf (EFFTB) at Tavg=0	kg ha^{-1} h^{-1} J^{-1} m^2 s		0.475	0.0353	1, 2, 3
at Tavg=40			0.2	0.01	1, 2, 3
Maximum CO_2 assimilation rate (AMAXTB) at DVS=0			55	2.75	2, 3

at DVS=1.25		50			3
at DVS=1.5			40	2	2, 3
at DVS=1.75		35			3
at DVS=2			21	1.05	2, 3
Reduction factor of AMAX (TMPFTB) at Tavg=0	°C;-	0			
at Tavg=9		0			
at Tavg=20			0.5	0.025	1, 2, 3
at Tavg=30		1			1
at Tavg=35			0.9	0.045	1, 2, 3
at Tavg=42		0.078			1
Reduction factor of AMAX (TMNFTB) at $Tmin^c$=5	°C;-	0			1
at Tmin=12		1			1
Efficiency of conversion into leaves (CVL)	kg ka^{-1}		0.7	0.028	1, 2, 3
Efficiency of conversion into storage organs (CVO)	kg ka^{-1}		0.695	0.035	1, 2, 3
Efficiency of conversion into roots (CVR)	kg ka^{-1}		0.705	0.021	1, 2, 3
Efficiency of conversion into stems (CVS)	kg ka^{-1}		0.674	0.023	1, 2, 3
Rel. incr. in respiration rate per 10°C (Q10)	-		2	0.1	1, 2
Rel. maintenance respiration rate for leaves (RML)	kg kg^{-1} d^{-1}		0.03	0.0015	1, 2, 3
Rel. maintenance respiration rate for storage organs (RMO)	kg kg^{-1} d^{-1}		0.01	0.0005	1, 2, 3
Rel. maintenance respiration rate for roots (RMR)	kg kg^{-1} d^{-1}		0.013	0.0035	1, 2, 3
Rel. maintenance respiration rate for stems (RMS)	kg kg^{-1} d^{-1}		0.015	0.00075	1, 2, 3
Reduction factor for senescence (RFSETB) at DVS=0	-;-	1			1
at DVS=2		1			1
Partitioning to roots (FRTB) at DVS=0	-;kg kg^{-1}		0.4	0.02	1, 2
at DVS=0.4			0.262	0.013	1, 2
at DVS=1		0			3
at DVS=1.2		0			3
Partitioning to leaves (FLTB) at DVS=0	-;kg kg^{-1}		0.62	0.031	1, 3

at DVS=0.5			0.52	0.031	1, 3
at DVS=0.88			0.215	0.09	1, 3
at DVS=1.2		0			3
at DVS=2		0			3
Partitioning to storage organs (FOTB) at DVS=0	-;kg kg^{-1}	0			1
at DVS=0.9		0.2			1
at DVS=1.1			0.63	0.18	1, 3
at DVS=1.2			0.95	0.05	1, 3
at DVS=2		2			1
Partitioning to stems (FSTB) (function of DVS)	-;kg kg^{-1}	Derived as 1 – (FLTB + FOTB)			
Relative death rate of roots (RDRRTB) at DVS=0	-;kg kg^{-1} d^{-1}	0			3
at DVS=1.5		0			3
at DVS=1.5001		0.02			33
at DVS=2		0.02			3
Relative death rate of stems (RDRSTB) at DVS=0	-;kg kg^{-1} d^{-1}	0			3
at DVS=1.5		0			3
at DVS=1.5001		0.02			3
at DVS=2		0.02			3

[a] mean air daily temperature

[b] development stage code (0: emergence; 1: flowering; 2: maturity)

[c] minimum air daily temperature

[d] 1: adapted from Van Heemst et al. (1988); 2: Ceglar et al. (2011); 3: JRC (2012)

Appendix D. WOFOST parameters used for sunflower and statistical settings used for sensitivity analysis (SA). Parameters with the field "Value" populated were not used for SA.

Parameter	Units	Value	Mean	Stand. dev.	Source[d]
Base temperature for emergence (TBASEM)	°C	6			1, 2
Maximum effective temperature for (TEFFMX)	°C	30			1
Thermal sums to reach emergence (TSUMEM)	°C-d	80			1
Daily increase in temperature sums (DTSMTB) at Tavg[a]=0	°C;°C-d	0			1, 2
at Tavg=2		0			1, 2
at Tavg=18		16			1, 2
at Tavg=40		38			1, 2
Thermal sums from emergence to anthesis (TSUM1)	°C-d	1600			1
Thermal sums from anthesis to maturity (TSUM2)	°C-d	1000			1
Leaf area index at emergence (LAIEM)	ha ha^{-1}		0.005	0.000265	1, 2
Maximum relative increase in leaf area index (RGRLAI)	ha ha^{-1} $°C^{-1}$ d^{-1}		0.029	0.00147	1, 2, 3, 4
Specific leaf area (SLATB) at DVS[b]=0	-; ha kg^{-1}		0.003	0.00015	1, 2, 4
at DVS=1			0.002	0.00011	1, 2, 4
at DVS=2.00		0.002			1, 2, 4
Specific pod area (SPA)	ha kg^{-1}	0			1
Specific stem area (SSATB) at DVS=0	ha kg^{-1}	0			1
at DVS=2		0			1
Life span of leaves growing at 35°C (SPAN)	D		30	1.5	1
Base temperature for leaf aging (TBASE)	°C		4.5	0.225	1, 2
Extinction coefficient for diffuse light (KDIFTB) at DVS=0	-;-		0.8	0.04	1, 2, 5
at DVS=2			0.8	0.04	1, 2, 5
Light use efficiency single leaf (EFFTB) at Tavg=0	kg ha^{-1} h^{-1} J^{-1} m^2 s		0.442	0.0221	1
at DVS=40			0.442	0.0221	1
Maximum CO_2 assimilation rate (AMAXTB) at DVS=0	-;kg ha^{-1} h^{-1}		43	2.15	1, 6, 7
at DVS=1.5			32.5	1.625	1, 6, 7

at DVS=2			15	0.75	1, 6, 7
Reduction factor of AMAX (TMPFTB) at Tavg=0	°C;-	0			1, 8
at Tavg=10			0.5	0.025	1, 2, 8
at Tavg=20		1			1, 8
at Tavg=30		1			1, 8
at Tavg=35			0.75	0.0375	1, 8
at Tavg=40		0.5			1, 8
Reduction factor of AMAX (TMNFTB) at $Tmin^c$=0	°C;-	0			1
at Tmin=3		1			1
Efficiency of conversion into leaves (CVL)	kg ka^{-1}		0.697	0.0348	1
Efficiency of conversion into storage organs (CVO)	kg ka^{-1}		0.695	0.0347	1
Efficiency of conversion into roots (CVR)	kg ka^{-1}		0.75	0.0375	1
Efficiency of conversion into stems (CVS)	kg ka^{-1}		0.69	0.0345	1
Rel. incr. in respiration rate per 10°C (Q10)	-		2	0.1	1
Rel. maintenance respiration rate for leaves (RML)	kg kg^{-1} d^{-1}		0.031	0.00155	1
Rel. maintenance respiration rate for storage organs (RMO)	kg kg^{-1} d^{-1}		0.012	0.000575	1
Rel. maintenance respiration rate for roots (RMR)	kg kg^{-1} d^{-1}		0.01	0.0005	1
Rel. maintenance respiration rate for stems (RMS)	kg kg^{-1} d^{-1}		0.015	0.000745	1
Reduction factor for senescence (RFSETB) at DVS=0	-;-	1			1
at DVS=2		1			1
Partitioning to roots (FRTB) at DVS=0	-;kg kg^{-1}		0.5	0.025	1
at DVS=0.5			0.325	0.0162	1
at DVS=1		0			1
at DVS=2		0			1
Partitioning to leaves (FLTB) at DVS=0	-;kg kg^{-1}		0.5	0.025	1
at DVS=0.8			0.2	0.01	1
at DVS=1		0			1
at DVS=2		0			1

Partitioning to storage organs (FOTB) at DVS=0	-;kg kg^{-1}	0			1
at DVS=1		0			1
at DVS=1.2			0.739	0.0369	1
at DVS=1.4			0.869	0.0434	1
at DVS=2		1			1
Partitioning to stems (FSTB) (function of DVS)	-;kg kg^{-1}	Derived as 1 – (FLTB + FOTB)			
Relative death rate of roots (RDRRTB) at DVS=0	-;kg kg^{-1} d^{-1}	0			1
at DVS=1.5		0			1
at DVS=1.5001		0.02			1
at DVS=2		0.02			1
Relative death rate of stems (RDRSTB) at DVS=0	-;kg kg^{-1} d^{-1}	0			1
at DVS=1.5		0			1
at DVS=1.5001		0.02			1
at DVS=2		0.02			1

[a] mean air daily temperature

[b] development stage code (0: emergence; 1: flowering; 2: maturity)

[c] minimum air daily temperature

[d] 1: adapted from Tomorovic et al. (2009); 2: Archontoulis et al. (2011); 3: Hall et al. (1995); 4: Trápani et al. (1999); 5: Casadebaig et al. (2011); 6: Zahoor et al. (2011); 7: Steduto et al. (2000); 8: Paul et el. (1990)

3.7 Supplementary material

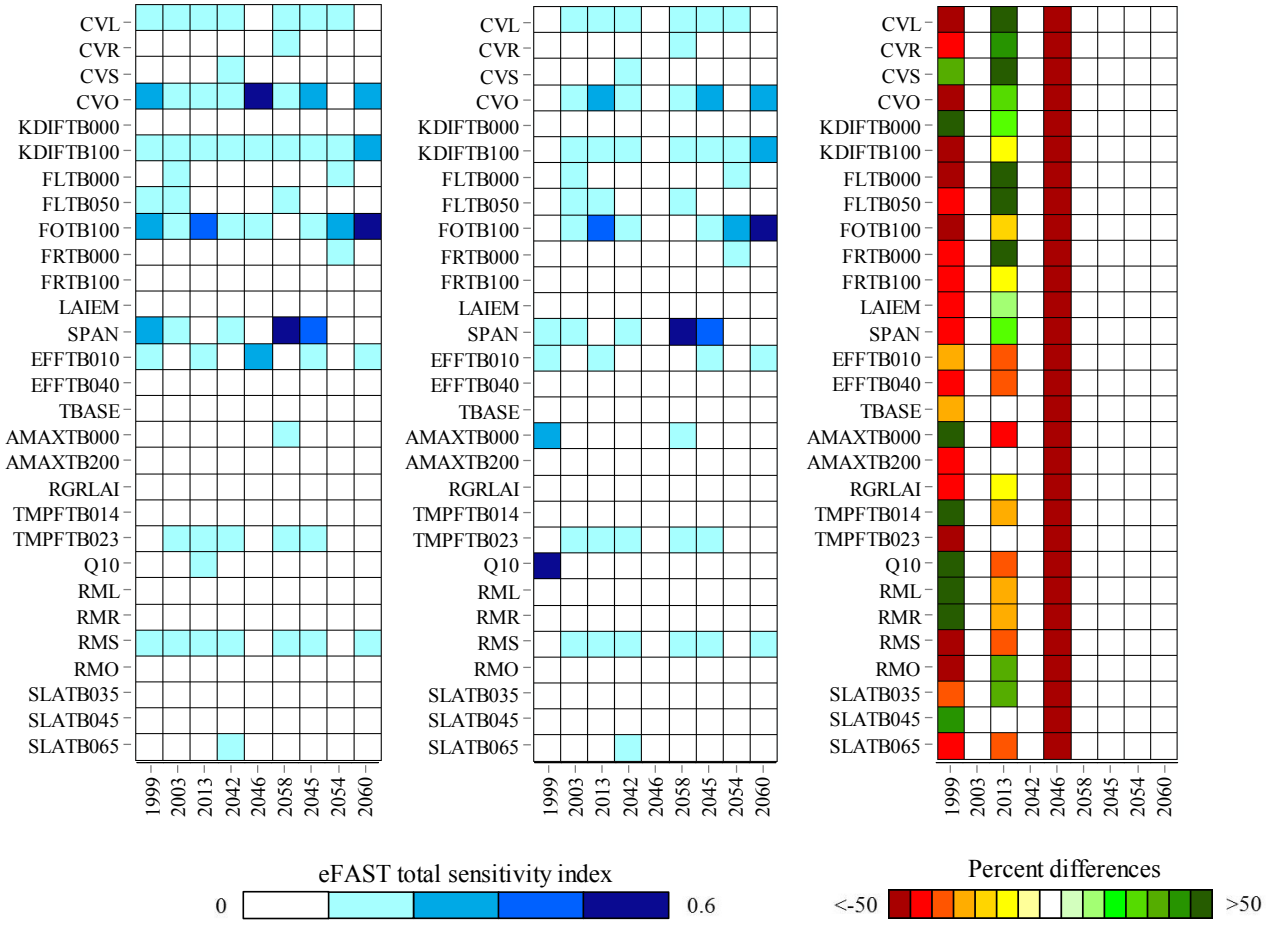

Figure S1. eFAST total sensitivity index for winter wheat yield simulated with WOFOST at the selected years in Switzerland (Ellighausen site). Left panel = EMS (existing modelling solution); central panel = MMS (modified modelling solution); right panel = percent differences between the two modelling solutions.

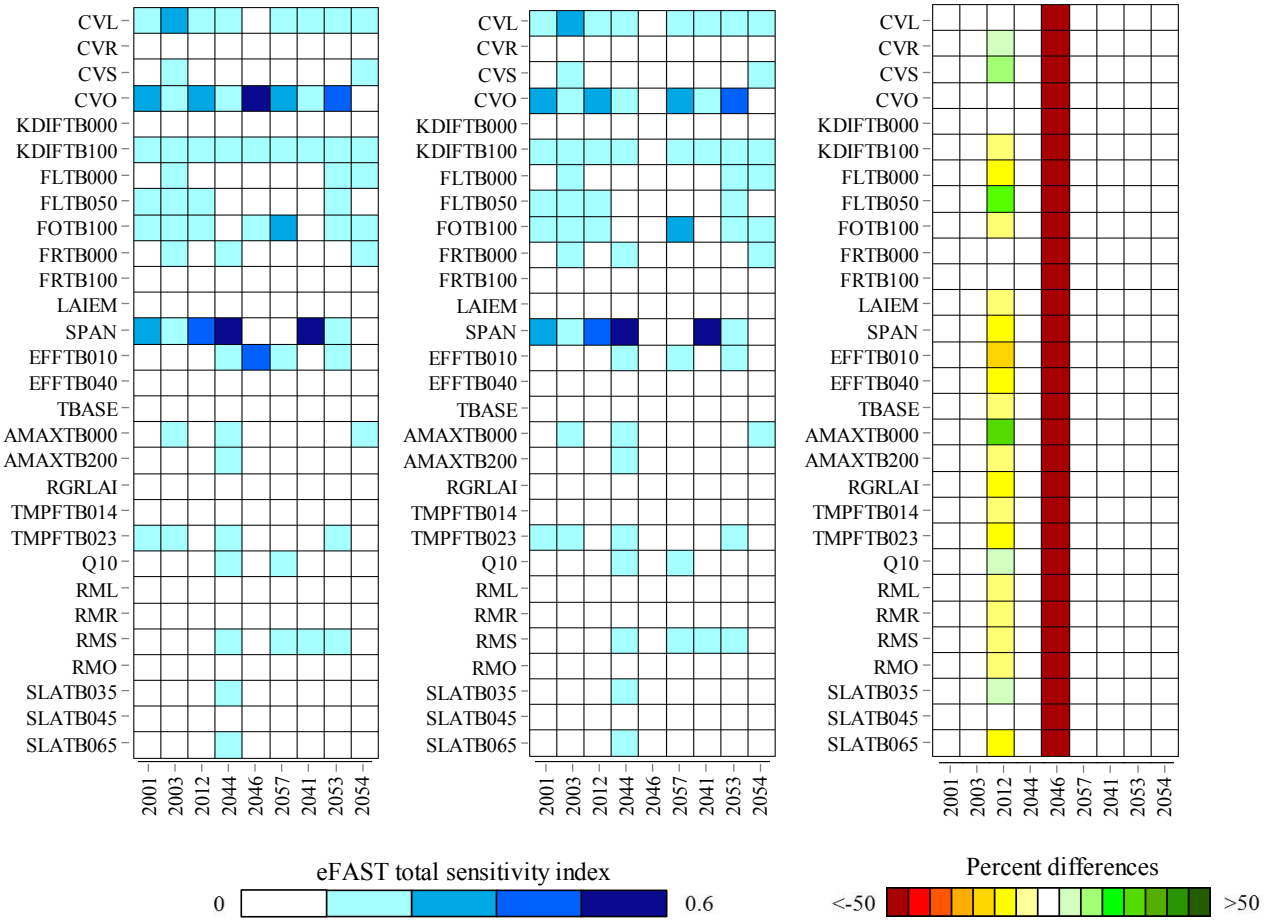

Figure S2. eFAST total sensitivity index for winter wheat yield simulated with WOFOST at the selected years in Switzerland (Reckenholz site). Left panel = EMS (existing modelling solution); central panel = MMS (modified modelling solution); right panel = percent differences between the two modelling solutions.

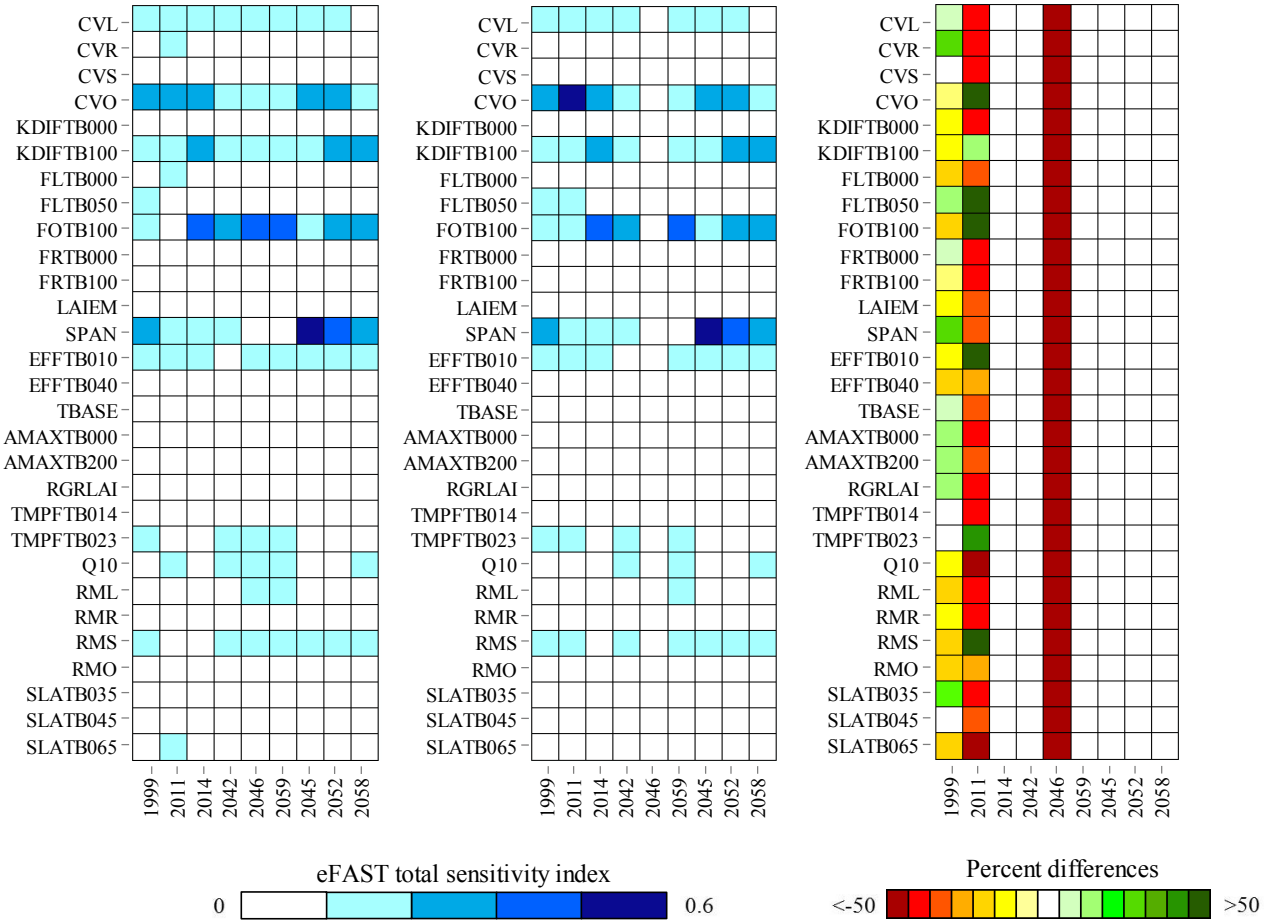

Figure S3. eFAST total sensitivity index for winter wheat yield simulated with WOFOST at the selected years in Switzerland (Therwil site). Left panel = EMS (existing modelling solution); central panel = MMS (modified modelling solution); right panel = percent differences between the two modelling solutions.

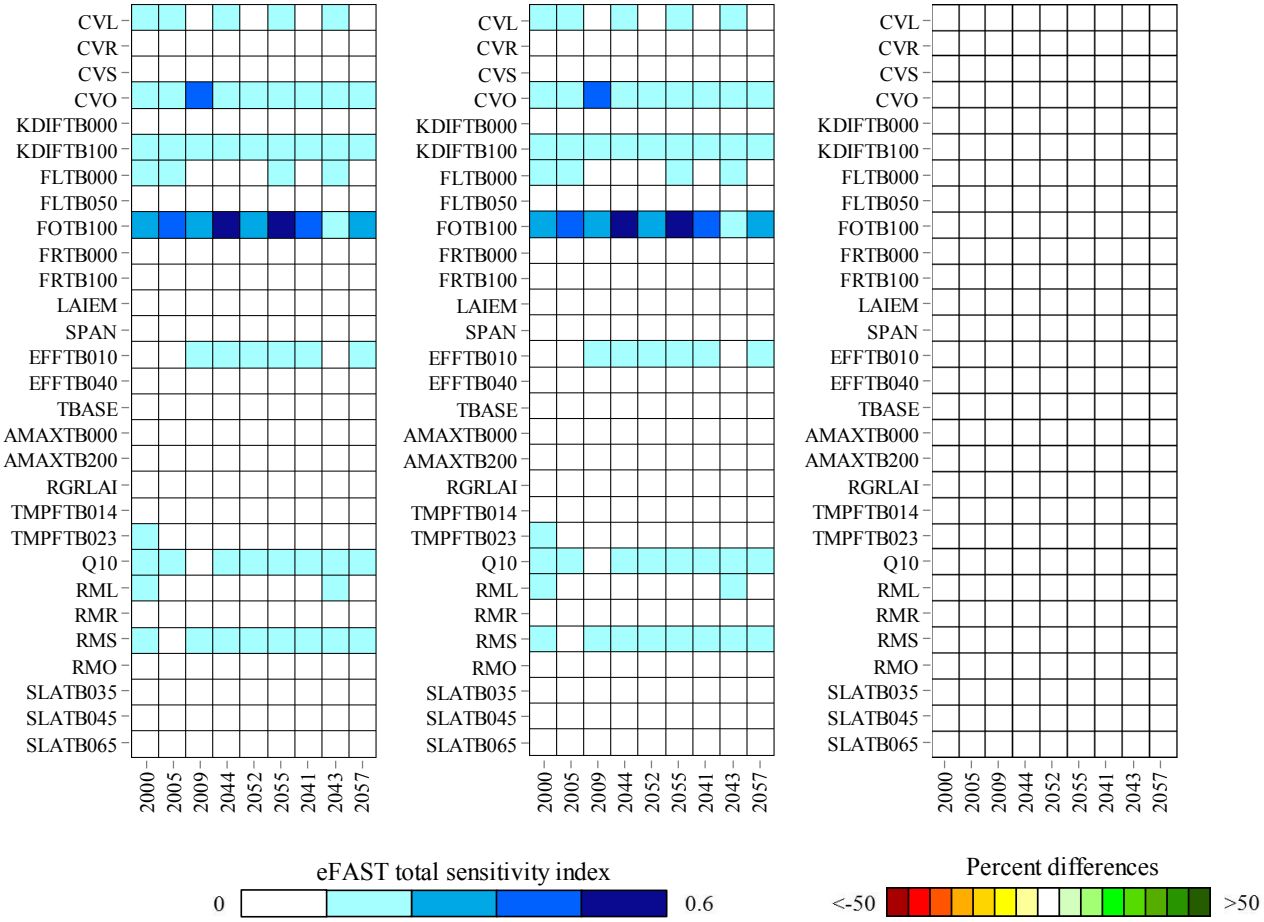

Figure S4. eFAST total sensitivity index for winter wheat yield simulated with WOFOST at the selected years in Italy (Foggia site). Left panel = EMS (existing modelling solution); central panel = MMS (modified modelling solution); right panel = percent differences between the two modelling solutions.

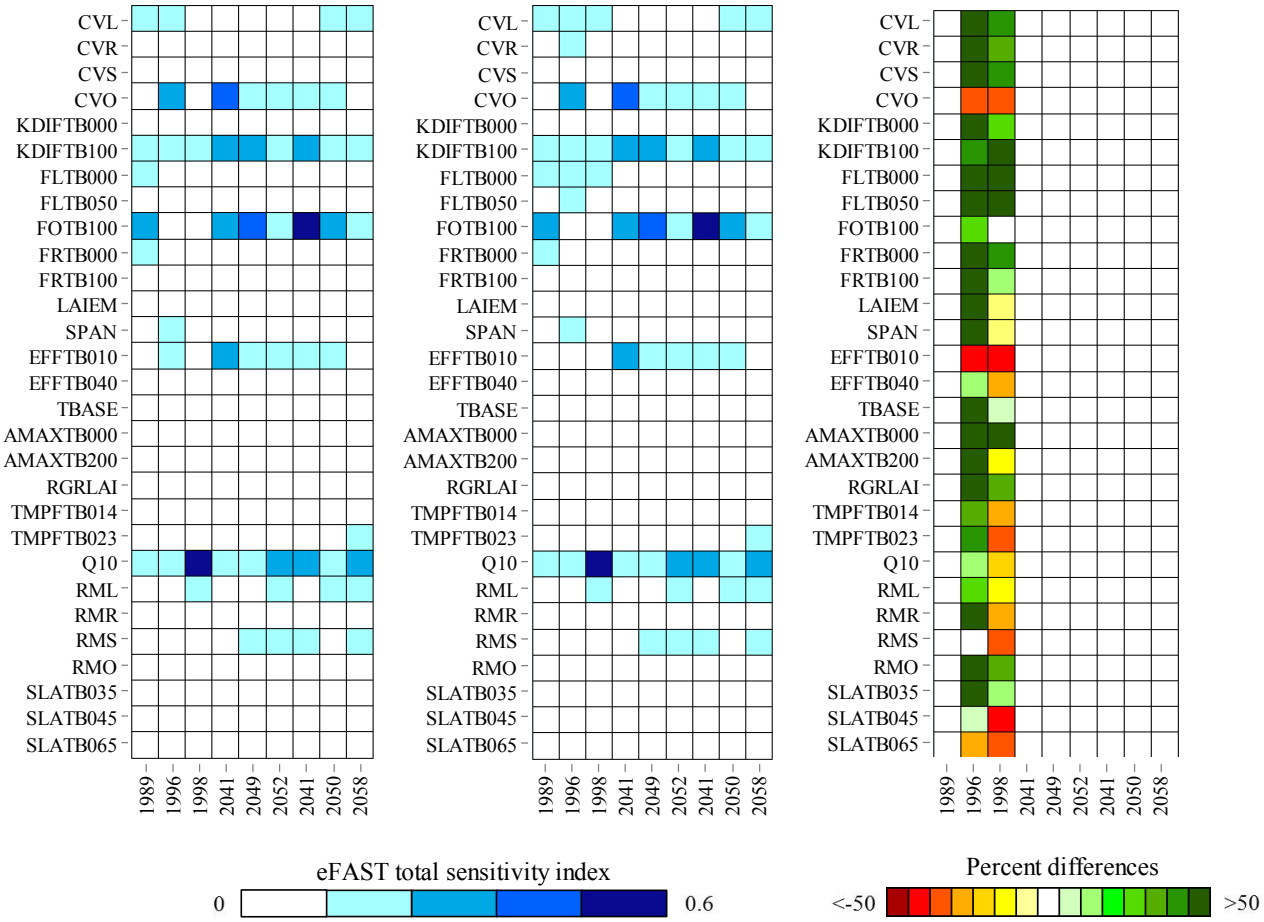

Figure S5. eFAST total sensitivity index for winter wheat yield simulated with WOFOST at the selected years in Spain (Cordoba site). Left panel = EMS (existing modelling solution); central panel = MMS (modified modelling solution); right panel = percent differences between the two modelling solutions.

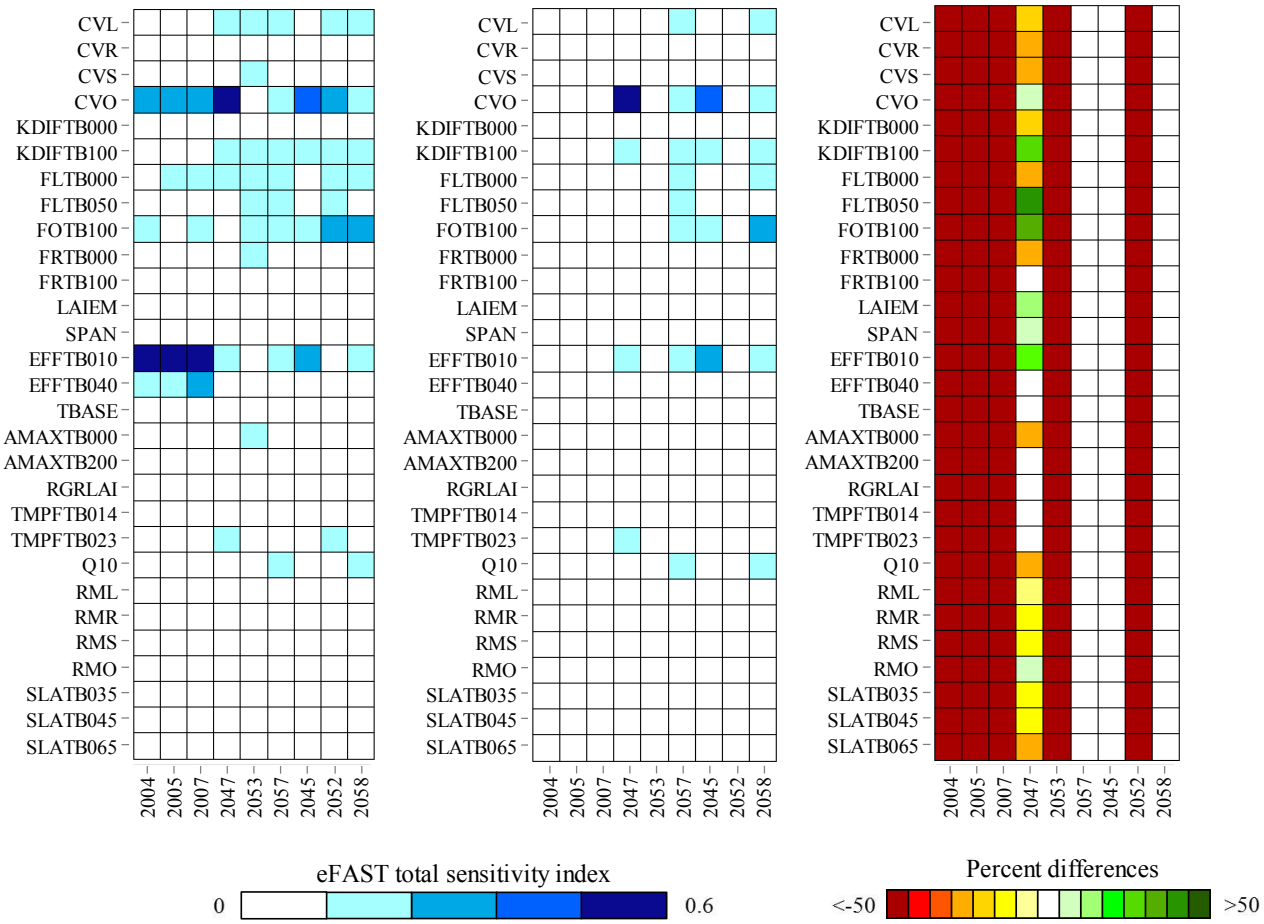

Figure S6. eFAST total sensitivity index for winter wheat yield simulated with WOFOST at the selected years in Ukraine (Mironivka site). Left panel = EMS (existing modelling solution); central panel = MMS (modified modelling solution); right panel = percent differences between the two modelling solutions.

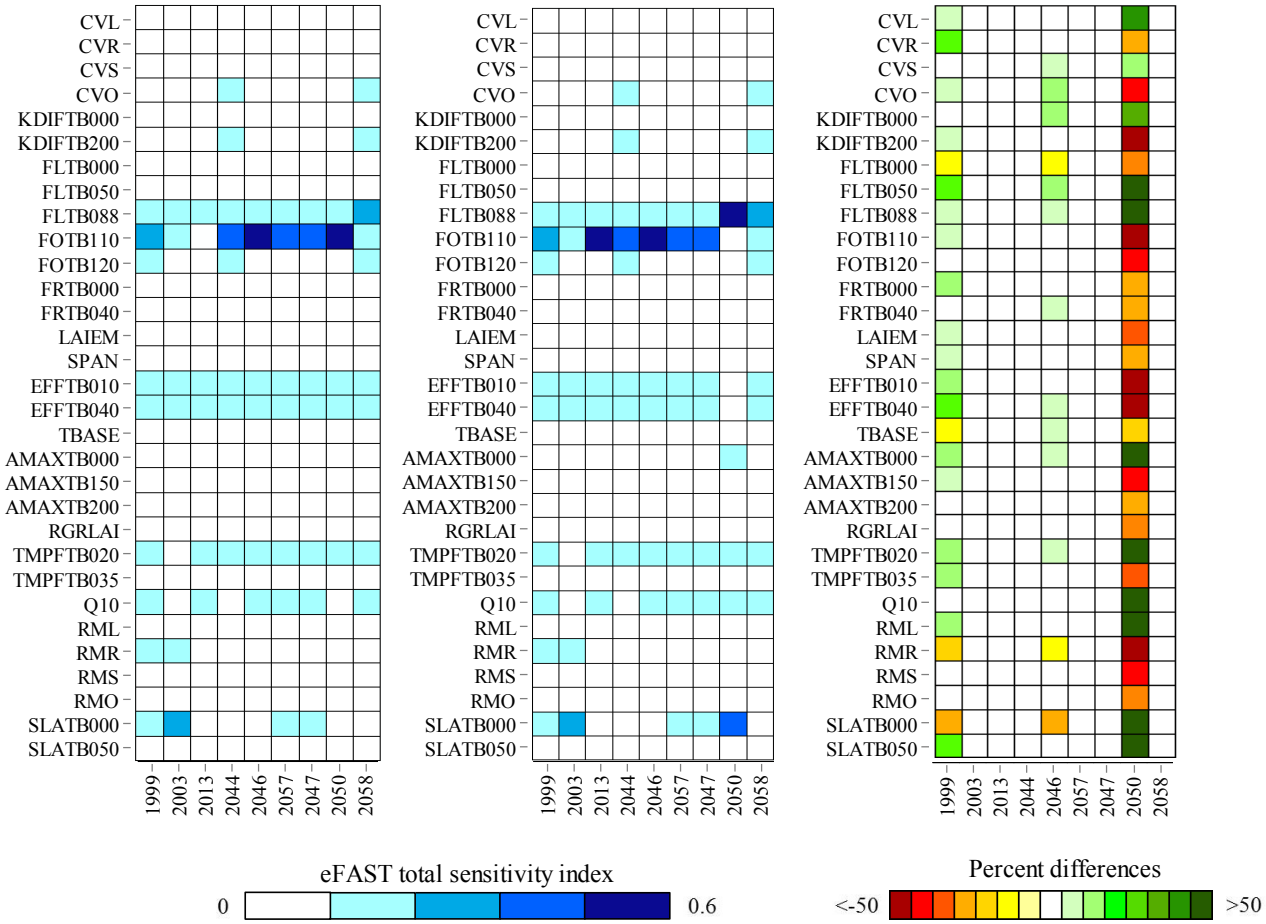

Figure S7. eFAST total sensitivity index for maize yield simulated with WOFOST at the selected years in Switzerland (Changins site). Left panel = EMS (existing modelling solution); central panel = MMS (modified modelling solution); right panel = percent differences between the two modelling solutions.

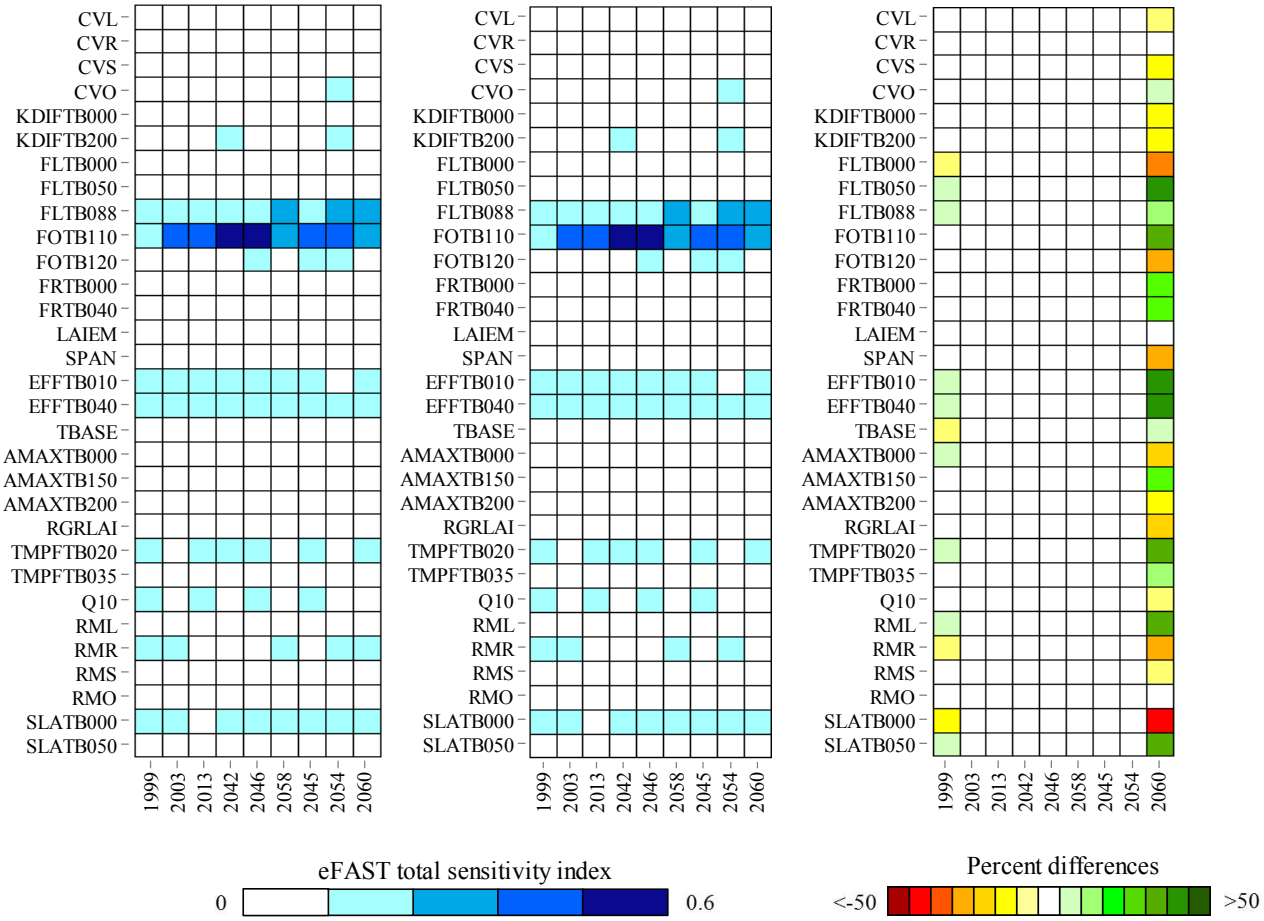

Figure S8. eFAST total sensitivity index for maize yield simulated with WOFOST at the selected years in Switzerland (Ellighausen site). Left panel = EMS (existing modelling solution); central panel = MMS (modified modelling solution); right panel = percent differences between the two modelling solutions.

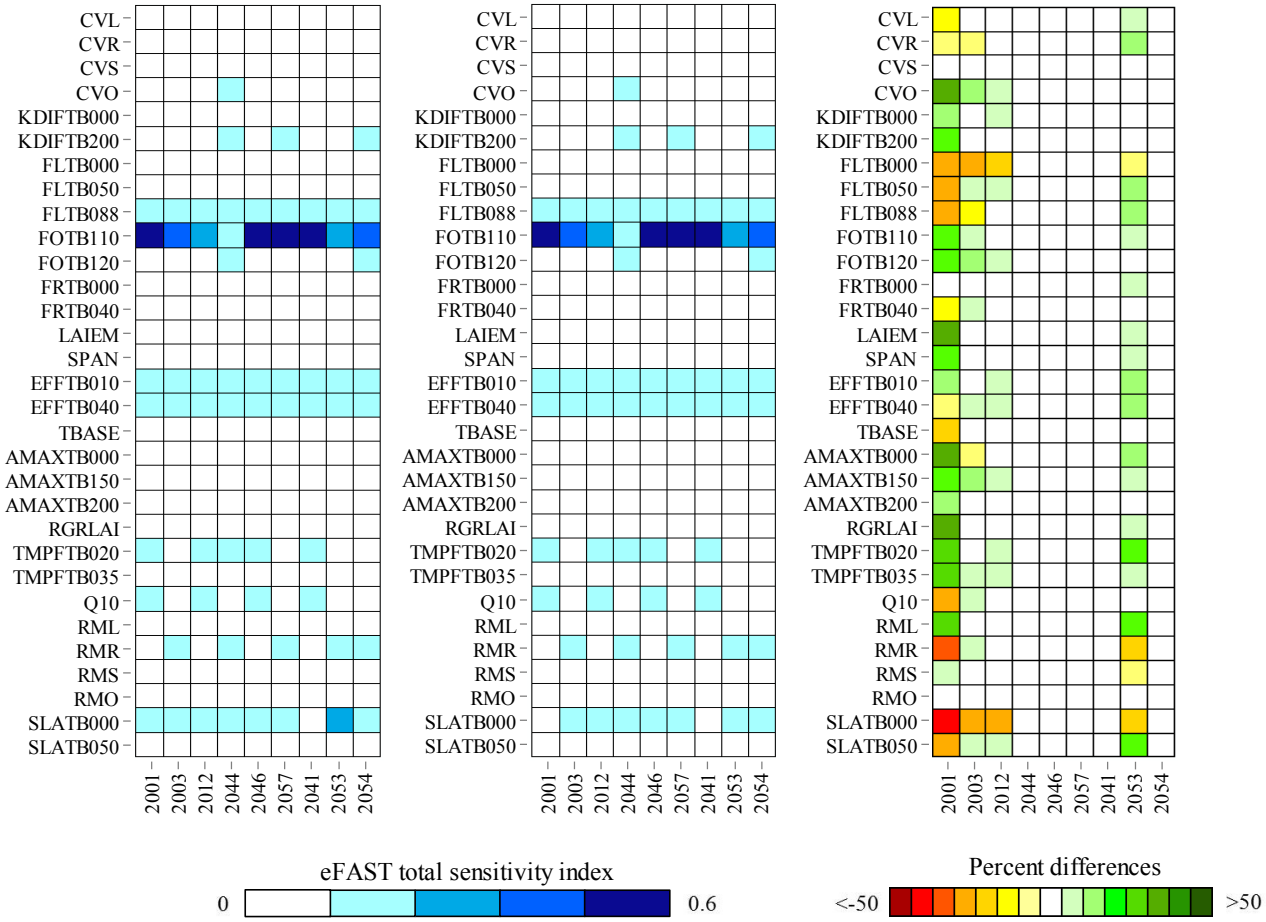

Figure S9. eFAST total sensitivity index for maize yield simulated with WOFOST at the selected years in Switzerland (Reckenholz site). Left panel = EMS (existing modelling solution); central panel = MMS (modified modelling solution); right panel = percent differences between the two modelling solutions.

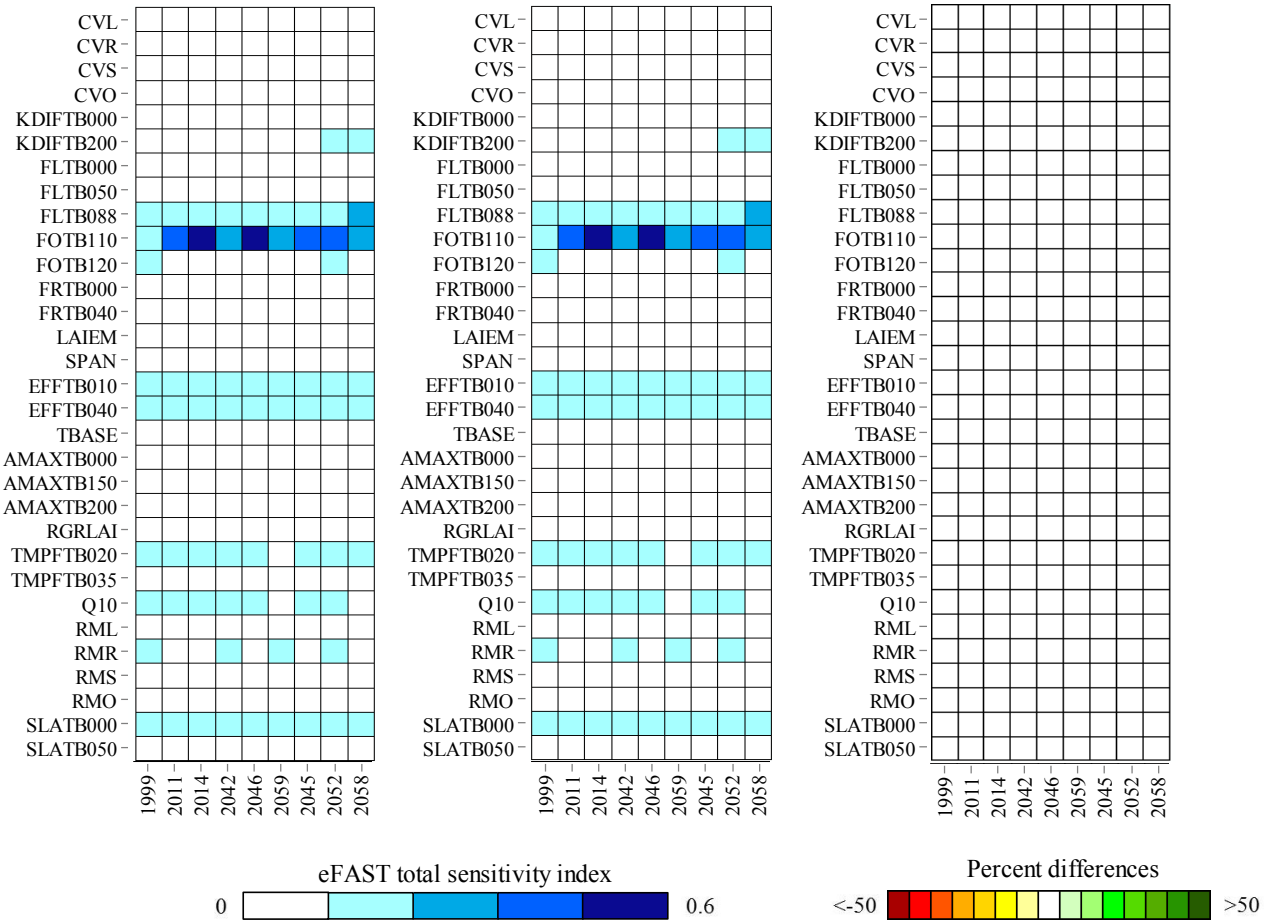

Figure S10. eFAST total sensitivity index for maize yield simulated with WOFOST at the selected years in Switzerland (Therwil site). Left panel = EMS (existing modelling solution); central panel = MMS (modified modelling solution); right panel = percent differences between the two modelling solutions.

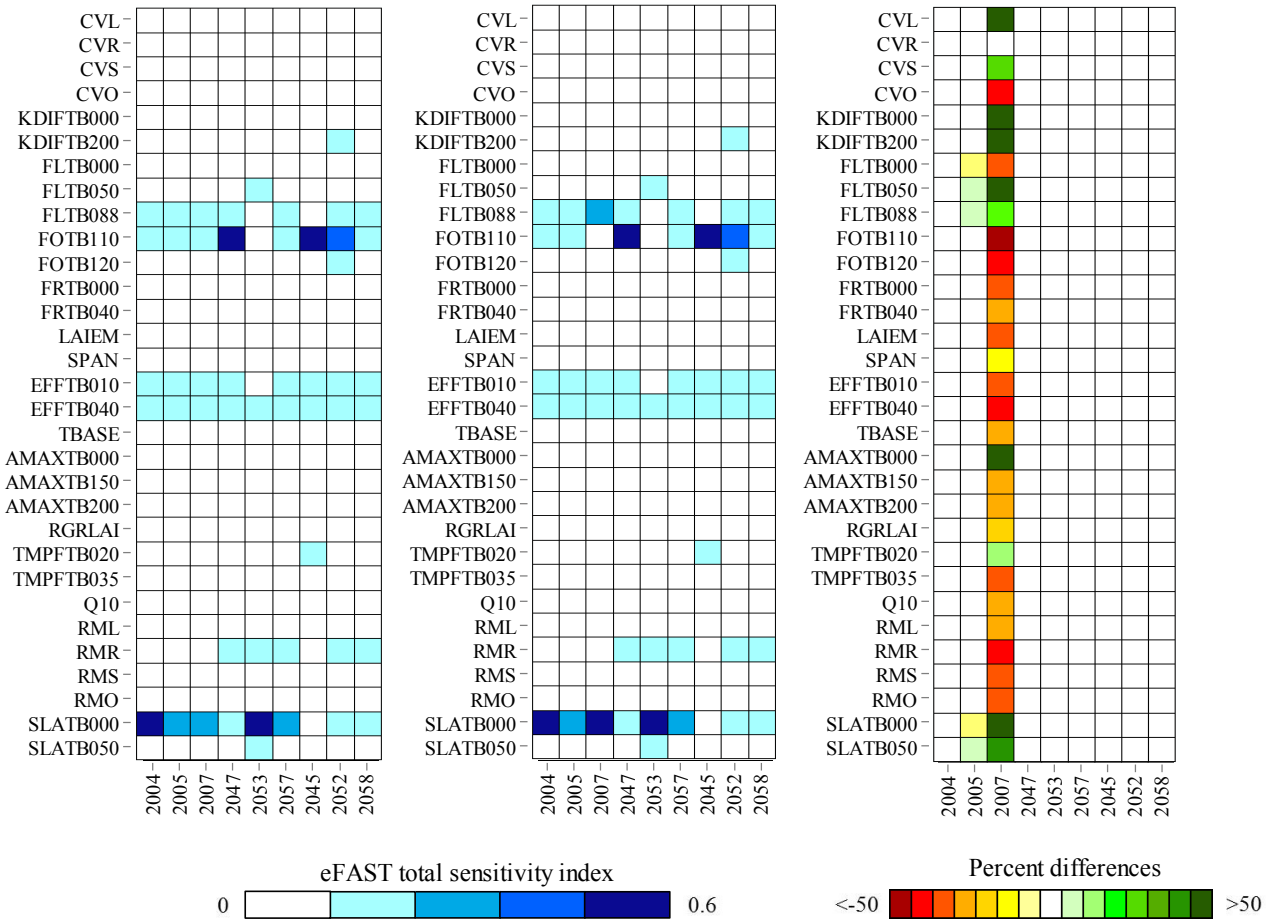

Figure S11. eFAST total sensitivity index for maize yield simulated with WOFOST at the selected years in Ukraine (Mironivka site). Left panel = EMS (existing modelling solution); central panel = MMS (modified modelling solution); right panel = percent differences between the two modelling solutions.

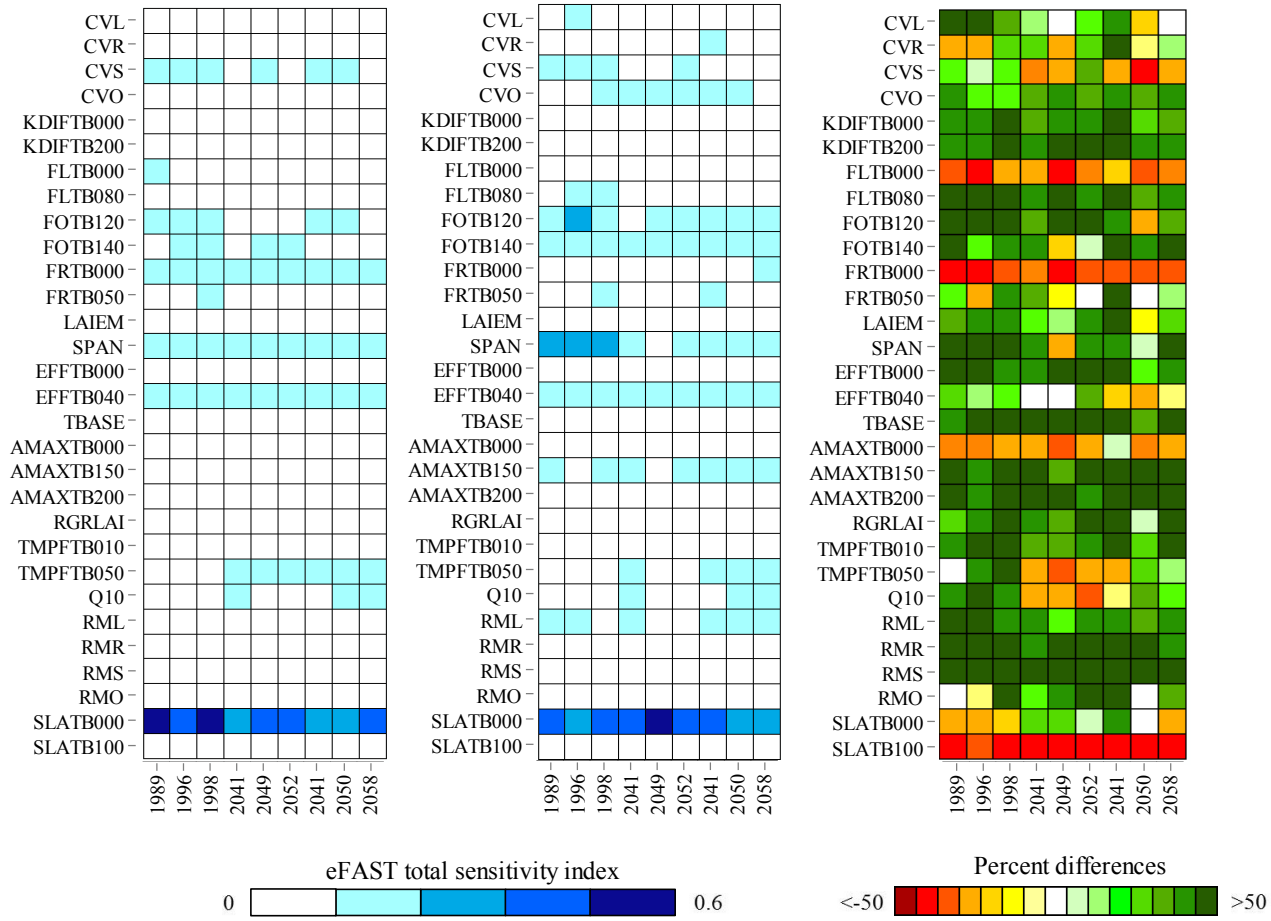

Figure S12. eFAST total sensitivity index for sunflower yield simulated with WOFOST at the selected years in Spain (Cordoba site). Left panel = EMS (existing modelling solution); central panel = MMS (modified modelling solution); right panel = percent differences between the two modelling solutions.

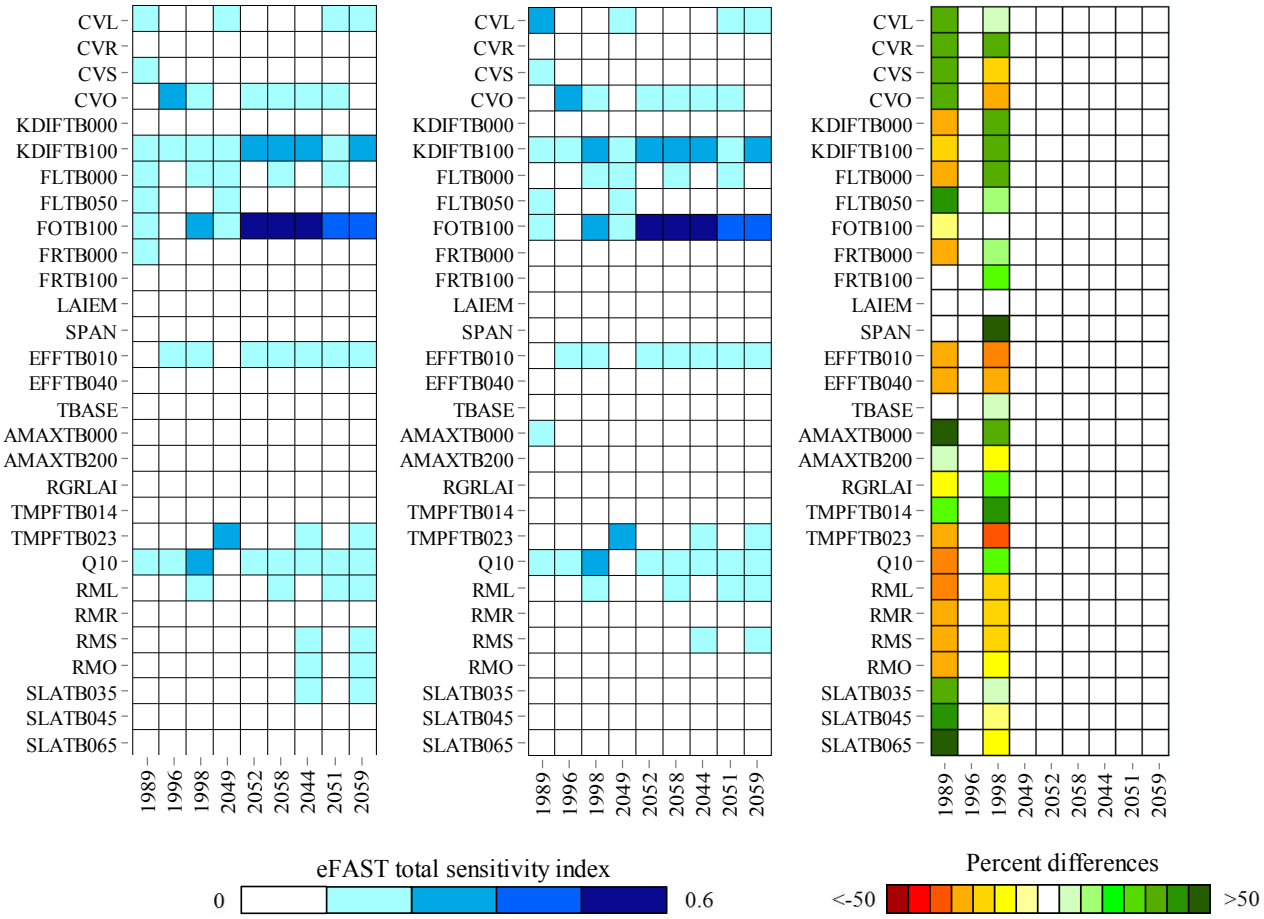

Figure S13. eFAST total sensitivity index for winter barley yield simulated with WOFOST at the selected years in Spain (Granada site). Left panel = EMS (existing modelling solution); central panel = MMS (modified modelling solution); right panel = percent differences between the two modelling solutions.

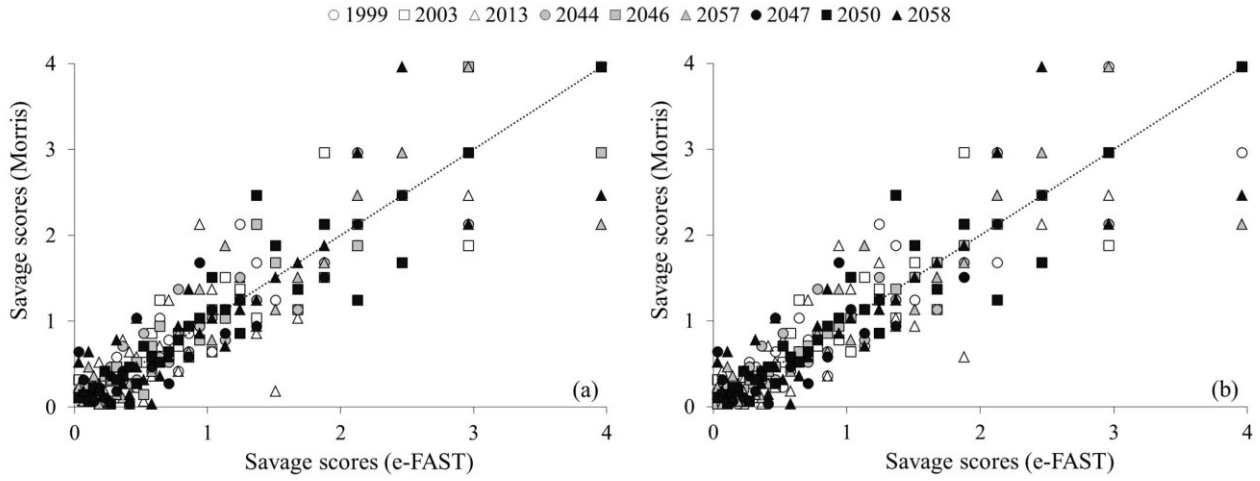

Figure S14. Comparison between results obtained with the Morris and eFAST sensitivity analysis methods for winter wheat simulation in Switzerland (Changins site). a) = savage scores for the EMS (existing modelling solution); b) = savage scores for the MMS (modified modelling solution); dotted line = 1:1 line.

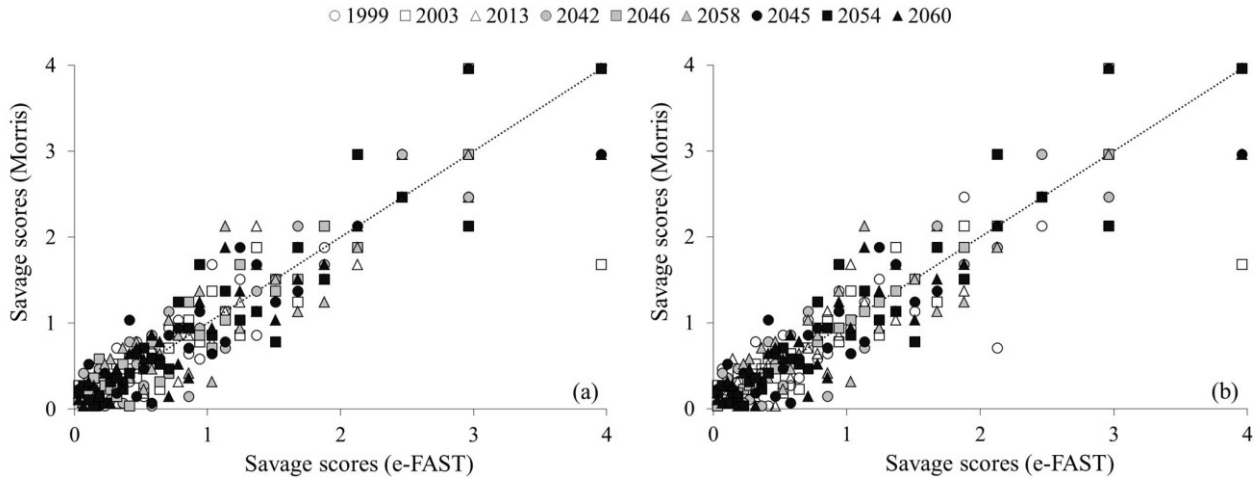

Figure S15. Comparison between results obtained with the Morris and eFAST sensitivity analysis methods for winter wheat simulation in Switzerland (Ellighausen site). a) = savage scores for the EMS (existing modelling solution); b) = savage scores for the MMS (modified modelling solution); dotted line = 1:1 line.

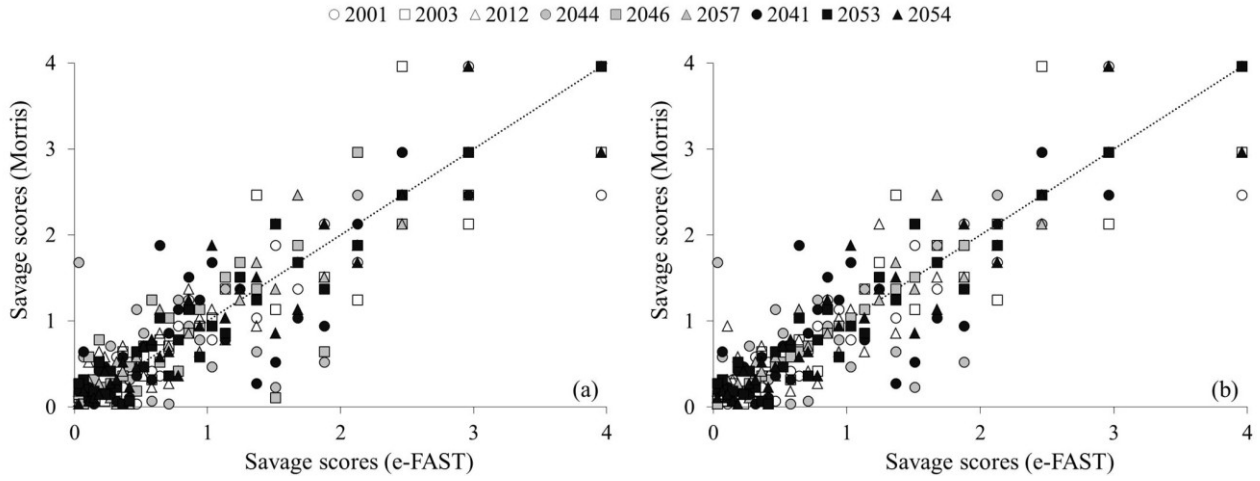

Figure S16. Comparison between results obtained with the Morris and eFAST sensitivity analysis methods for winter wheat simulation in Switzerland (Reckenholz site). a) = savage scores for the EMS (existing modelling solution); b) = savage scores for the MMS (modified modelling solution); dotted line = 1:1 line.

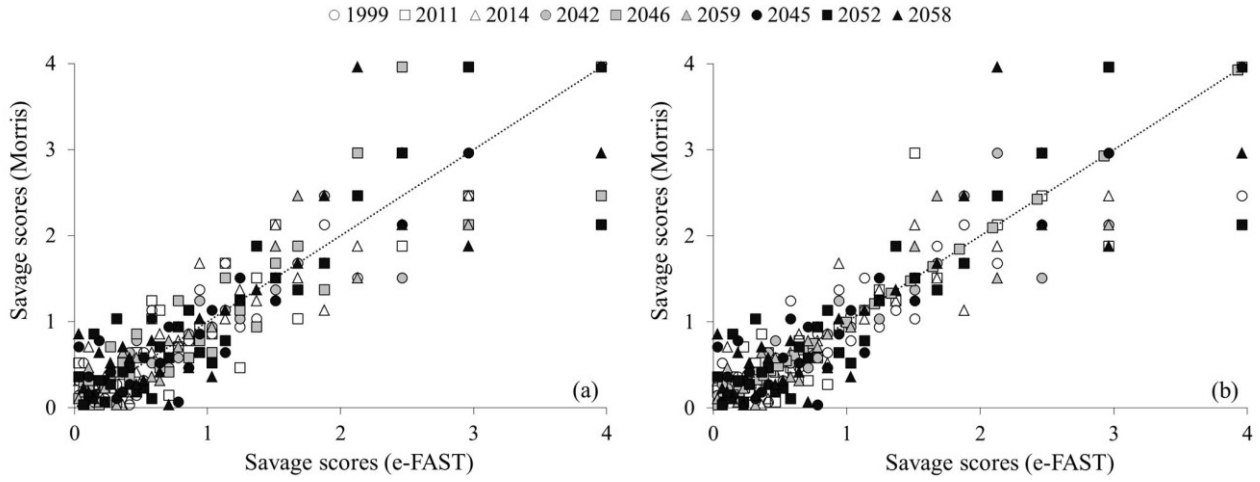

Figure S17. Comparison between results obtained with the Morris and eFAST sensitivity analysis methods for winter wheat simulation in Switzerland (Therwil site). a) = savage scores for the EMS (existing modelling solution); b) = savage scores for the MMS (modified modelling solution); dotted line = 1:1 line.

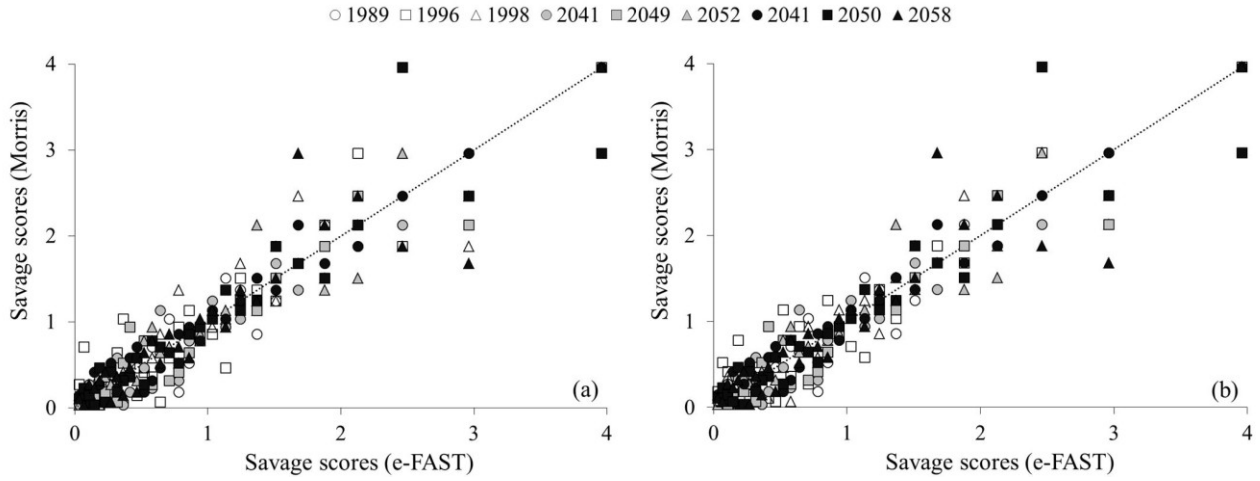

Figure S18. Comparison between results obtained with the Morris and eFAST sensitivity analysis methods for winter wheat simulation in Spain (Cordoba site). a) = savage scores for the EMS (existing modelling solution); b) = savage scores for the MMS (modified modelling solution); dotted line = 1:1 line.

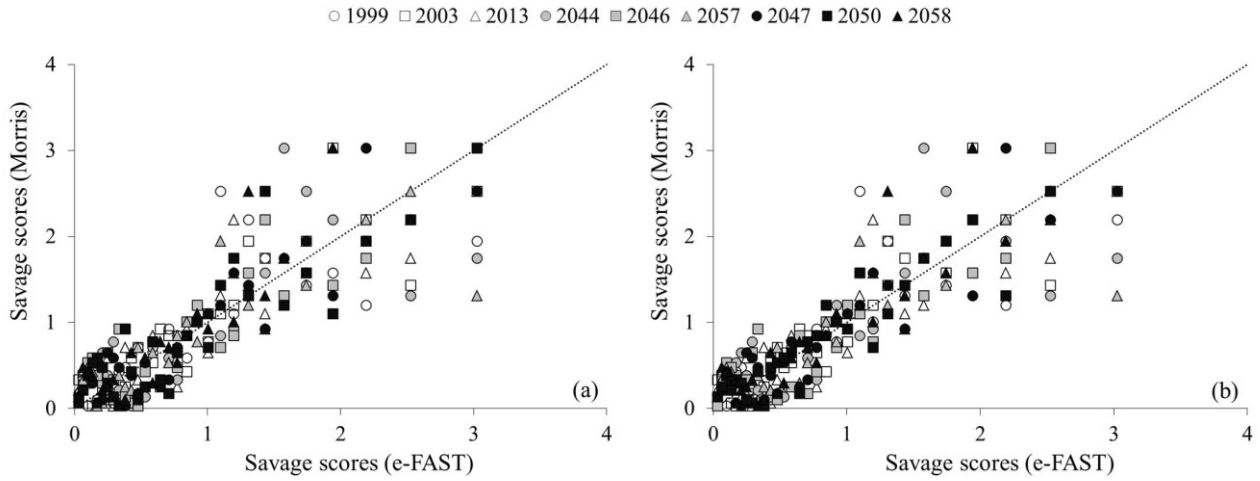

Figure S19. Comparison between results obtained with the Morris and eFAST sensitivity analysis methods for maize simulation in Switzerland (Changins site). a) = savage scores for the EMS (existing modelling solution); b) = savage scores for the MMS (modified modelling solution); dotted line = 1:1 line.

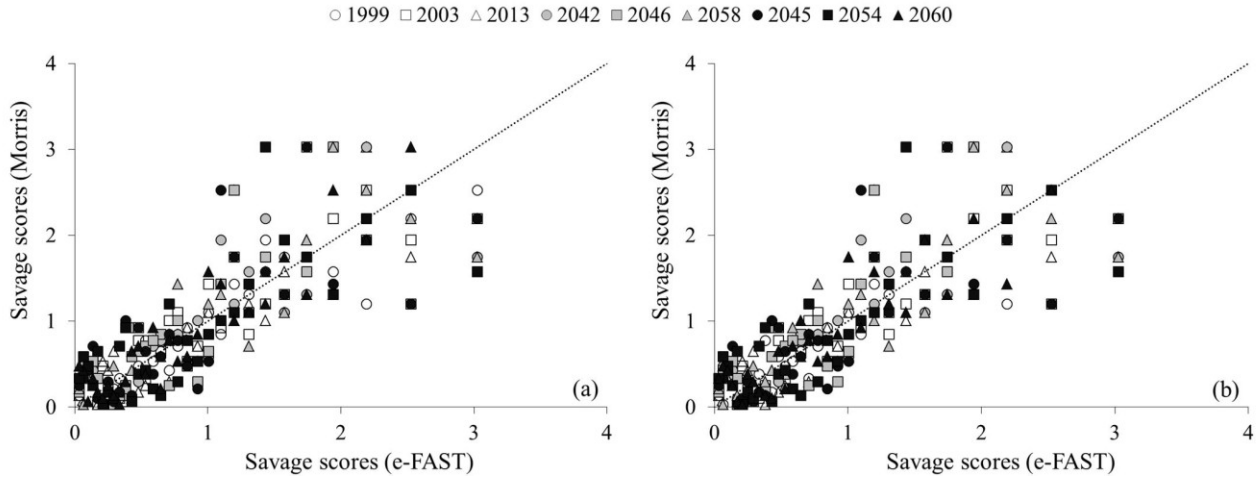

Figure S20. Comparison between results obtained with the Morris and eFAST sensitivity analysis methods for maize simulation in Switzerland (Ellighausen site). a) = savage scores for the EMS (existing modelling solution); b) = savage scores for the MMS (modified modelling solution); dotted line = 1:1 line.

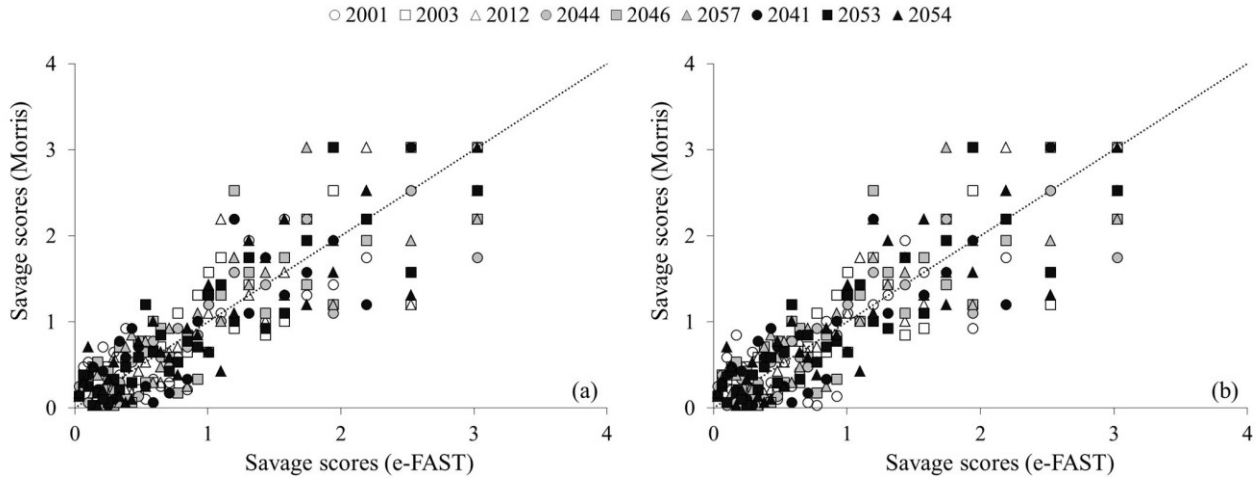

Figure S21. Comparison between results obtained with the Morris and eFAST sensitivity analysis methods for maize simulation in Switzerland (Reckenholz site). a) = savage scores for the EMS (existing modelling solution); b) = savage scores for the MMS (modified modelling solution); dotted line = 1:1 line.

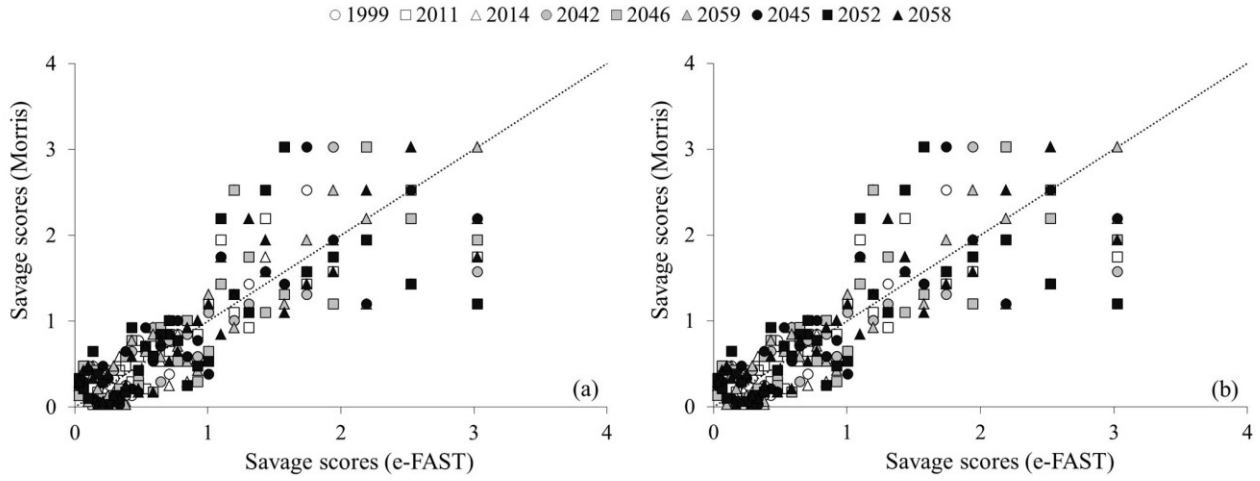

Figure S22. Comparison between results obtained with the Morris and eFAST sensitivity analysis methods for maize simulation in Switzerland (Therwil site). a) = savage scores for the EMS (existing modelling solution); b) = savage scores for the MMS (modified modelling solution); dotted line = 1:1 line.

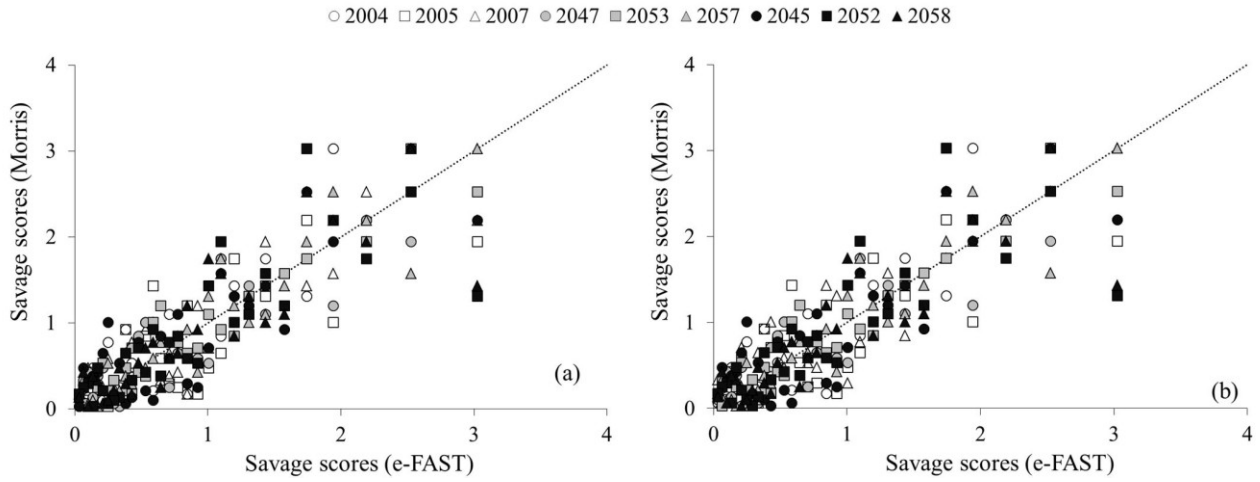

Figure S23. Comparison between results obtained with the Morris and eFAST sensitivity analysis methods for maize simulation in Ukraine (Mironivka site). a) = savage scores for the EMS (existing modelling solution); b) = savage scores for the MMS (modified modelling solution); dotted line = 1:1 line.

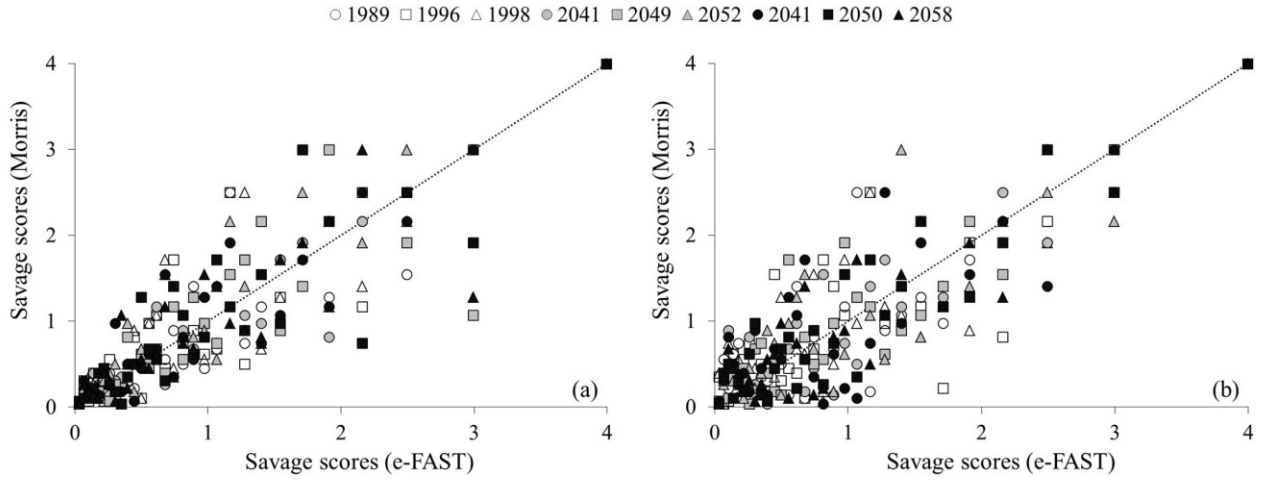

Figure S24. Comparison between results obtained with the Morris and eFAST sensitivity analysis methods for sunflower simulation in Spain (Cordoba site). a) = savage scores for the EMS (existing modelling solutions); b) = savage scores for the MMS (modified modelling solutions); dotted line = 1:1 line.

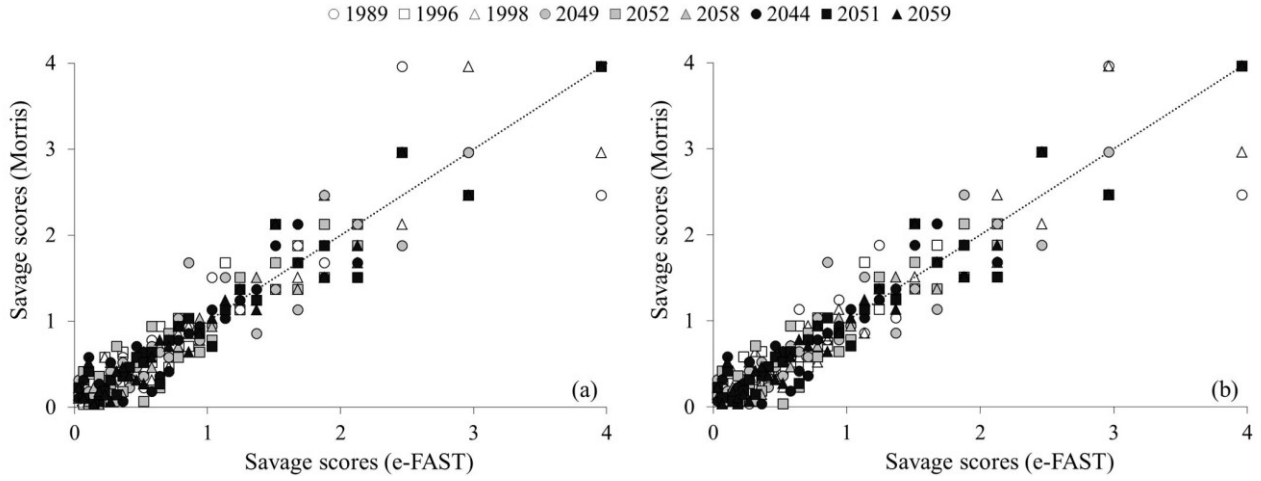

Figure S25. Comparison between results obtained with the Morris and eFAST sensitivity analysis methods for winter barley simulation in Spain (Granada site). a) = savage scores for the EMS (existing modelling solution); b) = savage scores for the MMS (modified modelling solution); dotted line = 1:1 line.

Chapter 4

QUANTIFYING REPEATABILITY AND REPRODUCIBILITY OF DIGITAL HEMISPHERICAL PHOTOGRAPHY FOR LAI ESTIMATES IN TREE SPECIES

Carlo Gilardelli, Francesca Orlando, Ermes Movedi,Roberto Confalonieri.

Submitted to Agricultural and Forest Meteorology

4.1 Abstract

Digital hemispherical photography (DHP) has been widely used to estimate leaf area index (LAI) in forestry. Despite the advancement in the processing of hemispherical images with dedicated tools, several steps are still manual and thus easily influenced by operator's subjectivity. The purpose of this study is to quantify the subjectivity component in the LAI estimates of woody canopies using the software Can-Eye. Following the ISO 5725 protocol, we quantified the repeatability and reproducibility limits defining the lower limits of the maximum accuracy obtainable in the estimation of LAI of a broad range of woody canopies differing from structure and dimension. Moreover we evaluated the effect of the segmentation method on LAI estimates of the same operator. The better results (restrained limits of repeatability and reproducibility), were obtained in case of high (>5) LAI values with limits which roughly correspond to 22% of the estimated LAI values. Poorer results were obtained in case of medium and low LAI values, with repeatability and reproducibility limits which exceeded the 40% of the estimated LAI values. Regardless of the LAI range explored, satisfactory results were achieved for trees in row-structured plantations (limits almost equal to the 30% of the estimated LAI values). The conducted paired t-test confirmed the relevant effect of the segmentation method on LAI estimates. Despite a non-negligible user effect, the precision metrics for DHP are consistent with those determined for other indirect methods for LAI estimates, thus confirming the overall reliability of DHP in woody canopies.

Keywords

Accuracy; digital hemispherical photography; leaf area index; precision, woody canopies.

4.2 Introduction

Leaf area index (LAI; total one-sided area of leaf tissue per unit ground surface) is widely recognized as a key variable for a broad range of agro-environmental studies, given its tight relationships with primary production (Duchemin et al., 2006), transpiration (Cleugh et al., 2007), energy exchange (Leuning et al., 2005), CO2 sequestration (Confalonieri et al., 2013), and with a variety of other eco-physiological processes (Asner et al., 2003). However, the direct measurement of LAI is often unfeasible, especially in operational context or when woody canopies are involved (Jonckheere et al., 2004). In these cases, LAI is usually estimated via indirect methods, based on the measurement of the amount of radiation (i) reflected/absorbed by (remote sensing techniques) or (ii) transmitted through the canopy (optical proximal instruments). The digital hemispherical photography (DHP) – like other methods based on image processing (e.g., PocketLAI, Confalonieri et al., 2013) – can be assimilated to the last category, although they derive gap fraction from image segmentation instead of the above-to-below canopy luminance ratio. DHP is one of the less expensive techniques and gives users the possibility to reprocess archives (e.g., correction of incorrect exposure, removal of unwanted objects) because of its permanent image recording. For these reasons and for the partial suitability of other indirect methods, it is widely used for LAI estimates in orchards and forest stands (Macfarlane et al., 2007; Khabba et al., 2009; Liu et al., 2013; Orlando et al., 2015). However, it is more time-consuming than other methods like the use of LiDAR images to estimate LAI (Tang et al., 2012; Zhao and Popescu, 2009); because of the need of asynchronous and not automated processing of the images acquired, which anyhow provides information to fully characterize the canopy in terms of openness and foliage density (Rich et al., 1993; Easter and Spies, 1994; Beaudet and Messier, 2002).

After acquisition, hemispherical images are processed using dedicated software packages (e.g., GapLightAnalyzer, Forest Renewal BC, Can-Eye), which classify pixels into two categories based on thresholds defined by the user through trial and error adjustments. Despite the widespread use of this method in forestry, some constraints still limit its reliability. For instance, the influence of camera exposure on LAI estimates (e.g., Englud et al., 2000; Zhang et al., 2005), the dependency on the view zenith angle detected by the device (Leblanc et al., 2005) and even the selection of the optimal segmentation thresholds, which is one of the main challenges (Jonckeere et al., 2004), involving high level of subjectivity due to the user's sensibility and experience (Glatthorn and Beckschäfer, 2014). Moreover, threshold identification can be influenced by the pixels' category (i.e., sky or green) from which the user decides to start (Jonckheere et al., 2005). Therefore, the

interference of these user-dependent steps on the accuracy of LAI estimates from DHP constitutes an important issue that deserve to be thoroughly investigated. Accuracy is composed by trueness and precision, the first being the agreement between real values and the means of replicated measurements, the latter – for in vivo methods – being the agreement within a series of replicated measurements, performed by the same user (repeatability) or by independent users under different conditions (reproducibility) (Confalonieri et al., 2014).

This study aims at quantifying the precision of DHP for LAI estimates in tree species, computing the limits of repeatability and reproducibility. These limits represent the lower limits of the maximum accuracy obtainable within several estimates of the same user and between estimates of different users. Given direct LAI measurement in tree canopies is unfeasible and the process of image acquisition (using standard protocol) should not lead to additional sources of uncertainty, we focused on the components of precision related with image processing.

4.3 Methods

The dataset used for precision determination on woody canopies was acquired with a smartphone Samsung GT-i9105 Galaxy S II Plus equipped with a fisheye lens AKASHI ALTLENS4IN1SG2,
during a previous work involving a wide range of canopy types (Orlando et al., 2015). In this study, only images from broad-leaved trees were used. The software used for image processing was Can-Eye (v. 6.314; www.avignon.inra.fr/can_eye; Weiss et al., 2004), which obtained the best results in a comparative study from Liu et al. (2013). Precision metrics were determined by following the adaptation of the ISO 5725 protocol (ISO, 1994) to in vivo field methods proposed by Confalonieri et al. (2014). To estimate the repeatability and reproducibility of DHP, three classes of broad-leaved tree species were considered (Table 1). This choice allowed complying with the ISO 5725 protocol, which indicates to perform the analysis on different batches of materials. Within each class, four plants were selected on the basis of the mean LAI values estimated by Orlando et al. (2015), by dividing LAI values into quartiles (25, 50, 75, 100%) and choosing one set of images within each quartile, in order to explore a wide ranges of LAI values (i.e., levels in the ISO 5725 protocol).

Table 1. Tree canopies used for determining digital hemispherical photography precision.

ID Class (as in Orlando et al., 2015)	Canopy class	Species for each quartile within the class
4	Broad-leaved trees in sparse or continuous canopy, with high scaffold branches	*Populus* spp. *Liriodendron tulipifera* L. *Fagus sylvatica* L. *Magnolia grandiflora* L.
3	Broad-leaved trees in plantation row, with low scaffold branches	*Populus* spp. *Robinia pseudoacacia* L. *Populus* spp. *Populus* spp.
1	Broad-leaved trees in sparse canopy, with medium scaffold branches	*Olea europaea* L. *Sorbus domestica* L. *Acer platanoides* L. *Fagus sylvatica* L.

The images of each of the entities reported in table 1 were processed by four independent users (laboratories A, B, C and D hereafter, according to the ISO 5725 terminology) familiar with the Can-Eye software in four different 10-day periods (four measurement replicates for each entity and for each user), leaving free choice for the Can-Eye segmentation method and threshold identification. According to ISO 5725, possible outliers were identified by applying the Cochran's (Cochran, 1941) and Grubbs' (Grubbs, 1969) tests, targeting outlying values detection, respectively, in variances and means from different laboratories.

According to the relationships between the test metrics and related tabulated values, laboratories were considered as non-outlying, stragglers (not enough different from others and thus maintained in following steps) or outliers (excluded from precision determination). Repeatability and reproducibility (as well as their relative values and limits; ISO, 1994) were quantified by targeting, respectively, the four sequential replicates from the same laboratory and all LAI values estimated by the laboratories that did not were identified as outliers for a certain entity.

Then, the uncertainty in LAI estimates due to the effect of the selected segmentation method was quantified by considering the whole 126-item dataset of tree broad canopy images from Orlando et al. (2015). To avoid mixing different sources of uncertainty, a single user processed all the images in this phase, using alternatively the two segmentation methods (based on sky or green pixel detection). A paired t-test was used to assess the significance of the differences due to the segmentation method.

4.4 Result and discussion

Table 2 shows the results of the statistical analyses performed on the three categories of tree canopies using DHP. The Grubbs' test led to identify one value as outlier (laboratory C for Magnolia grandiflora L.) and two values as stragglers (laboratories B and C for Olea europaea L.), whereas the Cochran's test led to identify laboratory B as outlier for Populus spp. The corresponding values were not used for repeatability and reproducibility determination.

Table 2. Precision (repeatability and reproducibility) of digital hemispherical photography (Can-Eye software) in estimating LAI in tree species. r: repeatability limit; RSDr: relative standard deviation of repeatability; R: reproducibility limit; RSDR: relative standard deviation of reproducibility. In case r was larger than R, R was set equal to r (Horwitz, 1995).

Canopy class	Species	Estimated values	Repeatability		Reproducibility	
			r	RSD_r	R	RSD_R
Broad-leaved trees in sparse or continuous canopy, with high scaffold branches	*Populus* spp.	1.45	0.65	15.89	0.69	17.04
	Liriodendron tulipifera L.	3.78	2.57	24.26	2.57	24.26
	Fagus sylvatica L.	3.33	1.81	19.35	1.81	19.35
	Magnolia grandiflora L.	5.22[a]	1.06	7.09	1.06	7.09
Broad-leaved trees in plantation row, with low scaffold branches	*Populus* spp.	1.48[b]	0.41	9.99	0.43	10.32
	Robinia pseudoacacia L.	2.32	1.12	17.24	1.12	17.24
	Populus spp.	3.66	0.85	8.27	1.09	10.69
	Populus spp.	3.72	0.55	5.25	0.73	7.03
Broad-leaved trees in sparse canopy, with medium scaffold branches	*Olea europaea* L.	0.82[c]	0.42	18.44	0.42	18.44
	Sorbus domestica L.	3.29	2.36	25.68	2.43	26.35
	Acer platanoides L.	5.11	1.66	11.58	1.66	11.58
	Fagus sylvatica L.	5.52	0.83	5.37	0.99	6.41

[a] Laboratory C is an outlier according to the Grubbs' test.
[b] Laboratory B is an outlier according to the Cochran test.
[c] Laboratories B and C are stragglers according to the Grubbs' test.

In general, the lowest values (and thus better) for repeatability and reproducibility limits were achieved for LAI higher than 5 (Fig. 1), corresponding to the 4th quartile of each canopy class (Table 1).

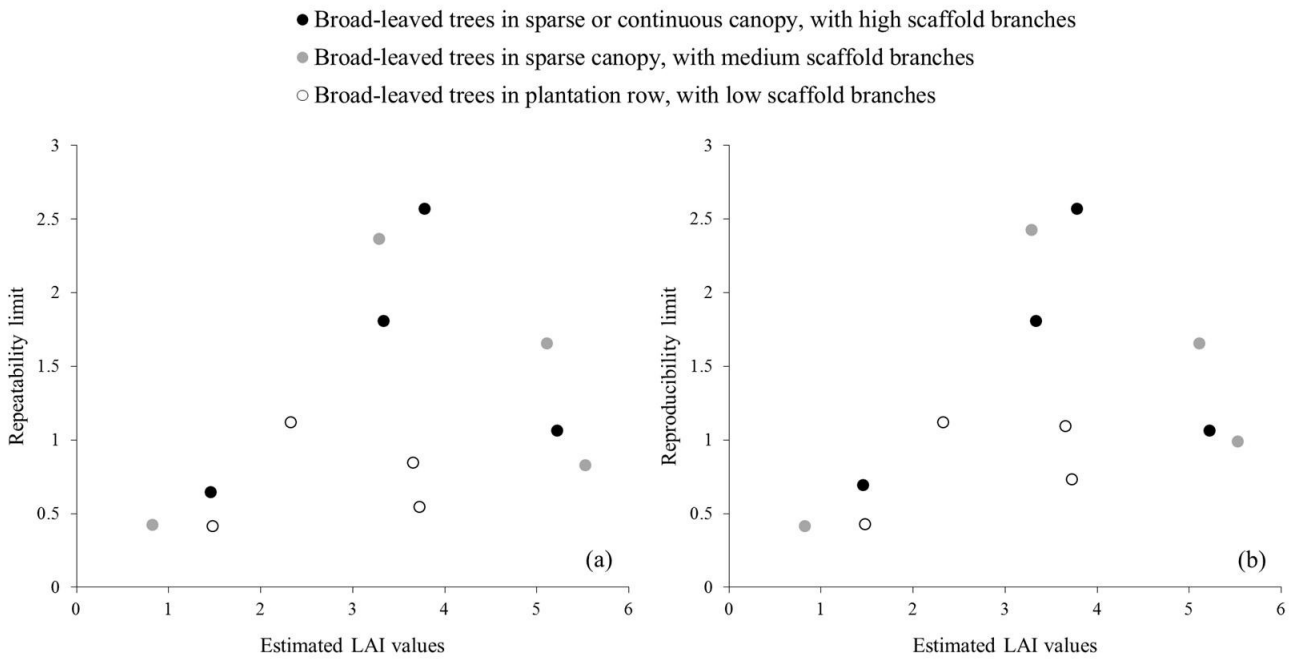

Figure 1. Relationships between repeatability (a) and reproducibility (b) limits of LAI estimates, and mean LAI values for the different canopy classes. Black circles refer to broad-leaved trees in sparse or continuous canopy, with high scaffold branches; grey circles refer to broad-leaved trees in sparse canopy, with medium scaffold branches; white circles refer to broad-leaved trees in plantation row, with low scaffold branches.

For this range of LAI values, indeed, mean values for repeatability and reproducibility limits were equal to 1.18, roughly corresponding to 22% of the estimated LAI. Results for medium (between 2.5 and 4) and low LAI values (lower than 1.5) were instead less satisfactory. For the medium LAI values, the average repeatability and reproducibility limits were equal to 1.54 and 1.56, corresponding to about 47% of the estimated LAI. Precision metrics were slightly better for low LAI values, with mean repeatability and reproducibility limits equal to 0.50 and 0.51 (almost 42% of the estimated values). These results suggest that, when hemispherical images were composed by a prevalent proportion of vegetation (high LAI values), the impact of the uncertainty in threshold definition during segmentation was negligible. In these cases, indeed, the limited relative presence of mixed pixels (or of image regions characterized by sky and vegetation pixels mixed up with a fine level of granularity) because of a large proportion of vegetation, simplified the determination of threshold values both between and within laboratories. On the contrary, when hemispherical images were either evenly composed by sky and vegetation pixels (intermediate LAI values) or characterized by an high proportion of sky (low LAI values), the determination of the threshold value – and thus the image segmentation – was more affected by the user sensibility and experience, because of a larger amount of pixels potentially subject to uncertain classification.

An exception to the positive relationship between mean LAI values and precision metrics was observed for broad-leaved trees in plantation row. For this class, intermediate value of the precision metrics were achieved, regardless of the mean LAI value (Table 2). Mean repeatability and reproducibility limits were indeed equal to 0.73 and 0.83, respectively (28.5% and 31.1% of the estimated LAI) and the corresponding relative standard deviations did not exceed 11.4%. Probably, the continuity of the canopy guaranteed by the planting layout and the position of branches (all the trees belonging to this canopy class were cultivated as short rotation forestry), as well as the protocol followed for images acquisition (Orlando et al., 2015), allowed obtaining close estimates both within and between laboratories, independently from the LAI values.

The values of precision metrics achieved in this study for DHP are slightly larger than those estimated – on homogeneous rice crops – by Confalonieri et al. (2013) for the smart app PocketLAI and for the AccuPAR ceptometer (Decagon, Pullman, WA, USA). The mean values of repeatability and reproducibility limits for DHP determined in this study (including all the canopy classes) were 1.19 and 1.25, respectively, whereas they were 0.80 and 0.82 for PocketLAI, and 0.73 and 0.82 for AccuPAR. Also, the variability among the precision metrics calculated for different samples for DHP was practically the same of that estimated for AccuPAR, whereas PocketLAI presented a larger variability. DHP achieved instead values for the precision metrics that were slightly better than those estimated for LAI-2000 (Decagon, Pullman, WA), regardless of the instrument 4- or 5-ring configuration (Confalonieri et al., 2013).

Figure 2 shows the comparison of LAI estimates obtained – for the whole dataset of DHP images collected by Orlando et al. (2015) – by the same user with the two segmentation methods (sky or green) available in the Can-Eye software.

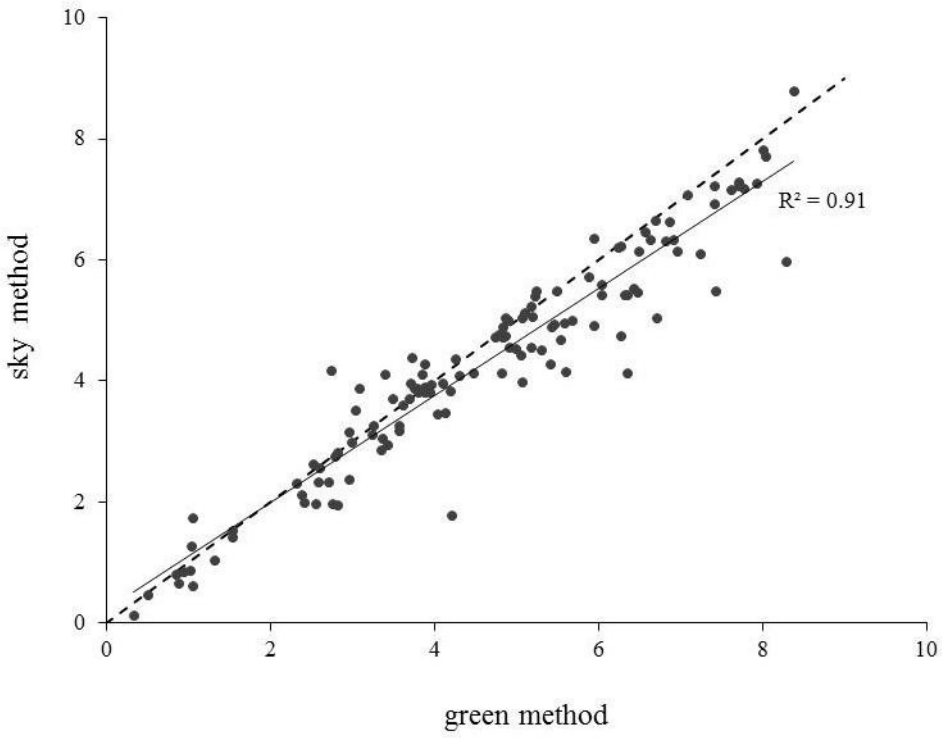

Figure 2. Comparison of LAI estimates obtained by the same user for 126 DHP images using the 'sky' and 'green' segmentation methods available in Can-Eye.

In more than 30% of the cases, the two segmentation methods led to differences in LAI estimates that exceeded 0.5, thus indicating that – beside the selection of thresholds – the choice of the segmentation method explain a large part of the variability in LAI estimates due to user subjectivity. This is confirmed by the paired t-test, which revealed that the differences between the two series of LAI estimates were significant ($p < 0.001$). In general, a tendency to estimate lower LAI values with the sky segmentation method was observed, likely due to the difficulty in threshold determination for the segmentation of pixels in the external profile of the canopies. Indeed, the corresponding portions of images were often characterized by canopy pixels that appeared very light because of light beams penetrating the vegetation. In these cases, the use of the sky method led to defining threshold values that segmented vegetation pixels as sky, thus determining lower LAI values compared to what achieved using the green segmentation method.

4.5 Conclusions

Here we quantified the source of uncertainty due to user's subjectivity, by calculating the repeatability and reproducibility of the segmentation procedure as offered by Can-Eye, the most popular software for DHP estimates. Indeed, compared to other indirect methods, the protocol for image acquisition is less subject to possible user's effects, which can instead affect LAI estimates during image processing. Although we observed a significant effect of the segmentation method

selected by the user, our study proved – once more – the reliability of LAI estimation with DHP. Indeed, this technique obtained values of repeatability and reproducibility consistent with those of the smart app PocketLAI and of the AccuPAR ceptometer, and slightly better than those estimated for LAI-2000. The best values for precision metrics were obtain in case of images characterized by high relative amounts of pixels entirely belonging to vegetation, whereas more uncertainty was observed for LAI estimates on images with many mixed pixels or with large image regions characterized by scattered presence of sky and vegetation pixels.

Chapter 5

DOWNSCALING RICE YIELD SIMULATION AT SUB-FIELD SCALE USING REMOTELY SENSED LAI DATA

Carlo Gilardelli, Tommaso Stella, Roberto Confalonieri, Luigi Ranghetti, Manuel Campos-Taberner, Francisco Javier Garcia-Haro, Mirco Boschetti.

5.1 Abstract

A deeper understanding of cropping system dynamics is fundamental to increase the sustainability of agricultural productions, and – to meet this goal – many resources have been recently invested on the refinement of technologies such as crop modeling and remote sensing. This study presents a system to estimate rice yields based on the integration of a biophysical model and remotely sensed products at sub-field scale. Leaf area index data derived from decametric optical imageries (i.e. Landsat-8, Landsat-7 and Sentinel–2A) were assimilated into the WARM model via automatic recalibration of model parameters at a fine spatial resolution (30 m × 30 m). The ability of the system to estimate rice yield was tested by comparing both output from default modelling and from assimilation solution with field data derived from yield maps acquired during 2014, 2015 and 2016 from about 40 paddy fields in northern Italy. The assimilation of remotely sensed information improved model performances (MAE = 0.6 t ha-1 and RRMSE = 13.8%) compared to what achieved using only the simulation model (MAE = 0.8 t ha-1 and RRMSE = 15.7%). Moreover, the system allowed to properly capture the within-field variability, thus to identify areas within each field characterized by different degrees of productivity.

Keywords

Yield predictions; Decision support system; Crop model; Remote sensing; Data assimilation

5.2 Introduction

The development and productivity of crops depend on a number of factors, such as cultivar/hybrid features, soil properties, weather conditions and agro-management practices (Lobell et al., 2005). Reliable tools able to capture the variability induced by changes in these factors are increasingly needed (Sørensen et al., 2010) to meet food demand of a growing population while complying with the most recent agricultural policies. Among available tools, process-based crop models have been widely used because of their capability to reproduce the interaction between genotypes and environmental factors under a variety of climate and management scenarios (Basso et al., 2001). Despite they are often used to run simulations at field scale or even on larger areas, these models estimate plant growth at point scale, i.e., on virtual areas for which all inputs are assumed to be uniform (Balcovič et al., 2013; Waha et al., 2015), thus requiring tailored strategies to properly assess spatial variability of yields and other relevant variables (Batchelor et al., 2002). A common approach is to split the simulation area into a number of spatial units small enough to reduce the uncertainty due to the unavoidable violation of the assumption of input homogeneity. The downside of this approach is the increased requirement of input data, which are often difficult and expensive to measure (Wong and Asseng, 2006). In order to reduce the acquisition costs for spatially distributed inputs and to allow the application of models at different scales, spatial variability can be analysed and transferred to the crop model using indirect methods. The recent advances in satellite technology and image processing make remote sensing one of the most intriguing techniques to downscale model applications (Lobell et al., 2015). Remote sensing can indeed provide information on how variables driving crop growth and development change in time and space (Panigada et al., 2014). Recent studies aimed at improving model performance using remotely sensed information focused on the spatial variability of crop reflectance (Launay and Guerif, 2005), crop nitrogen content (Jongschaap, 2006), sowing dates (Busetto et al., 2017), and the identification and quantification of possible stresses which affect crops (Baret et al., 2007). However, in most cases, the assimilation into crop models of remotely sensed information deals with estimates of leaf area index (LAI) (e.g., Casa et al., 2012; Zhao et al., 2013), i.e., the one-sided area of leaf tissue per unit ground surface (Campbell and Normann, 1989). The great interest for this variable is due to its influence on canopy spectral reflectance (Baret and Buis, 2007) and to its key role in mediating any relationship between plants and the atmosphere (Zhu et al., 2013). Moreover, LAI can be considered as a good indicator of canopy status, being closely linked with many other variables of interest, like aboveground biomass and plant nitrogen content (Casa et

al., 2012). Two main strategies are available to assimilate exogenous data in crop model simulations (e.g., Dorigo et al., 2007): (i) calibration, which entails the adjustment of model parameters or initial states by minimizing the error between exogenous data and corresponding model outputs, and (ii) forcing, which consists in periodic model re-initializations based on the replacement of simulated variables with exogenous ones. Both these methods have pros and cons, although the former is often preferred since it is able to preserve the conceptual and mathematical coherence during the entire simulation for both above- and belowground variables. To date, many studies succeeded in integrating remotely sensed data into dynamic models, even though the computational costs related to data assimilation via calibration is still a significant bottleneck for the dissemination of this technique in operational contexts (Dong et al., 2013).

Here we present the high-resolution application of a multiple downhill simplex optimization method (Nelder and Mead, 1965; Acutis and Confalonieri, 2006) to the assimilation of remotely sensed time series of LAI into the WARM rice model (Confalonieri et al., 2009). The aim is to improve model performances in predicting final yield while allowing for the simulation of within-field variability. With a view to applications at larger scale, computational costs are limited by performing assimilation only once in the growing season using all the available LAI data from the beginning of tillering to the end of flowering.

5.3 Material and methods

5.3.1 Study area and sub-field LAI data

The study area was located in Northern Italy in the Pavia province (latitude 45°15' N ± 1.5', longitude 8° 34' E ± 2', 112 m ± 15 m a.s.l.). Figure 1 shows the rice farm in which data were acquired, composed by 81 fields covering about 100ha cultivated with different varieties (i.e., Mare, Sirio, Augusto, Opale, Selenio, Sole, Ecco61, Oceano, Centauro).

Fertilizations, irrigations and treatments against weeds, pest and diseases guaranteed unlimiting conditions for rice growth and development. Sowings were carried out between mid-April and mid-May, depending on differences in cultivated varieties (long and short cycle) and on variability in meteorological conditions in the three years, whereas harvests were performed in late September or early October. For a sample of these fields (46, 40 and 37 fields in 2014, 2015 and 2016 respectively; fields with an area lower than 3000 m2 were excluded), information on cultivated rice varieties, sowing dates, techniques and yield maps estimated by a GPS equipped harvester were provided by the farmer.

Daily weather data were retrieved from a close weather station of the regional environmental agency "ARPA Lombardia" (data available here: https://www.dati.lombardia.it/Ambiente/Dati-sensori-meteo/647i-nhxk/data), assumed as representative for all the fields, since the latter are located in a flat area of about 20 km2. The LAI data used for assimilation into the model were generated during the EU FP7 ERMES project (http://www.ermes-fp7space.eu). LAI was derived from remote sensing high-resolution data such as Landsat-8 Operational Land Imager (OLI), Landsat-7 Enhanced Thematic Mapper (ETM+) and Sentinel–2A (S2A) Level 1C images (Table 1) by inverting a radiative transfer model (PROSAIL, Jacquemoud et al., 2009) specifically designed for rice crops. Details on the method and performance of retrieval algorithm can be found in Campos-Taberner et al. (2016) and Campos-Taberner et al. (2017).

An example of spatio-temporal variability of the LAI derived from satellite data is shown in Figure 2 as only one variety was sown in the same date in the three fields, within field spatial variability captured by satellite data can be mainly ascribed to local plant-soil interactions.

Table 1: Cardinality of exogenous LAI maps used in the assimilation process grouped by data source

Year	Start date	End date	ETM+	OLI	S2A	Tot.
2014	June 9th	October 23th	-	6	-	6
2015	April 1st	September 24th	6	6	-	12
2016	April 19th	September 27th	4	7	8	19

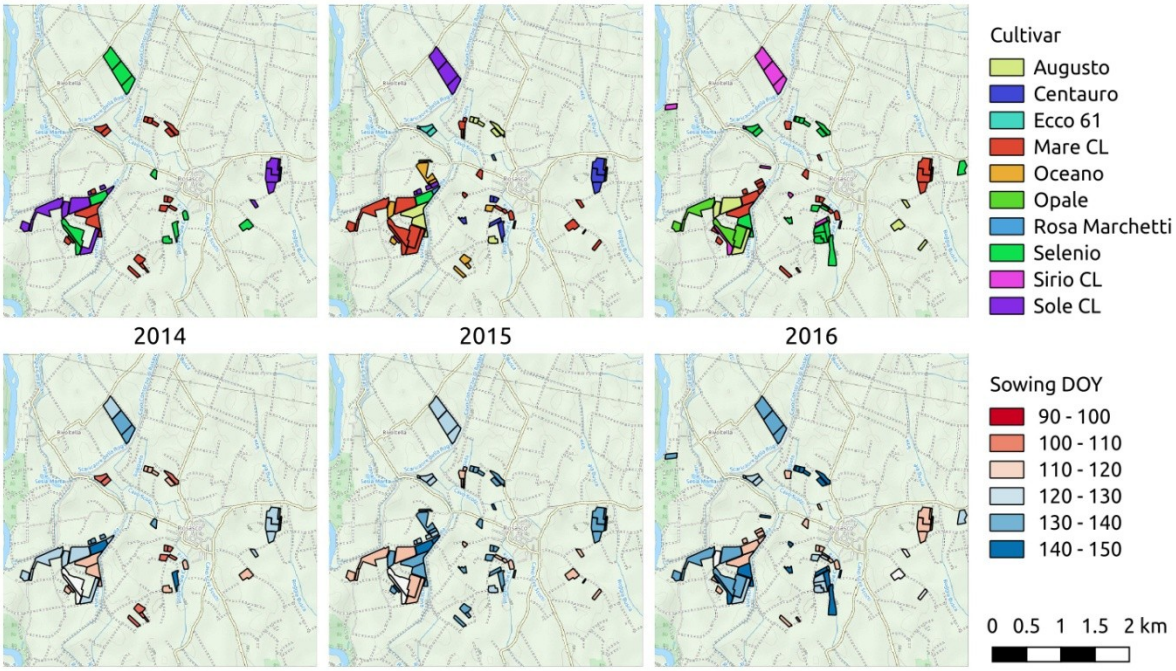

Figure 1: Fields distribution, cultivated varieties and sowing dates for the study area

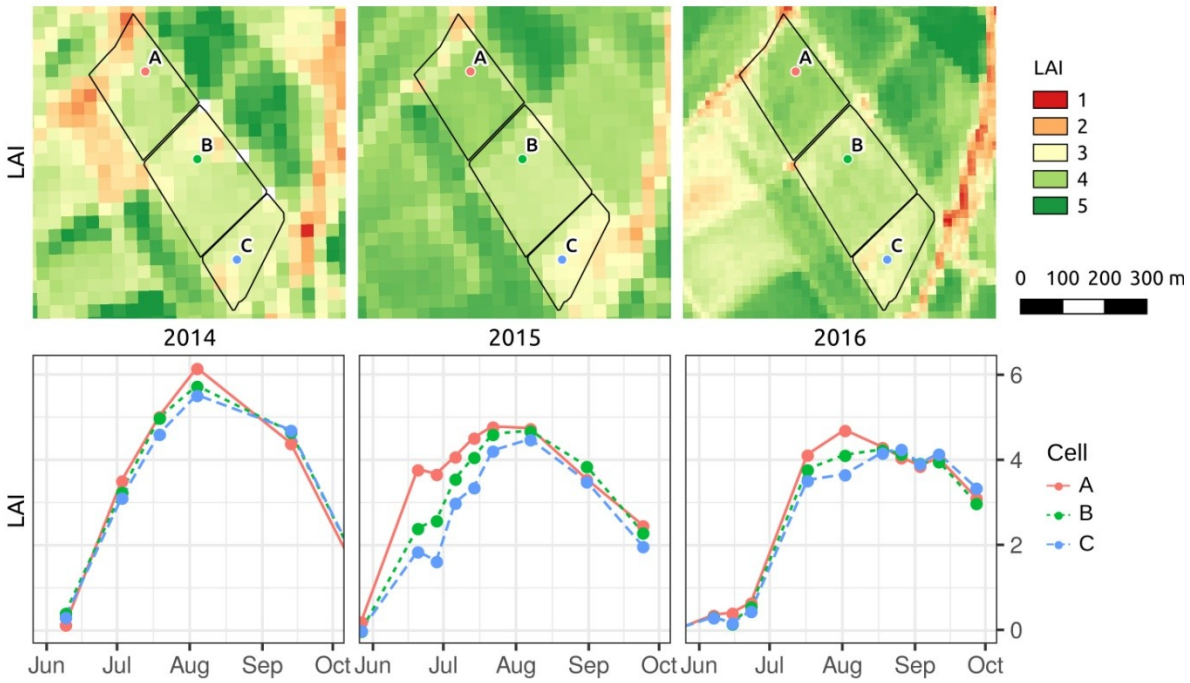

Figure 2: Example of LAI data spatial-temporal variability. Top panels show within field LAI variability as retrieved by OLI data (2014 and 2015) and Sentinel 2 (2016) in the first decade of July (DOY 184, 187 and 193 respectively). Bottom panels provide examples of LAI temporal profiles for the three specific locations.

5.3.2 Simulation model and assimilation procedure

The rice-specific simulation model WARM was selected, given its extensive use in the region for both research (e.g., Paleari et al., 2017) and operational purposes (Busetto et al., 2017). The model, fully described in the seminal literature, simulates photosynthesis (at daily or hourly time step) using a net photosynthesis approach, with radiation use efficiency modulated by temperature, atmospheric CO2 concentration, diseases, senescence, floret sterility, and saturation of enzymatic chains in case of high radiation levels. Daily accumulated biomass is partitioned to different plant organs using a set of parabolic and beta functions. Daily increase in green leaf area index (gLAI) is derived from the biomass partitioned to leaves and a development-specific specific leaf area (SLA). Leaf senescence is calculated by subtracting dead leaf area index units – when a thermal time threshold is reached – from total LAI.

The assimilation of exogenous LAI data was performed via recalibration of model parameters using a modified, multiple-start version of the downhill simplex method (Nelder and Mead, 1965). The simplex is a geometric concept with N+1 vertices in an N-dimensional parameter hyperspace; it moves through this space based on reflection, contraction, and expansion, following the gradient of an objective function. Changes to the standard version of the simplex deal with the use of multiple starting points (to reduce the risk of falling in local minima) and the adoption of boundaries to avoid the selection of parameter values outside a reasonable range (Acutis and Confalonieri, 2006). The relative root mean square error (RRMSE, obtained as the ratio between RMSE and the mean of observations; %) was used as objective function. Assimilation was performed using only LAI data estimated between beginning of tillering and end of flowering to avoid background effect on LAI estimates in case of limited vegetation (e.g., during early growth) or with the presence of senescent tissues (Haboudane et al., 2004). Phenological stages where dynamically estimated from the model for each combination of cultivated variety, sowing date and meteorological data, and then used to select relevant LAI data for each simulation unit. Parameters considered in the recalibration process were maximum radiation use efficiency (RUE, g MJ-1), being the most influential parameter in crop modelling as indicated by a previous sensitivity analysis study (Confalonieri et al., 2010), and specific leaf area at emergence (SLAini, m2 kg-1) and at tillering (SLAtill, m2 kg-1), both being strictly related with LAI dynamics. The other parameters were kept to the default values (Appendix A) for Indica- and Japonica-type cultivars, developed using data from dedicated trials carried out within the EU FP7 ERMES project.

For the simulations without assimilation, inputs were at field-scale were homogeneous, thus requiring one simulation for each combination field × year. In the case of assimilation of exogenous LAI data each field was further divided in 30 × 30 m simulation units, corresponding to Landsat 7/8 spatial grid. Sentinel-2A LAI retrieved, at 10 m spatial resolution, were aggregated to the same spatial resolution. Yield data collected by the harvester were spatially interpolated to obtain high resolution (2 × 2 m) maps; and aggregated on the same 30 m × 30 m regular grid, in order to allow for the evaluation of simulated yields and their variability within each field. The agreement between observed and simulated yields was first quantified at field level using the mean absolute error (MAE) and the relative root mean square error (RRMSE). In addition to these agreement indices, for each 30 m × 30 m simulation unit the relative bias error (RBE, eq.1) was applied to quantify the system ability to describe the yields spatial variability, because of its capability to indicate direction and magnitude of the bias.

$$RBE_i = \left(\frac{P_i - O_i}{O_i}\right) \cdot 100 \quad [1]$$

where P_i (t ha-1) and O_i (t ha-1) are the simulated and observed yield values for the i-th simulation unit.

In order to quantify the overall improvements in simulated yields due to LAI data assimilation, the integrals between -15% and +15% of the RBE probability distribution functions (∫RBE) were computed for each combination rice cultivar × year. This allowed to quantify the percentage of simulation units for which the error in yield simulation is less than 15% of the observed value, considered as a typical uncertainty associated with the estimation of yield in field experiments (Belder et al., 2007; Li et al., 2015).

5.4 Results and discussion

Yield simulation at field level was overall satisfactory using both approaches 1) default parameterizations and 2) LAI assimilation for parameters recalibration. Best results using the default parameterizations were achieved for the datasets collected in 2014, MAE and RRMSE being 0.70 t ha-1 and 14.5%, respectively. To a lesser extent, error metrics demonstrated the reliability of default parameterization also for datasets collected in 2015 (MAE = 0.85 t ha-1; RRMSE = 17.4%) and 2016 (MAE = 1.00 t ha-1; RRMSE = 17.5%). The assimilation of remotely sensed LAI data allowed improving model performances for 2015 (MAE = 0.74 t ha-1; RRMSE = 15.5%) and 2016 (MAE = 0.76 t ha-1; RRMSE = 12.9%). On the other hand, no relevant improvements were achieved through LAI assimilation for the 2014 datasets (MAE = 0.68 t ha-1;

and RRMSE = 14.9%), with respect to the results obtained using the default parameterizations. However, the available dataset of LAI estimated in 2014 (6 dates, of which 3 in the period tillering – flowering, used for calibration) was noticeably lower to 2015 (12 dates, of which 6 in the period tillering – flowering, suitable for calibration) and 2016 (19 samples, of which 9 in the period tillering – flowering, suitable for calibration). The availability of lesser LAI data for calibration, could lead to a no sensible improvement of assimilation procedure with respect to well calibrated modelling solution. These results are comparable with those obtained in other recent studies about the improvement of maize yield at field level through the integration of remotely sensed information in crop models (Ines et al., 2013; Zhao et al., 2013; Li et al., 2014). In all these studies the inclusion of remotely sensed data improved modelling performances with a reduction of RRMSE ranging between 12% and 16%.

The contribution of LAI assimilation can be better appreciated when data are analyzed at full resolution, comparing observed and predicted yield values for each simulation unit. Figure 3 shows the distributions of $\mathrm{RBE_i}$ values (i being the simulation unit) for the two approaches. LAI assimilation produced errors generally distributed more centrally around zero if compared to those calculated with the default parameterizations. This demonstrates the higher reliability of the assimilation-based simulations to reproduce the spatial distribution of rice yields, although over- and under-estimations were still present (tails of the distributions in Fig. 3). However, most of these errors were calculated for simulation units located at the margins of the rice fields, where border effects may greatly affect growth dynamics, as well as factors not accounted for by the simulation model (e.g., effects of traffic due to tractors and other machineries, anomalies in fungicide distributions). Moreover, these areas are the ones characterized by pixel mixture in satellite data with 30 meter spatial resolution. These factors contribute to make LAI estimation close to the field border less reliable and more affected by estimation uncertainty.

Only in two cases out of 14 (Augusto and Selenio varieties in 2015 and 2016, respectively), a worsening in model performance was observed when remotely sensed LAI data were assimilated. In these two cases, some inconsistencies were noticed in the relationship between remotely sensed LAI values and observed yields (data not showed). Many authors highlighted – although to a different extent – positive relationships between LAI and biomass values, and thus – under unlimiting conditions and without the presence of stressors leading to sterility – between LAI and yield (e.g., Takai et al., 2006; Li et al., 2009). Such relationship was not observed for the Augusto variety in 2015. Compared to the results obtained in 2014 for the same variety, remotely sensed

LAI at the end of flowering in the 2015 was higher, in light of the favorable weather conditions experienced by the crop during most of the season (i.e., between April and August: +1.93°C for average maximum temperature; +1°C for average minimum temperature; +1.46 MJ m-2 for global solar radiation). However, the larger LAI values did not correspond to larger observed yields, being yields in 2014 and 2015, respectively, equal to 5.32 ± 0.57 t ha-1 and 4.90 ± 0.53 t ha-1. This can be explained by possible errors in LAI estimates and, more likely, by factors that limited 2015 yields for that variety, not taken into account by the model (e.g., effects of the previous cover crop, extreme weather events near harvesting which deplete the productions). A similar inconsistency was observed for Selenio variety in 2016. Also in this case, 2016 was warmer (+0.8°C for average maximum temperature for the period April-August) and with higher radiation (+3.89 MJ m-2) compared to 2014, when Selenio variety was also sown. However, despite observed yields in 2016 were – as expected – larger than those recorded in 2014 (even by about 2 t ha-1), remotely sensed LAI values at the end of flowering were lower. This is the reason why assimilation of remotely sensed LAI led, in this case, to a general underestimation of yields for Selenio in 2016 (Figure 3).

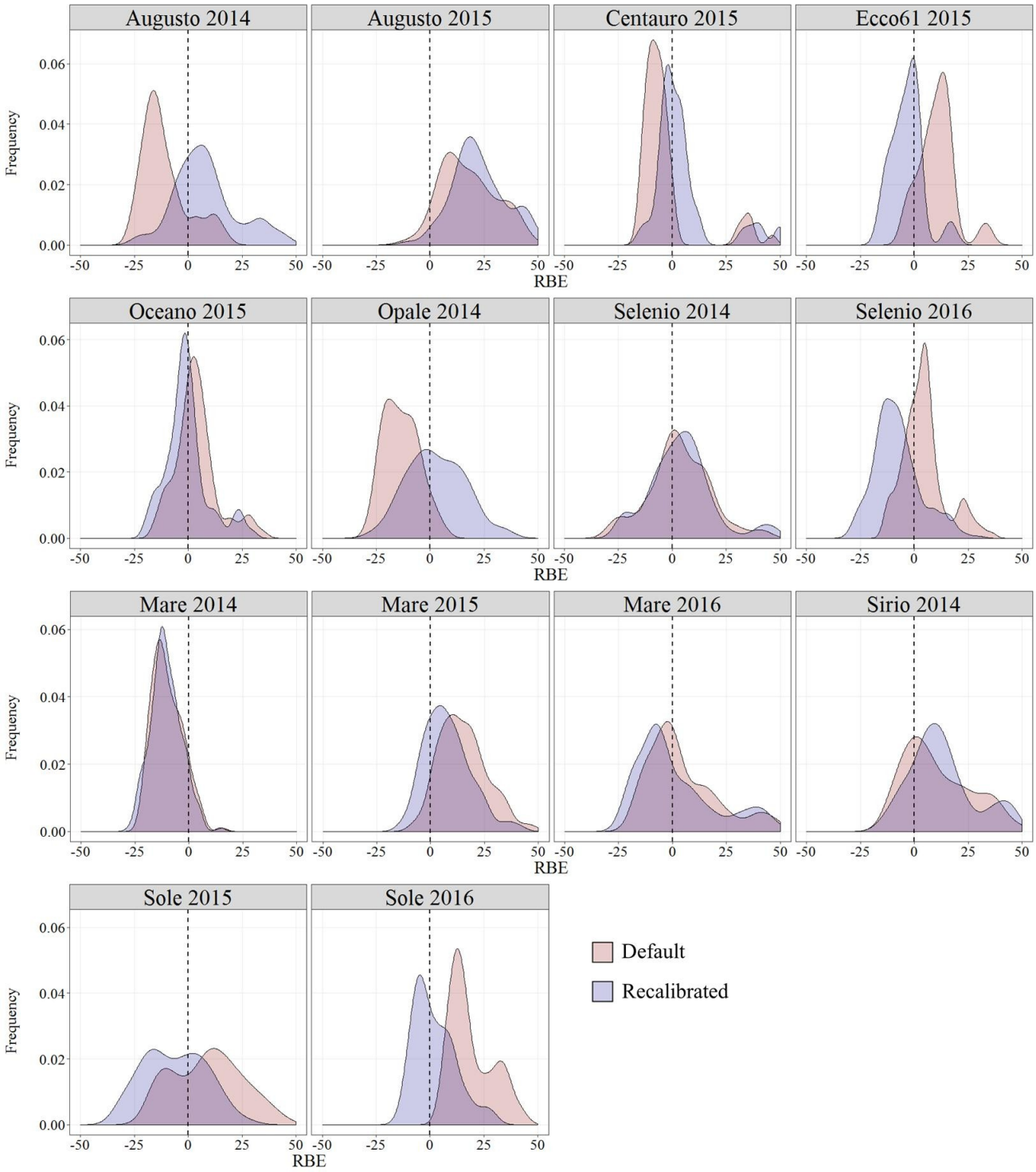

Figure 3. Frequency distributions of relative bias error (RBE; %) resulting from the comparison between observed and simulated yields for each simulation unit (corresponded to the cells of a 30 m × 30 m regular grid). Red and blue refer, respectively, to the values of RBE calculated for simulations performed with the default parameterizations and for those benefiting from LAI assimilation. Dotted black (vertical) lines indicate RBE = 0%, i.e., perfect agreement between observed and simulated yield values.

The good results achieved by assimilating remotely sensed LAI data were further underlined by the indices of agreement between simulated and observed yields (Table 2). Indeed, the model

capability to reproduce yield distribution within each field improved in almost all the cases, with mean values for MAE and RRMSE equal to 0.71 t ha-1 and 14.7% (while MAE = 0.80 t ha-1 and RRMSE = 15.7% using default parameterizations). Excluding the two cases discussed above (Augusto in 2015 and Selenio in 2016) where inconsistencies between LAI and observed yields were noticed, LAI assimilation overall led the indices of agreement to improve to a greater extent (average MAE and RRMSE = 0.66 t ha-1 and 13.8%).The use of the integrals between -15% and +15% of the RBE probability distribution functions ($\int \mathrm{RBE}$) confirmed the improvement in model performance when remotely sensed LAI were assimilated. The average $\int \mathrm{RBE}$ after the assimilation was indeed 0.70, whereas it was 0.65 with the default parameterizations. Even in this case, excluding the two cases discussed above, the average $\int \mathrm{RBE}$ would have been equal to 0.73, i.e., in 73% of the cells, the RBE for rice yield simulation was lower than 15%.

Table 2. Performances of the WARM model for simulating spatially distributed rice yields using the default parameterization (default) and after the assimilation of remotely sensed LAI data (recalibrated). $\int \mathbf{RBE}$ = integral of Relative Bias Errors between -15% and +15%; MAE = Mean Absolute Error (t ha-1; minimum and optimum = 0, maximum = +∞); RRMSE = Relative Root Mean Square Error, obtained as the ratio between RMSE and the mean of observations (%; minimum and optimum = 0, maximum= 100); default = results obtained with default parameterizations; recalibration = results obtained after parameters recalibration for LAI assimilation.

	Simulation units (# of fields)	∫ RBE		MAE		RRMSE	
		default	recalibration	default	recalibration	default	recalibration
Augusto 2014	118 (6)	0.53	0.69	0.78	0.63	16.4	15.1
Augusto 2015	94 (9)	0.46	0.26	0.85	1.19	20.1	26.9
Centauro 2015	61 (3)	0.74	0.78	0.73	0.61	16.7	16.6
Ecco61 2015	17 (2)	0.98	0.90	0.69	0.38	12.2	8.18
Oceano 2015	83 (8)	0.86	0.84	0.47	0.46	10.6	10.5
Opale 2014	52 (3)	0.54	0.70	0.78	0.57	16.8	12.9
Selenio 2014	146 (15)	0.68	0.70	0.64	0.67	15.3	16.2
Selenio 2016	247 (10)	0.86	0.69	0.58	0.81	9.59	13.9
Mare 2014	176 (16)	0.73	0.73	0.74	0.72	12.9	13.4
Mare 2015	278 (13)	0.52	0.75	0.98	0.63	18.2	12.6
Mare 2016	145 (18)	0.64	0.62	0.96	1.00	16.7	15.9
Sirio 2014	135 (6)	0.61	0.61	0.67	0.71	16.4	17.0
Sole 2015	118 (5)	0.53	0.60	1.09	1.01	17.0	16.7
Sole 2016	166 (9)	0.44	0.88	1.27	0.52	20.3	9.23

Results for the three sample fields shown in Figure 4 demonstrate the effectiveness of LAI assimilation for describing the within-field spatial variability of yields. Since the simulations obtained with the default parameterizations were performed using a single set of inputs (Fig. 4b), simulated yield is constant across field, without the possibility to reproduce the observed yield variability (Fig. 4a). On the contrary, LAI assimilation allowed to discriminate and quantify between highly and poorly productive areas (Fig. 4**Figure**c), thus providing useful information on the between-field and intra-field yield variability. As an example, looking at the upper field, LAI

assimilation allowed to properly simulate the higher yields in the top-right part of the field; the same can be discussed for the high productivity in the bottom-left part of the central field and for the low productivity in the bottom field.

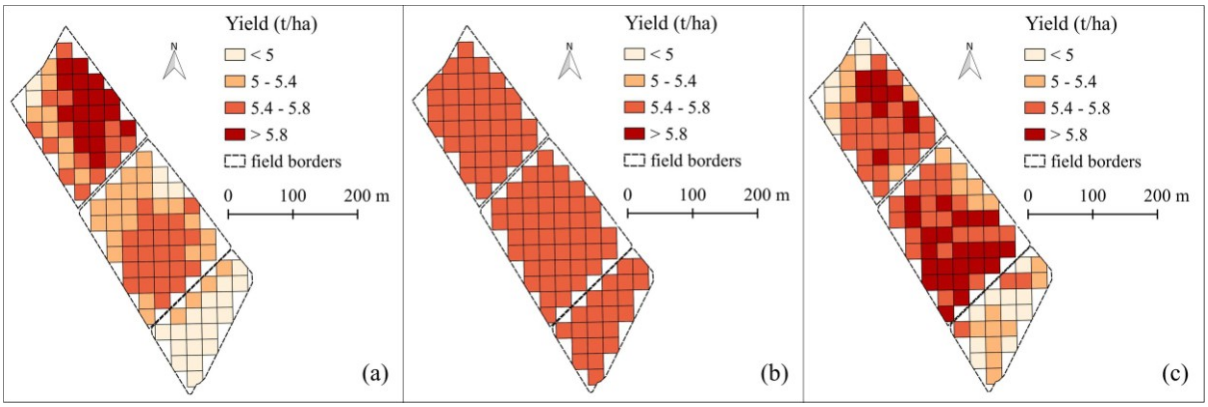

Figure 4: Spatially distributed yields (t ha-1) in three sample fields. Observed yields (a); simulated yields with the default parameterizations (b); simulated yields after remotely sensed LAI assimilation (c).

5.5 Concluding remarks

The parameterizations for the WARM model developed within the ERMES project demonstrated their reliability for the simulation of rice yield at field level, overall achieving satisfactory evaluation metrics. The assimilation of remotely sensed LAI data allowed improving model performances, although to a moderate extent, given default parameterizations were already developed using field observations collected under conditions very similar to those characterizing this study. For this reason, the contribution of LAI assimilation in case of less specific parameter sets is expected to be more impacting in yield estimation. Moreover, LAI assimilation allowed reproducing yield variability within fields, providing the model with an implicit spatial dimension despite all other inputs were constant at field level. Despite remotely sensed LAI data were used to recalibrate model parameters just once during the growing season, the agreement between simulated and observed within-field yield distributions (at 30 m × 30 m resolution) can be considered satisfactory. This makes this approach one of those eligible to provide high-resolution estimates of crop productivity. In the perspective of a more rationale use of inputs, possible applications of the methodology evaluated here deal with precision agriculture. Considering the fact that errors resulted higher at the margins of the rice fields (where the effect of mixed pixels is higher), it is reasonable to expect that the improvement of LAI spatial resolution could lead to a better estimations of the yield spatial variability. This will be possible from 2018, with the use of Sentinel-2A (here used for 2016) and Sentinel-2B (available since July 2017): the joint use of these two datasets will allow to have more dense time series at a better spatial resolution (10 × 10 m),

so reducing the effect of mixed pixels and allowing to estimate spatial variability also for smaller fields. Nonetheless, some aspects need to be further investigated, like those related with the inconsistencies found for two datasets (variety Augusto in 2015 and Selenio in 2016) in terms of relationships between LAI expansion and biomass/yield production, and between crop state variables and canopy reflectance properties.

Acknowledgement

This study was supported by the ERMES FP7 project (http://www.ermes-fp7space.eu) funded by the European Union Seventh Framework Program (FP7/2007-2013) under Grant 606983.

5.6 Appendix

Appendix A. Parameters values used as default for the WARM model. The Japonica-early parameter set was used for the varieties Augusto, Opale and Centauro, whereas the Japonica-medium was used for Selenio and SoleCL. Indica-medium and Indica-late parameter sets were instead used, respectively, for SirioCL and Ecco61, and for MareCL and Oceano.

Parameter	Japonica early	Japonica Medium	Indica medium	Indica late
Specific Leaf Area at Emergence	36	28	34	28
Partitioning to Leaves at Emergence	0.61	0.67	0.65	0.6
PAR to Global Radiation Factor	0.5	0.5	0.5	0.5
Specific Leaf Area at Tillering	19	17	16	17
Maximum Panicle Height	66.24	66.24	66.24	66.24
Growing Degree Days to Reach Emergence	80	120	100	100
Growing Degree Days to Reach Flowering	840	830	830	1050
Growing Degree Days to Reach Maturity	340	400	400	390
Growing Degree Days to Reach Harvest	100	100	100	100
Base Temperature for Development	11	11	11	11
Optimum Temperature for Development	25	25	25	25
Maximum Temperature for Development	42	42	42	42
Photoinhibition	1	1	1	1
PhotoInsensitivity	20	20	20	20
Maximum Radiation Use Efficiency	2.2	3	3.1	3.15
Threshold Radiation for Saturation	25	25	25	25
Maximum Rooting Depth	100	100	100	100
Full Canopy Water Uptake Maximum	8	8	8	8
Full Canopy Coefficient	1.05	1.05	1.05	1.05
Base Temperature for Growth	12	12	12	12
Optimum Temperature for Growth	30.5	32	30.8	30.8
Maximum Temperature for Growth	40	40	38	38
Development Susceptibility to Water Stress	0.3	0.3	0.3	0.3
Leaf Life	620	600	500	500
Extinction Coefficient for Solar Radiation	0.5	0.5	0.5	0.5

Chapter 6

GENERAL DISCUSSION AND PERSPECTIVES

6.1 Specific and overall conclusion

The ultimate goal of this research was the setup and evaluation of procedures to support decision-making based on the integration of process based crop model and remotely sensed information. Before the formalization and the evaluation of the tool with measured data, some activities were carried out to guarantee the reliability of the proposed methodologies. This led the following tasks to be performed:

- The improvement in the simulation of canopy structure for a widespread crop model;
- The evaluation of modelling solutions sensitivity to their parameters under a wide range of agro-climatic conditions;
- The quantification of the precision of one of the most popular method for LAI estimates.

The first task, presented in Chapter 2, was carried out for improving the simulation of crop growth and production dynamics via an increase in the level of adherence of the simulated system to the underlying one. The new model (WOFOST-GTC) allowed to satisfactorily reproduce rapeseed growth and productivity, as well as the quality of production.

The second task (described in Chapter 3) was about a series of sensitivity analysis experiments performed on two WOFOST-based modelling solutions. Sensitivity analysis is a useful technique to obtain information about model structure and to identify the most influential parameters and it is usually applied before the operational use of modelling solution. It allows identifying the parameters on which the largest efforts should invested during the parameterization, as well as the parameters to automatically re-calibrate in case of exogenous data assimilation. Within this task, sensitivity analysis experiments were targeted to major crops in different European sites under different weather regimes. Moreover, the effect of extreme weather events on crop growth and productivity was considered by running simulation using different model configurations. The simulation of the final yield was mostly influenced by the parameters related with storage organs dynamics. Indeed, the parameters identified as the most influential were those related with biomass partitioning to storage organs and its conversion efficiency. Exceptions were found in case of anomalous weather conditions. In these cases, the modelling solutions were mostly influenced by the parameters driving the simulation during early crop stages.

The third task, well documented in the chapter 4, was targeted to the validation (determination of repeatability and reproducibility) of the LAI estimates from hemispherical images, one of the most widespread indirect methods for LAI estimates. This activity is particularly important, given LAI estimates are also adopted to calibrate radiative transfer models used in remote sensing. The

quantification of the impact of subjectivity and the determination of precision metrics using rigorous validation protocols allowed to conclude that the hemispherical photography, despite its low cost, can be considered as a valuable technique for LAI estimates also in case of complex canopy structures.

All the activities briefly summarized above allowed defining sound bases for the integration of crop models and remote sensing. In this sense, a case study is shown in chapter 5, where remote sensing LAI data collected during 2014, 2015 and 2016 were assimilated in the WARM rice model to analyze intra-field variability at 30 m × 30 m spatial resolution. Unless few cases, the inclusion of remotely sensed LAI data contributed to reduce the uncertainty in yield simulation. Moreover, the yield variability within each field was accurately simulated thorough the identification of the most and less productive areas. Results were obtained starting from default parameterizations and automatically recalibrating model parameters once during the growing season, thus improving model performances while saving computational costs. This allows the system to be adopted to derive spatially distributed information on crop status and to support the decision-making under operational contexts.

6.2 Future perspectives

Despite the promising results achieved, some weakness emerged during its validation. The inclusion of remotely sensed data did not improve modelling performance in two cases. Some inconsistencies were founded in the relationship between crop state variables and LAI data. In particular, a high LAI value at canopy closure did not correspond to a high final yield. So, further investigations about the mutual relationship between LAI and final yield are required. Within this issue, the refinement of LAI description will be of certain importance. Other works will be directed to the improvements of the techniques to include remotely sensed LAI values into crop models, thus avoiding unexpected unbalances in the relationship between crop state variables. The downscaling of model simulation to a fine resolution accompanied with low requirements in terms of computational costs make the system proposed a valid approach for large scale applications. Further researches will target the adoption of other modelling solutions which explicitly describe the effect of agro-management practices, to further validate this tool for supporting crop management.

PUBLICATIONS DURING THE DOCTORAL WORK

Submitted

Gilardelli, C., Orlando, F., Movedi, E., Confalonieri, R,. 2017. Quantifying repeatability and reproducibility of digital hemispherical photography for LAI estimates on tree species.

Published

Gilardelli, C., Confalonieri, R., Cappelli, G., Bellocchi, G., 2017. Sensitivity of WOFOST-based modelling solutions to crop parameters under climate change. Ecological Model 368, 1-14.

Gilardelli, C., Stella, T., Frasso, N., Cappelli, G., Bregaglio, S., Chiodini, M.E., Scaglia, B., Confalonieri, R., 2016. WOFOST-GTC: A new model for the simulation of winter rapeseed production and oi quality. Field Crops Research 197, 125-132.

Confalonieri. R., Orlando, F., Paleari, L., Stella, T., Gilardelli, C., Movedi, E., Pagani, V., Cappelli, G., Vertemara, A., Alberti, L., Alberti, P., Atanassiu, S., Bonaiti, M., Cappelletti, G., Ceruti, M., Confalonieri, A., Corgatelli, G., Corti, P., Dell'Oro, M., Ghidoni, A., Lamarta, A., Maghini, A., Mambretti, M., Manchia, A., Massoni, G., Mutti, P., Pariani, S., Pasini, D., Pesenti, A., Pizzamiglio, G., Ravasio, A., Rea, A., Santorsola, D., Serafini, G., Slavazza, M., Acutis, M., 2016. Uncertainty in crop model predictions: What is the role of users? Environmental Modelling and Software 81, 165-173.

Orlando, F., Movedi, E., Paleari, L., Gilardelli, C., Foi, M., Dell'Oro, M., Confalonieri, R., 2015. Estimating leaf area index in three species using the PocketLAI smart app. Applied Vegetation Science 18, 716-723.

REFERENCES

Acutis, M., Confalonieri, R., 2006. Optimization algorithms for calibrating cropping systems simulation models. A case study with simplex-derived methods integrated in the WARM simulation environment. Italian Journal of Agrometeorology 3, 26-34.

Akaike, H., 1974. A new look at the statistical model identification. IEEE Trans. Automatic Control 19, 716-723.

Annan, J.D., 2001. Modelling under uncertainly: Monte Carlo methods for temporally varying parameters. Ecol. Model. 136, 297-302.

Archontoulis, S.V., Vos, J., Yin, X., Bastiaans, L., Danalatos, N.G., Struik, P.C., 2011. Temporal dynamics of light and nitrogen vertical distributions in canopies of sunflower, kenaf and cynara. Field Crop. Res.. 122, 186-198.

Arora, V.K., Gajri, P.R., 1998. Evaluation of a crop growth-water balance model for analysing wheat response to climate- and water-limited environments. Field Crop. Res. 59, 213-224.

Asner, G.P., Scurlock, J.M.O. & Hicke, J.A. 2003. Global synthesis of leaf area index observations: implications for ecological and remote sensing studies. Global Ecology and Biogeography 12: 191-205.

Asseng, S., Ewert, F., Rosenzweig, C., Jones, J.W., Hatfield, J.L., Ruane, A., Boote, K.J., (…) & Wolf, J. (2013) Uncertainties in simulating wheat yields under climate change. Nat. Clim. Change 3, 827–832.

Balkovič, J., van der Velde, M., Schmid, E., Skalský, R., Khabarov, N., Obersteiner, M., Stürmer, B., Xiong, W., 2013. Pan-European crop modelling with EPIC: Implementation, up-scaling and regional crop yield validation. Agricultural Systems 120, 61-75.

Baret, F., Buis, S., 2007. Estimating canopy characteristics from remote sensing observation: review of methods associated problems. In: Liang, S. (Eds.), Advances in Land Remote Sensing: System Modelling, Inversion and Applications. Springer, New York, pp. 171-200.

Baret, F., Houles, V., Guérif, M., 2007. Quantification of plant stress using remote sensing observations and crop models: the case of nitrogen management. Journal of Experimental Botany 58, 869-880.

Barlow, K.M., Christy, B.P., O'Leary, G.J., Riffkin, P.A., Nuttal, J.G., 2015. Simulating the impact of extreme heat and frost events on wheat crop production: A review. Field Crop. Res. 171, 109-119.

Barnett, C., Hossel, J., Perry, M., Procter, C., Hughes, G., 2006. A handbook of climate trends across Scotland. Scotland and Northern Ireland Forum for Environmental Research, SNIFFER Project CC03, Edinburgh, United Kingdom.

Basso, B., Ritchie, J.T., Pierce, F.J., Braga, R.P., Jones, J.W., 2001. Spatial validation of crop models for precision agriculture. Agricultural Systems 68, 97-112.

Bassu, S., Brisson, N., Durand, J.L., Boote, K., Lizaso, J., Jones, J.W., Rosenzweig, C., (…) & Waha, K., 2014. How do various maize crop models vary in their responses to climate change factors? Global Change Biol. 20, 2301-2320.

Batchelor, W.D., Basso, B., Paz, J.O., 2002. Examples of strategies to analyze spatial and temporal yield variability using crop models. European Journal of Agronomy 18, 141-158.

Baux, A., Hebeisen, T., Pellet, D., 2008. Effect of minimal temperatures on low-linolenic rapeseed oil fatty-acid composition. Eur. J. Agron. 29, 102-107.

Baux, A., Colbach, N., Pellet, D., 2011. Crop management for optimal low-linolenic rapeseed oil production - Field experiments and modelling. Europ. J. Agronomy 35, 144-153
Baux, A., Colbach, N., Allirand, J.M. Jullien, A., Ney, B., Pellet, D., 2013. Insight into temperature effects on the fatty acid composition of oilseed rape varieties. Eur. J. Agron. 49, 12-19.
Beaudet, M. & Messier, C. 2002. Variation in canopy openness and light transmission following selection cutting in northern hardwood stands: an assessment based on hemispherical photographs. Agricultural and Forest Meteorology 110: 217-228.
Belder, P., Bouman, B.A.M., Spiertz, J.H.J., 2007. Exploring options for water saving in lowland rice using a modeling approach. Agricultural Systems, 92, 91-114.
Bell, J.G., McGhee, F., Campbell, P.J., Sargent, J.R., 2003. Rapeseed oil as an alternative to marine fish oil in diets of post-smolt Atlantic salmon (Salmo salar): changes in flesh fatty acid composition and effectiveness of subsequent fish oil "wash out". Aquaculture 218, 515-528.
Bhardwaj, H.L., Hamama, A.A., 2008. Oil quality of winter hardy rapeseed germplasm relative to biodiesel production. World J. Agric. Sci. 4, 01-06.
Biernath, C., Gayler, S., Bittner, S., Klein, C., Högy, P., Fangmeier, A., Priesack, E., 2011. Evaluating the ability of four crop models to predict different environmental impacts on spring wheat growth in open-top chambers. Eur. J. Agron. 35, 71-82.
Blackshaw, R.E., O'Donovan, J.T., Harker, K.N., Clayton, G.W., Stougaardd, R.N., 2006. Reduce herbicide doses in field crops: A review. Weed Biology and Management 6, 10-17.
Boogaard, H., Wolf, J., Supit, I., Niemeyer, S., van Ittersum, M., 2013. A regional implementation of WOFOST for calculating yield gaps of autumn-sown wheat across the European Union. Field Crop. Res. 143, 130−142.
Brun, R., Reichert, P., Kunsch, H.R., 2001. Practical identifiability analysis of large environmental simulation models. Water Resour. Res. 37, 1015-1030.
Busetto, L., Casteleyn, S., Granell, C., Pepe, M., Barbieri, M., Campos-Taberner, M., (…) & Boschetti, M., 2017. Downstream services for rice crop monitoring in Europe: from regional to local scale. IEEE Journal of Selected Topics in Applied Earth Observations and Remote Sensing 10.1109/JSTARS.2017.2679159.
Campbell, G.S., Normann, J.M., 1989. The description and measurement of plant canopy structure. In: Russel, G., Marshall, B. (Eds.) Plant Canopies: Their Growth, Form and Function. SEB Seminar Series, vol. 31.Cambridge University Press, Cambridge, UK, pp. 1-19.
Campolongo, F., Cariboni, J., Saltelli, A., 2007. An effective screening design for sensitivity analysis of large models. Environ. Modell. Softw. 22, 1509-1518.
Campos-Taberner, M., García-Haro, F.J., Camps-Valls, G., Grau_Muerda, G., Nutini, F., Crema, A., Boschetti, M., 2016. Multitemporal and multiresolution leaf area index retrieval for operational local rice crop monitoring. Remote Sensing of Environment 187, 102-118.
Campos-Taberner, M., García-Haro,F.J., Camps-Valls, G., Grau-Muedra,G., Nutini, F., Busetto, L., Katsantonis, D., (…) & Boschetti, M., 2017. Exploitation of SAR and Optical Sentinel Data to Detect Rice Crop and Estimate Seasonal Dynamics of Leaf Area Index. Remote Sensing 9 (3), 248. doi:10.3390/rs9030248
Cappelli, G., Yamaç, S.S., Stella, T., Francone, C., Paleari, L., Negri, M., Confalonieri, R., 2015. Are advantages from the partial replacement of corn with second-generation energy crops undermined by climate change? A case study for giant reed in northern Italy. Biomass Bioenerg. 80, 85-93.

Cariboni, J., Gatelli, D., Liska, R., Saltelli, A., 2007. The role of sensitivity analysis in ecological modelling. Ecol. Model. 203, 167-182.
Casa, R., Varella, H., Buis, S., Guérif, M., De Solan B., Baret, F., 2012. Forcing a wheat crop model with LAI data to access agronomic variables: Evaluation of the impact of model and LAI uncertainties and comparison with an empirical approach. European Journal of Agronomy 37, 1-10.
Casadebaig, P., Guilioni, L., Lecoeur, J., Christophe, A., Champolivier, L., Debaeke, P., 2011. SUNFLO, a model to simulate genotype-specific performance of the sunflower crop in contrasting environments. Agr. Forest Meteorol. 151, 163-178.
Ceglar, A., Črepinsek, Z., Kajfez-Bogataj, L., Pogacar, T., 2011. The simulation of phenological development in dynamic crop model: the Bayesian comparison of different methods. Agr. Forest Meteorol. 151, 101-115.
Cleugh, H.A., Leuining R., Mu, Q. & Running, S.W. 2007. Regional evapotranspiration estimates from flux tower and MODIS satellite data. Remote Sensing of Environment 106: 285-304.
Cochran, W.G. 1941. The distribution of the largest of a set of estimated variances as a fraction of their total. Annals of Human Genetics 11: 47-52.
Confalonieri, R., 2010. Monte Carlo based sensitivity analysis of two crop simulators and considerations on model balance. Eur. J. Agron. 33, 89-93.
Confalonieri, R., Acutis, M., Bellocchi, G., Donatelli, M., 2009a. Multi-metric evaluation of the models WARM, CropSyst and WOFOST for rice. Ecol. Model. 220, 1395-410.
Confalonieri, R., Bellocchi, G., Bregaglio, S., Donatelli, M., Acutis, M., 2010a. Comparison of sensitivity analysis techniques: a case study with the rice model WARM. Ecol. Model. 221, 1897-1906.
Confalonieri, R., Rosenmund, A.S., Baruth, B., 2009. An improved model to simulate rice yield. Agronomy for Sustainable Development 29, 463-474.
Confalonieri, R., Bellocchi, G., Donatelli, M., 2010b. A software component to compute agro-meteorological indicators. Environ. Modell. Softw. 25, 1485-1486.
Confalonieri, R., Foi, M., Casa, R., Aquaro, S., Tona, E., Peterle, M., Boldini, A.,(…) & Acutis, M. 2013. Development of an app for estimating leaf area index using a smartphone. Trueness and precision determination and comparison with other indirect methods. Computer and Electronics in Agriculture 96: 67-74.
Confalonieri, R., Francone, C., Chiodini, M.E., Cantaluppi, E., Caravati, L., Colombi, V., Fantini, D.,(…) & Acutis, M. 2014. Any chance to evaluate in vivo field methods using standard protocols? Field Crops Research 161: 128-136.
Confalonieri, R., Orlando, F., Paleari, L., Stella, T., Gilardelli, C., Movedi, E., Pagani, V., (…) & Acutis, M., 2016. Uncertainty in crop model predictions: What is the role of users? Environ. Modell. Softw. 81, 165-173.
Council of the European Community (2013). Overview of CAP reform (2014-2020). Agricultural Policy Perspective Brief, n°5* December 2013.
Cryer, S.A., Havens, P.L., 1999. Regional sensitivity analysis using a factorial method for the USDA model GLEAMS. Environ. Modell. Softw. 14, 613-624.
Cukier, R.I., Fortuin, C.M., Shuler, K.E., Petschek, A.G., Schaibly, J.H., 1973. Study of the sensitivity of coupled reaction systems to uncertainties in rate coefficients. I. Theory. J. Chem. Phys. 59, 3873-3878.

Daniel, C., Triboi, E., 2002. Changes in wheat protein aggregation during grain development: effects of temperatures and water stresses. Eur. J. Agron. 16, 1-12.
De Carvalho Lopes, D., Steidle Neto, A.J., 2011. Simulation models applied to crops with potential for biodiesel production. Comput. Electron. Agr. 75, 1-9.
Deligios, P.A., Farci, R., Sulas, L., Hoogenboom, G., Ledda, L., 2013. Predicting growth and yield of winter rapeseed in a Mediterranean environment: Model adaptation at a field scale. Field Crop. Res. 144, 100-112.
De Martonne, E., 1942. Nouvelle carte mondiale de l'indice d'aridité. Ann. Géogr. 51, 242-250 (in French).
de Wit, A., Duveiller, G., Defourny, P., 2012. Estimating regional winter wheat yield with WOFOST through the assimilation of green leaf area index retrieved from MODIS observations. Agr. Forest Meteorol. 164, 39-52.
Diepenbrock, W., 2000. Yield analysis of winter oilseed rape (Brassica napus L.): a review. Field Crop. Res. 67, 35-49.
Diodato, N., Ceccarelli, M., 2004. Multivariate indicator Kriging approach using a GIS to classify soil degradation for Mediterranean agricultural lands. Ecol. Indic. 4, 177-187.
Donatelli, M., Confalonieri, R., 2011. Biophysical models for cropping system simulation. In: Flichman, G. (Ed.) Bio-economic models applied to agricultural systems. Springer, München, Germany, pp. 59-86.
Dong, Y., Wang, J., Li, C., Yang, G., Wang, Q., Liu, F., Zhao, J., Wang, H., Huang, W., 2013. Comparison and analysis of data assimilation algorithms for predicting the leaf area index of crop canopies. IEEE Journal of Selected Topics in Applied Earth Observation and Remote Sensing 6, 188-201.
Dorigo, W.A., Zurita-Milla, R., De Wit, A.J.W., Brazile, J., Singh, R., Schaepman, M.E., 2007. A review on reflective remote sensing and data assimilation techniques for enhanced agroecosystem modeling. International Journal of Applied Earth Observation and Geoinformation 9, 165-193.
Du, T., Kang, S., Sun, J., Zhang, X., Zhang, J., 2010. An improved water use efficiency of cereals under temporal and spatial deficit irrigation in north China. Agricultural Water Management 97, 66-74.
Duchemin, B., Hadria, R., Erraki, S., Boulet, G., Maisongrande, P., Chehbuoni, A., Escadafal, R., (…) & Simonneaux, V. 2006. Monitoring wheat phenology and irrigation in Central Morocco: On the use of relationship between evapotranspiration, crops coefficients, leaf area index and remotely-sensed vegetation indices. Agricultural Water Management 79: 1-27.
Duveiller, G., Donatelli, M., Fumagalli, D., Zucchini, A., Nelson, R., Baruth, B., 2017. A dataset of future daily weather data for crop modelling over Europe derived from climate change scenarios. Theor. Appl. Climatol. 127, 573-585.
Easter, M.J. & Spies, T.A. 1994. Using hemispherical photography for estimating photosynthetic photon flux density under canopies and in gaps in Douglas-fir forests of the Pacific Northwest Canadian Journal of Forest Research 24: 2050-2058.
EEA, 2017. Climate change, impacts and vulnerability in Europe 2016. European Environmental Agency, Europe, pp. 424. http://www.eea.europa.eu/publications/climate-change-impacts-and-vulnerability-2016/at_download/file.

Englud, S.R., O'Brien, J.J., Clark, D.B., 2000. Evaluation of digital and film hemispherical photography and spherical densiometry for measuring forest light environments. Canadian Journal of Forest Research 30, 1999-2005.
Ethier, G.J., Livingston N.J., 2004. On the need to incorporate sensitivity to CO2 transfer conductance into the Farquhar-von Caemmerer–Berry leaf photosynthesis model. Plant, Cell Environ. 27, 137-153.
Evensen, G., 1994. Sequential data assimilation with a nonlinear quasi-geostrophic model using Monte Carlo methods to forecast error statistics. Journal of Geophysical Research 99, 10143-10162.
Ewert, F., Rounsevell, M.D.A., Reginster, I., Metzger, M.J., Leemans, R., 2005. Future scenarios of European land use I. Estimating changes in crop productivity. Agr. Ecosyst. Environ. 107, 101-116.
Falloon, P., Betts, R., 2010. Climate impacts on European agriculture and water management in the context of adaptation and mitigation – The importance of an integrated approach. Sci. Total Environ. 408, 5667-5687.
Fernandes, E.C.M., Soliman, A., Confalonieri, R., Donatelli, M., Tubiello, F., 2012. Climate change and agriculture in Latin America, 2020–2050. Projected impacts and response to adaptation strategies. World Bank, Report No. 69265, Washington DC, USA, 88 p.
Fess, T.L., Kotcon, J.B., Benedito, V.A., 2011. Crop breeding for low input agriculture: a sustainable response to feed a growing world population. Sustainability 3, 1742-1772.
Field, C.B., Barros, V., Stocker, T.F., Qin, D., Dokken, D.J., Ebi, K.L., Mastrandrea, M.D., (…) & Midgley, P.M., 2012. Managing the risks of extreme events and disasters to advance climate change adaptation. A special report on working groups I and II of the Intergovernmental Panel on Climate Change. Cambridge University Press, Cambridge and New York, p. 582.
Food and Agriculture Organization of the United Nations (FAO), 2014. FAOSTAT Online Statistical Service. FAO, http://faostat3.fao.org/ [Last accessed: 12/05/2015].
Fox Maule, C., Christensen, O., 2015. Report on methods, guidance and recommendations. EU-FP7 MODEXTREME (http://modextreme.org), Deliverable number: D3.3.Frère M., Popov, G.F.,1979. Agrometeorological crop monitoring and forecasting, FAO Plant Production and Protection, Paper No. 17, Rome, pp. 64. ISBN 9251008078, 1979.
Gabrielle, B., Denoroy, P., Gosse, G., Justes, E., Andersen, M.N., 1998. Development and evaluation of CERES-type model for winter oilseed rape. Field Crop. Res. 57, 95-111.
Gabrielle, B., Laville, P., Duval, O., Nicoullaud, B., Germon, J.-C., Hénault, C., 2006. Process-based modelling of nitrous oxide emissions from wheat-cropped soils at the sub-regional scale. Global Biogeochem. Cy. 20, GB4018.
Gaudin, A. C.M., Janovicek, K., Martin, R.C., Deen, W., 2014. Approaches to optimizing nitrogen fertilization in a winter – red clover (Trifolium pratense L.) relay cropping system. Field Crops Research 155, 192-201.
García-Vila., M., Fereres, E., 2012. Combining the simulation crop model AquaCrop with an economic model for the optimization of irrigation management at farm level. European Journal of Agronomy 36, 21-31.
Glatthorn,J. & Beckschäfer, P. 2014. Standardizing the protocol for hemispherical photographs: accuracy assessment of binarization algorithms. Plos One 9 (11).

Godfray, H.C.J., Beddington, J.R., Crute, I.R., Haddad, L., Lawrence, D., Muir, J.F., Pretty, J., Robinson, S., Thomas, S.M., Toulmin, C., 2010. Food security: the challenge of feeding 9 billion people. Science 327, 812-818.
Grubbs, F.E. 1969. Procedures for detecting outlying observations in samples. Technometrics 11: 1-21.
Haag, I., 2006. A basic water quality model for the river Neckar: part 1 - model development, parameter sensitivity and identifiability, calibration and validation. Acta Hydroch. Hydrob. 34, 533-548.
Habekotté, B., 1997. A model of the phenological development of winter oilseed rape. Field Crop. Res. 54, 127-136.
Haboudane, D., Miller, J.R., Pattey, E., Zarco-Tejada, P.J., Strachan, I.B., 2004. Hyperspectral vegetation indices and novel algorithms for predicting green LAI of crop canopies: Modeling and validation in the context of precision agriculture. Remote Sensing of Environment 90, 337-352.
Haines, T.D., Adlaf, K.J., Pierceall, R.M., Lee, I., Venkitasubramanian, P., Collison, M.W., 2011. Direct determination of MCPD fatty acid esters and glycidyl fatty acid esters in vegetable oils by LC–TOFMS. J. Am. Oil Chem. Soc. 88, 1-14.
Hall, A.J., Connor, D.J., Sadras, V.O., 1995. Radiation use efficiency of sunflower crops: effects of specific leaf nitrogen and ontogeny. Field Crop. Res. 41, 65-77.
Holland, K.H., Schepers, J.S., 2010. Derivation of a variable rate nitrogen application model for in-season fertilization of corn. Agronomy Journal 102, 1415-1424.
Horwitz, W. 1995. Protocol of the design. Conduct and interpretation of method performance studies. Pure Applied Chemistry 67: 331-343.
Ines, A.V.M., Das, N.N., Hansen, J.W., Njoku, E.G., 2013. Assimilation of remotely sensed soil moisture and vegetation with a crop simulation model for maize yield prediction. Remote Sensing of Environment 138, 149-164.
ISO, 1994. Accuracy (trueness and precision) of measurements methods and results-part 2: basic method for the determination of reproducibility of a standard measurement method. ISO 5725/2.
IPCC (Intergovernmental Panel on Climate Change), 2013. IPCC 5th Assessment Report “Climate Change 2013: the Physical Science Basis. University Press, Cambridge. http://www.ipcc.ch/report/ar5/wg1/#.Uk7O1xBvCVq.
Jacquemoud, S., Verhoef, W., Baret, F., Bacour, C., Zarco-Tejada, P.J., Asner, G.P., Franois, C., Ustin, S.L., 2009. PROSPECT + SAIL models: a review of use for vegetation characterization. Remote Sensing of Environment 113, Supplement 1, S56-S66.
Jacquez, J.A., Perry, T., 1990. Parameter estimation: local identifiability of parameters. Endocrinol. Metab. 258, 727-736.
Jonckheere, I., Fleck, S., Nackaerts, K., Muys, B., Coppin, P., Weiss, M. & Baret, F. 2004. Review of methods for in situ leaf area index determination. Part I. Theories, sensor and hemispherical photography. Agricultural and Forest Meteorology 121: 19-35.
Jonckheere, I., Nackaerts, K., Muys, B. & Coppin, P. 2005. Assessment of automatic gap fraction estimation of forest from digital hemispherical photography. Agricultural and Forest Meteorology 132: 96-114.
Jongschaap, R.E.E., 2006. Run-time calibration of simulation models by integrating remote sensing estimates of leaf area index and canopy nitrogen. European Journal of Agronomy 24, 316-324.
JRC, 2012. Joint Research Centre of the European Commission, Agriculture Project Action 3.

Khabba, S., Duchemin, B., Hadria, R., Er-Raki, S., Ezzahar, J., Chehbouni, A., Lahrouni, A. & Hanich, L. 2009. Evaluation of digital hemispherical photography and plant canopy analyser for measuring vegetation area index of orange orchards. Journal of Agronomy 8: 67-72.
Knox, J.W., Kay, M.G., Weatherhead, E.K., 2012. Water regulation, crop production, and water management–Understanding farmer perspectives on irrigation efficiency. Agricultural Water Management 108, 3-8.
Kumaraswamy, P., 1980. A generalized probability density function for double-bounded random processes. J. Hydrol. 46, 79-88.
Launay, M., Guérif M., 2005. Assimilating remote sensing data into a crop model to improve predictive performance for spatial applications. Agriculture, Ecosystem and Environment 111, 321-339.
Leblanc, S.G., Chen, J.M., Fernandes, R., Deering, D.W., Conley, A., 2005. Methodology comparison for canopy structure parameters extraction from digital hemispherical photography in boreal forest. Agricultural and Forest Meteorology 129, 187-207.
Lehmann, N., Finger, R., Klein, T., Calanca, P., Walter, A., 2013. Adapting crop management practices to climate change: modeling optimal solutions at the field scale. Agricultural Systems 117, 55-65.
Lesk, C., Rowhani, P., Ramankutty, N., 2016. Influence of extreme weather disasters on global crop production. Nature 529, 84-87.
Leuning R., Cleugh, H.A., Zegelin, S.J. & Hughes, D. 2005. Carbon and water fluxes over a temperate Eucalyptus forest and a tropical wet/dry savanna in Australia: measurements and comparison with MODIS remote sensing estimates. Agricultural and Forest Meteorology 129: 151-173.
Li, G., Xue, L., Gu, W., Yang, C., Wang, S., Ling, Q., Qin, X., Ding, Y., 2009. Comparison of yield components and plant type characteristics of high-yield rice between Taoyuan, a 'special eco-site' and Nanjing, China. Field Crops Research 112, 214-221.
Li, T., Hasegawa, T., Yin, X., Zhu, Y., Boote, K., Adam, M., Bregaglio, S., (…) & Bouman, B., 2014. Uncertainties in predicting rice yield by current crop models under a wide range of climatic conditions. Global Change Biol. 21, 1328–1341.
Li, X., Koike, T., Pathmathevan, M., 2004. A very fast simulated re–annealing (VFSA) approach for land data assimilation. Computers & Geosciences 30, 239-248.
Li, Y., Zhou, Q., Zhou, J., Zhang, G., Chen, C., Wang, J., 2014. Assimilating remote sensing information into a coupled hysrology-crop growth model to estimate regional maize yield in arid regions. Ecological Modelling 291, 15-27.
Liu, C., Kang, S., Li, F., Li, S. & Du, T. 2013. Canopy leaf area index for apple tree using hemispherical photography in arid region. Scientia Horticulturae 164: 610-615.
Liu, H., Weng, Q., 2012. Enhancing temporal resolution of satellite imagery for public health studies: a case study of West Nile Virus outbreak in Los Angeles in 2007. Remote Sensing of Environment 117, 57-71.
Lobell, D.B., Ortiz-Monasterio, J.I., Asner, G.P., Naylor, R.L., Falcon, W.P., 2005. Combining field surveys, remote sensing and regression trees to understand yield variations in an irrigated wheat landscape. Agronomy Journal 97, 241-249.
Lobell, D.B., Thau, D., Seifert, C., Engle, E., Little, B., 2015. A scalable satellite-based crop yield mapper. Remote Sensing of Environment 164, 324-333.

Long, S.P., Ainsworth, E.A., Leakey, A.D.B., Nösberger, J., Ort, D.R., 2006. Food for thought: lower-than-expected crop yield simulation with rising CO2 concentrations. Science 312, 1918-1921.
Luo, Y., Ficklin, D.L., Liu, X., Zhang, M., 2013. Assessment of climate change impacts on hydrology and water quality with a watershed modelling approach. Sci. Total Environ. 450-451, 72-82.
Macfarlane, C., Hoffman, M., Eamus, D., Kerp, N., Higginson, S., McMurtrie, R. & Adams, M. 2007. Estimation of leaf area index in eucalypt forest using digital photography. Agricultural and Forest Meteorology 143:176-188.
Marletto, V., Zinoni, F., Criscuolo, L., Fontana, G., Marchesi, S., Morgillo, A., (…) & Andersen, U., 2005. Evaluation of downscaled DEMETER multi-model ensemble seasonal hindcast in a northern Italy location by means of a model of wheat growth and soil water balance. Tellus, 57, 488-497.
Morari, F., Lugato, E., Borin, M., 2004. An integrated non-point source model-GIS system for selecting criteria of best management practices in the Po valley, North Italy. Agriculture, Ecosystem & Environment 102, 247-262.
Morris, M.D., 1991. Factorial sampling plans for preliminary computational experiments. Technometrics 33, 161-174.
Moss, R.H., Edmonds, J.A., Hibbard, K.A., Manning, M.R., Rose, S.K., van Vuuren, D.P., Carter, T.R., (…) & Wilbanks, T.J., 2010. The next generation of scenarios for climate change research and assessment. Nature 463, 747-756.
Movedi, E., Borras, D., Testi, L., Pagani, V., Guarneri, T., Paleari, L., Confalonieri, R., 2015. Abiotic stress model component: v1. EU-FP7 MODEXTREME (http://modextreme.org), Deliverable number: D2.1.
Müller, J., Behrens, T., Diepenbrock, W., 2005. Measurement and modelling of canopy gas exchange of oilseed rape. Agr. Forest Meteorol. 132, 181-200.
MupangwaW., Twomlow, S., Walker, S., Hove, L., 2007. Effect of minimum tillage and mulching on maize (Zea mais L.) yield and water content of clayey and sandy soils. Physics and Chemistry of the Earth 32, 1127-1134.
Nelder, J.A., Mead, R., 1965. A simplex method for function minimization. Computer Journal 7, 308-313.
Nelson, G.C., Valin, H., Sands, R.D., Havlik, P., Ahammad, H., Deryng, D., Elliott, J., (…) & van Meijl, H., 2014. Climate change effects on agriculture: Economic responses to biophysical shocks. Proceedings of the National Academy of Sciences of the United States of America 111, 3274-3279.
Novak, R.S., 2017. CO2 fertilization: Average is best. Nat. Clim. Change 7, 101-102.
Obermeier, W.A., Lehnert, L.W., Kammann, C., Müller, C., Grünhage, L., Luterbacher, J., Erbs, M., (…) & Bendix, J., 2016. Reduced CO2 fertilization effect in temperate C3 grasslands under more extreme weather conditions. Nat. Clim. Change 7, 137-141.
Omlin, M., Brun, R., Reichert, P., 2001. Biogeochemical model of lake Zurich: sensitivity, identifiability and uncertainty analysis. Ecol. Model. 141, 105-123.
Orlando, F., Movedi, E, Paleari, L., Gilardelli, C., Foi, M., Dell'Oro, M. & Confalonieri, R. 2015. Estimating leaf area index in tree species using the PocketLAI smart app. Applied Vegetation Science 18: 716-723.
Paleari, L., Movedi, E., Cappelli, G., Wilson, L.T., Confalonieri, R., 2017. Surfing parameter hyperspaces under climate change scenarios to design future rice ideotypes. Global Change Biology, doi: 10.1111/gcb.13682.

Palosuo, T., Kersebaum, K, C., Angulo, C., Hlavinka, P., Moriondo, M., Olesen, J.E., Patil, R.H.,(…) & Rötter, R., 2011. Simulation of winter wheat yield and its variability in different climates of Europe: A comparison of eight crop growth models. Eur. J. Agron. 35, 103-114.
Panda, S., Amatya, D.M., Hoogenboom, G., 2014. Stomatal conductance, canopy temperature and leaf area index estimation using remote sensing and OBIA techniques. Journal of Spatial Hydrology 12 (1).
Panigada, C., Rossini, M., Meroni, M., Cilia, C., Busetto, L., Amaducci, S., Boschetti, M., (…) & Colombo, R., 2014. Fluorescence, PRI and canopy temperature for water stress detection in cereal crops. Internation Journal of Applied Earth Observation and Geoinformation 30, 167-178.
Pastres, R., Ciavatta, S., 2005. A comparison between the uncertainties in model parameters and in forcing functions: its application to a 3D water-quality model. Environ. Modell. Softw. 20, 981-989.
Perego, A., Sanna, M., Giussani, A., Chiodini, M.E., Fumagalli, M., Pilu, S.R., Bindi, M., Moriondo, M., Acutis, M., 2014. Designing a high-yielding maize ideotype for a changing climate in Lombardy plain (northern Italy). Sci. Total Environ. 499, 497-509.
Peterson, T.C., Folland, C., Gruza, G., Hogg, W., Mokssit, A., Plummer, N., 2001. Report on the activities of the Working Group on Climate change detection and related rapporteurs 1998-2001. WMO, Rep. WCDMP-47, WMO-TD 1071, Geneva, Switzerland, 143 p.
Prando, P., 2011. Risposta morfo-fisiologica e produttiva del colza (B. napus L. var. oleifera) a dosi crescenti di azoto. Ms Thesis, University of Padova, Italy, 115 pp.
Priesack, E., Gayler, S., Hartmann, H.P., 2006. The impact of crop growth sub-model choice on simulated water and nitrogen balances. Nutr. Cycl. Agroecosys. 75, 1-13.
Rabitz, H., 1989. System analysis at molecular scale. Science 246, 221-226.
Ramos, M.J., Fernandez, C., M., Casas, A., Rodriguez, L., Perez, A., 2009. Influence of fatty acid composition of raw materials on biodiesel properties. Bioresource Technol. 100, 261-268.
Raun, W.R., Solie, J.B., Johnson, G.V., Stone, M.L., Mullen, R.W., Freeman, K.W., Thomason, W.E., Lukina, E.V., 2002. Improving nitrogen use efficiency in cereal grain production with optical sensing and variable rate application. Agronomy Journal 94, 815-820.
Rich, P.M., Clark, D.B., Clark, D.A. & Oberbauer, S.F. 1993. Long-term study of solar radiation regimes in a tropical wet forest using quantum sensors and hemispherical photography. Agricultural and Forest Meteorology 65: 107-127.
Richter, G.M., Acutis, M., Trevisiol, P., Latiri, K., Confalonieri, R., 2010. Sensitivity analysis for a complex crop model applied to Durum wheat in the Mediterranean. Eur. J. Agron. 32, 127-136.
Richter, O., Sondgerath, D., 1990. Parameter estimation in ecology: the link between data and models. VCH Publishers, New York, NY, USA, p. 300.
Rossato, M., 2012. Effetti dell'epoca di semina su resa in seme, fitomassa e sua ripartizione in colza invernale da olio. Bs Thesis, University of Padova, Italy, 51 pp.
Rossini, M., Panigada, C., Cilia, C., Meroni, M., Busetto, L., Cogliati, St., Amaducci, S., Colombo, R., 2015. Discriminating irrigated and rainfed maize with diurnal fluorescence and canopy temperature airborne maps. ISPRS International Journal of Geo-Information 4, 626-646.
Rötter, R.P., Carter, T.R., Olesen, J.E., Porter, J.R., 2011. Crop–climate models need an overhaul. Nat. Clim. Change 1, 175-177.

Rötter, R.P., Palosuo, T., Pirttioja, N.K., Dubrovsky, M., Salo, T., Fronzen, S., Aikasalo, R., (…) & Carter, T.R., 2011. What would happen to barley production in Finland if global warming exceeded 4°C? A model based assessment. Eur. J. Agron. 35, 205-214.
Rötter, R.P., Palosuo, T., Kersebaum, K.C., Angulo, C., Bindi, M., Ewert, F., Ferrise, R., (…) & Trnka, M., 2012. Simulation of spring barley yield in different climatic zones of Northern and Central Europe: A comparison of nine crop models. Field Crops Research 133, 23-36.
Saltelli, A., Tarantola, S., Campolongo, F., 2000. Sensitivity analysis as an ingredient of modeling. Stat. Sci. 15, 377-395.
Saltelli, A., Tarantola, S., Chan, K.P.S., 1999. A quantitative model-independent method for global sensitivity analysis of model output. Technometrics 41, 39-56.
Sándor, R., Barcza, Z., Acutis, M., Doro, L., Hidy, D., Köchy, M., Minet, J., (…) & Bellocchi, G., 2016. Multi-model simulation of soil temperature, soil water content and biomass in Euro-Mediterranean grasslands: Uncertainties and ensemble performance. Eur. J. Agron. doi:10.1016/j.eja.2016.06.006.
Savage, I.R., 1956. Contributions to the theory of rank order statistics – the two-sample case. Ann. Math. Stat. 27, 590-615.
Singh, A.K., Tripathy, R., Chopra, U.K., 2008. Evaluation of CERES-Wheat and CropSyst models for water-nitrogen interactions in wheat crop. Agricultural Water Management 95, 776-786.
Solie, J.B., Monroe, A.D., Raun, W.R., Stone, M.L., 2012. Generalized algorithm for variable-rate nitrogen application in cereal grains. Agronomy Journal 104 ,378-387.
Sørensen, C.G., Fountas, S., Nash, E., Pesonen, L., Bochtis, D., Pedersen, S.M., Basso, B., Blackmore, S.B., 2010. Conceptual model of a future farm management information system. Computers and Electronics in Agriculture 72, 37-47.
Spasibionek, S., 2006. New mutants of winter rapeseed (Brassica napus L.) with changed fatty acid composition. Plant Breeding 125, 259-267.
Stearns, S.C., 1992. The Evolution of Life Histories. Oxford University Press, Oxford.
Steduto, P., Albrizio, R., Giorio, P., Sorrentino, G., 2000. Gas-exchange response adn stomatal and not-stomatal limitations to carbon assimilation of sunflower under salinity. Environ. Exp. Bot. 44, 243-255.
Stella, T., Frasso, N., Negrini, G., Bregaglio, S., Cappelli, G., Acutis, M., Confalonieri, R., 2014. Model simplification and development via reuse, sensitivity analysis and composition: a case study in crop modelling. Environ. Modell. Softw. 59, 44-58.
Subedi, K.D., Ma, B.L., 2009. Assessment of some major yield-limiting factors on maize production in humid temperature environment. Field Crop. Res. 110, 21-26.
Supit, I., van Diepen, C.A., de Wit, A.J.W., Wolf, J., Kabat, P., Baruth, B., Ludwig, F., 2012. Assessing climate change effects on European crop yields using the Crop Growth Monitoring System and weather generator. Agr. Forest Meteorol. 164, 96-111.
Takai, T., Matsuura, S., Nishio, T., Ohsumi, A., Shiraiwa, T., Horie, T., 2006. Rice yield potential is closely related to crop growth rate during late reproductive period. Field Crops Research 96, 328-335.
Tang, H., Dubayah, R., Swatantran, A., Hofton, M., Sheldon, S., Clark, D.B., Blair, B., 2012. Retrieval of vertical LAI profiles over tropical rain forest using waveform lidar at La Selva, Costa Rica. Remote Sensing of Environment 124, 242-250.

Tilman, D., Cassman, K.G., Matson, P.A., Naylor, R., Polasky, S., 2002. Agricultural sustainability and intensive production practices. Nature 418, 671-677.
Tingem, M., Rivington, M., Bellocchi, G., 2009. Adaptation assessments for crop production in response to climate change in Cameroon. Agron. Sustain. Dev. 29, 247-256.
Tester, M., Langridge, P., 2010. Breeding technologies to increase crop production in a changing world. Science 327, 818-822.
Todorovic, M., Albrizio, R., Zivotic, L., Abi Saad, M.T., Stöckle, C., Steduto, P., 2008. Assessment of AquaCrop, CropSyst, and WOFOST model in the simulation of sunflower growth under different water regimes. Agron. J. 101, 509-521.
Trápani, N., Hall, A.J., Weber, M., 1999. Effects of constant and variable nitrogen supply on sunflower (Helianthus annuus L.) leaf cell number and size. Ann. Bot. – London 84, 599-606.
Turral, H., Svendsen, M., Faures, J.M., 2010. Investing in irrigation: reviewing the past and looking to the future. Agricultural Water Management 97, 551-560.
Ursin, V.M., 2003. Modification of plant lipids for human health: development of functional land-based omega-3 fatty acids. J. Nutr. 133, 4271-4274.
van der Velde, M., Tubiello, F.N., Vrieling, A., Bouraoui, F., 2012. Impacts of extreme weather on wheat and maize in France: evaluating regional crop simulations against observed data. Climatic Change 113, 751-765.
Van der Werf, H.M.G., Petit, J., 2002. Evaluation of the environmental impact of agriculture at farm level: a comparison and analysis of 12 indicator-based methods. Agriculture, Ecosystem and Environment 93, 131-145.
van Diepen, C.A., Rappoldt, C., Wolf, J., van Keulen, H., 1988. Crop Growth Simulation Model WOFOST. Documentation Version 4.1. Centre for World Food Studies, Wageningen, 299 pp.
van Diepen, C.A., Wolf, J., Van Keulen, C., Rappoldt, C., 1989. WOFOST: a simulation model of crop production. Soil Use Manage. 5, 16-24.
van Heemst, H., 1988. Plant data values required for simple and universal simulation models: review and bibliography. Simulation report CABO-TT, Wageningen, The Netherlands.
van Meijgaard, E., van Ulft, L.H., van de Berg, W.J., Bosveld, F.C., van den Hurk, B.J.J.M., Lenderink, G., Siebesma, A.P., 2008. The KNMI regional atmospheric climate model RACMO version 2.1. Technical Report; TR-302.
van Vuuren, D.P, Edmonds, J., Kainuma, M., Riahi, K., Thomson, A., Hibbard, K., Hurtt, G.C., Kram, T., Krey, V., Lamarque, J.-F., Masui, T., Meinshausen, M., Nakicenovic, N., Smith, S.J., Rose, S.K., 2011. The representative concentration pathways: an overview. Climatic Change 109, 5-31.
Villalobos, F., Tardieu, F., Bellocchi, G., de Melo e Abreu, J.P., Parent, B., Morales, A., (…) & Testi, L., 2015. Report on modelling approaches for simulating the impact of extreme events on agricultural production. EU-FP7 MODEXTREME (http://modextreme.org), Deliverable number: D1.2.
Voldoire, A., Sanchez-Gomez, E., Salas y Mélia, D., Decharme, B., Cassou, C., Sénési, S., Valcke, S., (…) & Chauvin, F., 2013. The CNRM-CM5.1 global climate model: description and basic evaluation. Clim. Dynam. 40, 2091-2121.
Wagner, H., Luther, R., Mang, T., 2001. Lubricant base fluids based on renewable raw materials. Their catalytic manufacture and modification. Appl. Catal. A-Gen. 221, 429-442.
Waha, K., Huth, N., Carberry, P., Wang, E., 2015. How model and input uncertainty impact maize yield simulations in West Africa. Environmental Research Letters 10, 024017.

Walton, G.H., 1999. Environmental impact on canola yield and oil. In: Wratten, N., Mailer, R.J. (Eds.), Proceedings of the 10th International Rapeseed Congress. Canberra, Australia. 26-29 Sept., p. 23-28.
Wang, D., Heckathorn, S.A., Wang, X., Philpott, S.M., 2012. A meta-analysis of plant physiological and growth responses to temperature and elevated CO2. Oecologia 169, 1-13.
Wang, J., Li, X., Lu, L., Fang, F., 2013. Parameter sensitivity analysis of crop growth models based on the extended Fourier Amplitude Sensitivity Test method. Environ. Modell. Softw. 48, 171-182.
Weiss, M., Baret, F., Smith, G.J., Jonckheere, I. & Coppin, P. 2004. Review of methods for in situ leaf area index (LAI) determination. Part II. Estimation of LAI, errors and sampling. Agricultural and Forest Meteorology 121: 37-53.
White, J.W., Hoogenboom, G., Kimbali, B.A., Wall, G.W., 2011. Methodologies for simulating impacts of climate change on crop production. Field Crop. Res. 124, 357-368.
Wong, M.T.F., Asseng, S., 2006. Determining the causes of spatial and temporal variability of wheat yields at sub-field scale using a new method of upscaling a crop model. Plant and Soil 283, 203-2015.
Wood, G.A., Welsh, J.P., Godwin, R.J., Taylor, J.C., Earl, R., Knight, S.M., 2003. Real-time measures of canopy size as a basis for spatially varying nitrogen application to winter wheat sown at different seed rates. Biosystems Engineering 84, 513-531.
Xu, C., Gertner, G., 2007. Extending a global sensitivity analysis technique to models with correlated parameters. Comput. Stat. Data An. 51, 5579-5590.
Youping, M., Shili, W., Li, Z., Yingyu, H., Liwei, Z., Yanbo, H., Futang, W., 2008. Monitoring winter wheat growth in North China by combining a crop model and remote sensing data. International Journal of Applied Earth Observation and Geoinformation 10,426-437.
Zahoor, R., Basra, S.M.A., Munir, H., Nadeem, M.A., Yousaf, S., 2011. Role of boron in improving assimilate partitioning and achene yield in sunflower. J. Agric. Soc. Sci. 7, 49-55.
Zeleke, K.T., Luckett, D.J., Cowley, R.B., 2011. Calibration and testing of the FAO AquaCrop model for canola. Agron. J. 103, 1610-1618.
Zeleke, K.T., Luckett, D.J., Cowley, R.B., 2014. The influence of soil water conditions on canola yields and production in Southern Australia. Agr. Water Manage. 144, 20-32.
Zhang, Y., Chen, J.M., Miller, J.R., 2005. Determining digital hemispherical photograph exposure for leaf area index estimation. Agricultural and Forest Meteorology 133, 166-181.
Zhao, K., Popescu, S., 2009. Lidar-based mapping of leaf area index and its use for validating GLOBCARBON satellite LAI product in a temperate forest of the southern USA. Remote Sensing of Environment 113, 1628-1645.
Zhao, Y., Chen, S., Shen, S., 2013. Assimilating remote sensing information with crop model using Ensemble Kalman Filter for improving LAI monitoring and yield estimation. Ecological Modelling 270, 30-42.
Zhu, Z., Bi, J., Pan, Y., Ganguly, S., Anav, A., Xu, L., Samanta, A., Piao, S., Nemani, R.R., Myneni, R.B., 2013. Global data set of vegetation leaf area index (LAI) and fraction of photosynthetically active radiation (FPAR) derived from global inventory modeling and mapping studies (GIMMS) normalized difference vegetation index(NDVI) for the period 1981 to 2011. Remote Sensing 5, 927-948.
Zinyengere, N., Crespo, O., Hachigonta, S., Tadross, M., 2014. Local impacts of climate change and agronomic practices on dry land crops in Southern Africa. Agr. Ecosyst. Environ. 197, 1-10.